Pancreatic cancer cell proliferation, glucose metabolism and chemosensitivity is affected by pancreatic stellate cells

Aina Balto

Thesis for the degree Master of Science
Molecular Biology and Biochemistry
60 credits

Department of Biosciences
Faculty of Mathematics and Natural Sciences

UNIVERSITY OF OSLO

May 2021

Pancreatic cancer cell proliferation, glucose metabolism and chemosensitivity is affected by pancreatic stellate cells

2021

Pancreatic cancer cell proliferation, glucose metabolism, and chemosensitivity is affected by pancreatic stellate cells

Aina Balto

http://www.duo.uio.no/

Print: Reprosentralen, University of Oslo

Acknowledgements

The experiments carried out and presented in this thesis were performed at the Institute of Pharmacology at Rikshospitalet and were funded by the Norwegian Cancer Society (Kreftforeningen), project number 212734-2019. The work was conducted under the supervision of Caroline Sophie Verbeke and Manoj Amrutkar.

A big thanks to Manoj Amrutkar for guidance and support throughout this whole process. I am very grateful for all the time you have spent teaching me practical lab work and for all the support you have provided in the writing process. Thanks for helping me to finish this thesis on time, although a pandemic decided to join us throughout the entire process. I would also like to thank Caroline Sophie Verbeke for support in the writing process and for taking care of all the practical things, and Anette Vefferstad Finstadsveen for guidance in the lab. Thanks to my fellow master student Miguel Garcia Skilbrei for all the good conversations in the reading room and the lab.

Finally, I would like to thank my family and friends for providing me a social life besides the master thesis during this pandemic.

Oslo, May 2021

Aina Balto

Abstract

Pancreatic ductal adenocarcinoma (PDAC), commonly referred to as pancreatic cancer, is associated with profound chemoresistance, resulting in an extremely poor prognosis with a 5-year survival rate of less than 8%. The presence of abundant stroma in PDAC creates a tumor environment with low oxygen and nutrient availability. Under such challenging conditions, to maintain their high metabolic demands, the pancreatic cancer cells (PCCs) get help from neighboring pancreatic stellate cells (PSCs) to acquire nutrients through unconventional ways, a process called metabolic rewiring, which results particularly in altered glycolysis. Furthermore, increasing evidence suggests that PSCs are key to the acquired chemoresistance of PCCs. However, if and how PSC-induced metabolic changes and chemoresistance in PCCs are interlinked is currently unknown. The aim of this study is to investigate PSC-induced changes in glycolysis and chemosensitivity in human pancreatic cancer cells.

The conditioned medium of PSCs (PSC-CM) that were isolated from a treatment-naïve PDAC (PSC-1), a neoadjuvantly treated PDAC (PSC-2), and a healthy donor (HPaSteC) were used to investigate the impact of PSCs on the cancer cell phenotype, glucose metabolism, and chemosensitivity using a panel of pancreatic cancer cells - Capan-2, HPAF-II and Mia PaCa-2. The phenotypic changes were determined by studying morphology on H&E staining, cell viability by MTT assay, and cell proliferation by BrdU incorporation. The glycolytic changes were investigated by measuring glucose transport using [^{3}H]-2-deoxy-D-glucose, and by measuring lactate secretion using the Glycolysis Cell-Based Assay Kit. Chemosensitivity was determined with the MTT assay. Lastly, proteomic analysis of PSC-CMs and western blot analysis of protein expression in PCCs was performed.

The results showed that cell growth, viability and proliferation were in most cases increased in PCCs incubated with PSC-CM compared with serum-free DMEM medium (SFM). Glucose transport was significantly lower in Mia PaCa-2 compared to the other two PCCs. It was increased in Capan-2 and Mia PaCa-2 by exposure to PSC-CM as compared to SFM. While PSC-CM had a variable impact on lactate secretion under normal conditions, under nutrient-poor conditions there was a trend towards increased lactate secretion by PCCs exposed to PSC-CM as compared to SFM. The PCCs showed reduced chemosensitivity when exposed to PSC-CM. When compared with SFM, incubation with PSC-CM showed a similar impact on the

PCCs. However, when compared between themselves, the impact of the three different PSCs on the different PCCs was quite variable. Similarly, western blot analysis demonstrated variation in protein expression between the three PCCs, while secretome analysis revealed considerable differences in the number and levels of proteins that were detected in the three different PSC-CMs.

In conclusion, a general trend of increased viability, proliferation, glucose transport, glycolysis and reduced chemosensitivity was seen in PCCs exposed to PSC-CM as compared to PCCs incubated with SFM. Notably, the observed changes varied strongly between the PCCs as well as between the PSC-CMs. Further investigations are required to gain insight into the molecular mechanisms that underlie the PSC-CM induced changes in glucose metabolism and chemosensitivity in PCCs.

Table of contents

1 Introduction

1.1 Pancreas

The human pancreas is an organ of around 15-25 cm in length and its weight is approximately 100–150 g. It has a hammer-like shape with a larger head and a more slender body and tail. It is located in the retroperitoneal space of the upper abdomen and lies in close relationship with the spleen and other organs of the digestive system, including the stomach, duodenum and colon, as illustrated in Figure 1.1. The pancreas consists of an endocrine and an exocrine compartment, which regulate digestion and blood glucose, respectively [1].

The exocrine pancreas accounts for approximately 80% of the cellular mass of the entire organ and consists of acinar and ductal cells. The exocrine gland secretes pancreatic juice, which is drained along the pancreatic duct and into the duodenum [1]. The pancreatic juice contains digestive enzymes such as lipases, proteinases, and amylases which break down fats, proteins, and carbohydrates into smaller molecules that can be absorbed by the small bowel mucosa [2]. In addition, pancreatic juice contains bicarbonate, which neutralizes the acid that enters the duodenum from the stomach [3].

The endocrine pancreas consists of five types of hormone-secreting cells that form small clusters, the so-called islets of Langerhans, which lie dispersed throughout the exocrine pancreas. The different endocrine cell types within the islets are pancreatic polypeptide (PP) cells, alpha-(α), beta- (β), delta- (δ) and epsilon- (ε) cells [1, 2]. α-cells secrete glucagon to increase blood glucose levels, while β-cells secrete insulin to decrease blood glucose levels. δ-cells secrete somatostatin, which among various other functions, decreases the release of insulin and glucagon. ε-cells secrete ghrelin, which modulates the release of insulin and glucagon. PP cells secrete pancreatic polypeptides, which regulate the exocrine and endocrine secretory activity of the pancreas [2]. The islet cells are intimately related to a delicate network of capillaries, into which they secrete their respective hormones. The latter enter the microvasculature of the exocrine tissue before entering the general circulation [4].

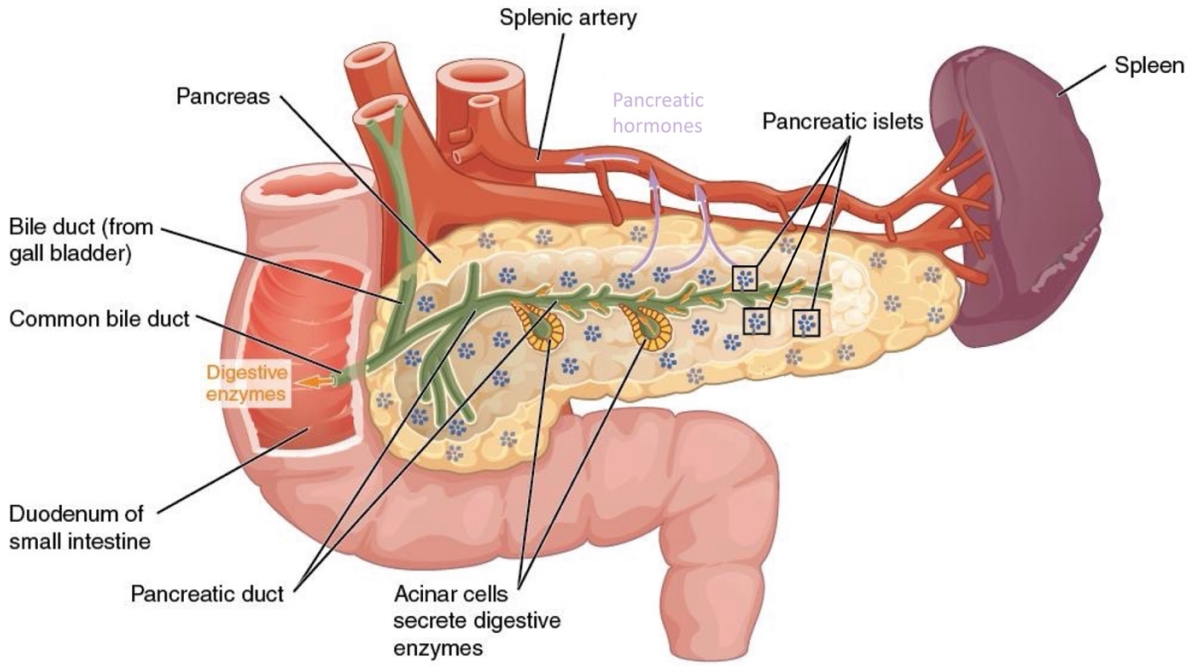

Figure 1.1. Schematic representation of the human pancreas: anatomy, function and nearby organs. Adapted and modified from Human Anatomy and Physiology, an OpenStax College resource [5].

1.2 Pancreatic cancer

Cancer refers to a neoplastic growth that has breached the confines of its tissue of origin and has the potential to invade and spread to other tissues. Cancer is mainly caused by an accumulation of mutations and other genetic alterations [6]. Mutations can take place in a reproductive cell, and therefore be passed on to the offspring (germline mutation), or it can take place in any of the other cells in the body and not be passed on to the offspring (somatic mutation) [7].

Cancer is classified either according to the organ it arises in or according to the type of tissue or cell it originated from. Cancers arising in the pancreas are therefore referred to as pancreatic cancer. Pancreatic cancer can be further classified based on which type of cell it has arisen from. The main type of epithelial cells in the pancreas are enzyme-producing acinar cells (85%), followed by endocrine cells (3-5%) and ductal cells, i.e., the epithelial cells that line the entire pancreatic duct system (up to 3%) [8]. Despite the low proportion of ductal cells in the normal pancreas, the most prevalent pancreatic tumor type is pancreatic ductal adenocarcinoma (PDAC), which arises from the duct epithelium and accounts for more than 90% of all pancreatic carcinomas [9]. Adenocarcinoma is the term for cancer arising from secretory

epithelial cells [6]. Pancreatic neoplasms with a non-ductal cellular origin such as acinar cell carcinomas, solid pseudopapillary neoplasms, and pancreatoblastomas are rare [8]. PDAC is therefore commonly referred to as pancreatic cancer, and is the subject of this thesis [10].

1.3 Pancreatic ductal adenocarcinoma

1.3.1 Epidemiology

PDAC is the fourth leading cause of cancer-related deaths at present, and by 2030 it is predicted to become the second leading cause of cancer-related deaths in the western world [11]. The International Agency for Research on Cancer estimated 495 773 new cases of pancreatic cancer and 466 003 deaths globally in 2020 [12]. Europe has the highest incidence with a crude rate of 18.7 cases per 100 000 inhabitants, while the lowest incidence has been reported in Africa with 1.3 cases per 100 000 inhabitants [13]. According to the estimates from the Norwegian Cancer Registry, 884 new cases of pancreatic cancer and 800 pancreatic cancer-related deaths were reported in Norway in 2019 [14].

1.3.2 Risk factors

Lifestyle-related risk factors for PDAC include smoking, heavy alcohol use, and obesity. In addition, diabetes, chronic pancreatitis and *Helicobacter pylori* infections have been reported as risk factors for PDAC [9, 15]. Non-modifiable risk factors include age, gender, blood type, and genetic predisposition [9, 15]. PDAC is rarely diagnosed in individuals younger than 40, and the worldwide incidence of PDAC is higher in males than in females [9, 15]. In addition, large epidemiological studies have shown that individuals with blood type O have a lower risk of developing PDAC compared to the other blood types [9]. Approximately 10% of patients with pancreatic cancer have a genetic predisposition due to a particular germline mutation. Approximately 5-10% of PDAC patients have so-called familial pancreatic cancer, which means that they have a strong family history of PDAC, but an underlying germline mutation cannot be identified [15].

1.3.3 Symptoms

Pancreatic cancer often remains asymptomatic for a long time or causes only mild and non-specific symptoms. Therefore, the disease is often detected at an advanced stage, which makes it difficult to treat. Jaundice is a common and alarming but fairly late symptom because it is

caused by tumor infiltration and obstruction of the bile duct, which runs through the head of the pancreas. When the bile duct is blocked, bilirubin accumulates in the body giving dark urine and yellow color to the skin and mucous membranes. Other PDAC symptoms are pain in the abdomen or the back, nausea, diarrhea, weight loss, poor appetite and a feeling of illness or low energy. Newly discovered diabetes is also one of the possible symptoms, as around 20% of PDAC patients developed diabetes within 6-12 months prior to the detection of their cancer [15, 16].

1.3.4 Diagnosis

Computed tomography (CT) is the diagnostic standard. A CT scan can show the location of the tumor, if it has grown into surrounding blood vessels or organs and if it has spread to the liver or lungs. If required, other imaging modalities can be used, including magnetic resonance (MR) or endoscopic ultrasound. The latter allows that a biopsy is taken from the pancreatic tumor, which can be used to clarify if the tumor is a neuroendocrine tumor or adenocarcinoma [16].

1.3.5 Genetics

There are two main types of cancer-critical genes, which are genes that when mutated contribute to the development of cancer. One type is the tumor suppressor genes that suppress abnormal cell proliferation and cause cancer when inactivated. The other type is the proto-oncogenes, which in contrast, cause cancer when they are activated into oncogenes by accelerating cell proliferation and invasiveness [6, 17]. The most common PDAC mutation is a missense mutation in glycine-12 in the proto-oncogene Kirsten rat sarcoma viral oncogene homolog (*KRAS*). This mutation is found in more than 90% of all PDACs [18]. *KRAS* codes for the protein Ras, a small GTPase that switches between an active guanosine triphosphate (GTP)-bound state and an inactive guanosine diphosphate (GDP)-bound state. The mutant *KRAS* gene produces a Ras protein that is “locked” in its activated form resulting in overstimulation of signaling pathways that drive cancer growth [19, 20]. *KRAS* is also the first genetic alteration in the great majority of PDACs. It is present in more than 90% of low-grade pancreatic intraepithelial neoplasia (PanIN), a non-invasive neoplastic lesion assumed to be the most common precursor of PDAC [21].

High-grade PanIN usually acquires mutations in the tumor suppressor genes tumor protein P53 (*TP53*), cyclin-dependent kinase inhibitor 2A (*CDKN2A*) and mothers against decapentaplegic

homolog 4 (*SMAD4*) [21]. Mutations in the *TP53* gene, which are present in 70% of PDACs, result in inactivation of the transcription factor p53. As a consequence, p53 is not able to induce the expression of genes promoting cell cycle arrest or apoptosis when the cell is subject to stress or DNA damage [18]. Inactivation of the *CDKN2A* gene, which is present in 46% of PDACs, results in loss of the p16 protein. Loss of p16 leads to increased cell proliferation as p16 is a regulator of the G1-S transition of the cell cycle [18]. Mutations in *SMAD4*, which are present in 38% of PDACs, leads to a non-functional, degraded or truncated Smad4 protein. Loss of Smad4 leads to alterations in tumor necrosis factor-β (TGF-β) signaling, which in turn increases cell proliferation [18, 22, 23].

Approximately 10% of PDAC patients have a form of genetic predisposition. Syndromes that increase the risk of developing PDAC include Lynch syndrome caused by mutated DNA mismatch repair (*MMR*) genes, familial atypical multiple mole melanoma syndrome caused by mutated *CDKN2A*, Peutz-Jeghers syndrome caused by mutated serine/threonine kinase 11 (*STK11*), hereditary breast and ovarian cancer syndrome caused by mutated breast cancer gene 2 (*BRCA2*), hereditary pancreatitis caused by mutated serine protease 1 (*PRSS1*), familial adenomatous polyposis caused by mutated adenomatous polyposis coli (*APC*) and Li-Fraumeni syndrome caused by mutated *TP53* [9, 15].

1.3.6 Treatment

Surgery is the only treatment that offers a potential cure for PDAC. Due to few and non-specific symptoms, PDAC is often detected at an advanced stage. Only around 20% of patients with PDAC have a resectable tumor at the time of detection [24]. In the remaining 80%, the tumor is unresectable because it has grown into adjacent large blood vessels or because it has metastasized to distant organs. A successful surgical resection gives a five-year survival rate of 25%, which is a significant increase compared to the general worldwide PDAC survival rate of 2-9% [9, 24].

Pancreatoduodenectomy (Whipple´s procedure) is the most common surgical procedure for PDAC. It is performed on the tumors in the pancreatic head region and involves removal of the head of the pancreas, the gallbladder, the duodenum, the distal part of the stomach and the distal bile duct. The small intestine is then connected to the remaining bile duct, stomach and the rest of the pancreas. This surgery is not performed if the cancer has spread to other organs such as

the liver or lungs, or if the tumor has grown extensively into blood vessels. If the cancer is located in the body or tail of the pancreas, a distal pancreatectomy is performed. Very rarely, the entire pancreas is removed (total pancreatectomy) [16, 25, 26].

If the tumor has grown into blood vessels, it is recommended to give neoadjuvant chemotherapy before considering surgery. When surgery is not possible at all, which is the case for most PDAC patients, chemotherapy and radiation therapy can be used to give life-prolonging and relieving effects [16]. The two chemotherapeutic first-line treatment options for patients with metastases are the combination of 5-fluorouracil, oxaliplatin, irinotecan and leucovorin (FOLFIRINOX) or gemcitabine combined with nanoparticle albumin-bound paclitaxel (GEM-NAB) [18]. A meta-analysis from 2019, including 3813 metastatic pancreatic cancer patients (2123 treated with GEM-NAB and 1690 treated with FOLFIRINOX), showed the overall risk of death and progression to be similar between the two treatment options. There is so far no evidence of a major benefit of one of the treatments compared with the other [27].

1.4 Pancreatic tumor microenvironment

1.4.1 Stromal architecture

The tumor microenvironment (TME) in PDAC, illustrated in Figure 1.2, is characterized by a dense fibrous stroma which may account for as much as 90% of the tumor mass [6, 28]. The acellular components of the stroma include extracellular matrix (ECM) components, growth factors and cytokines. The ECM is a mesh of secreted proteins that surrounds cells and creates structure in the intercellular space. Activated pancreatic stellate cells (PSCs) secrete excessive amounts of ECM components such as collagen (mainly type I, III and IV), fibronectin and hyaluronic acid [6, 29]. The increased presence of hyaluronic acid and rigid collagen network results in a high interstitial fluid pressure (IFP), which causes the collapse of a large part of the microvasculature inside the tumor. This leads to a hypoxic and nutrient-poor TME and impairs drug delivery in PDAC. Moreover, the interactions between the cancer cells and various cellular and acellular components of the pancreatic TME also contribute to therapy resistance and tumor progression [18, 28, 30-32].

The cellular components of the stroma include cancer-associated fibroblasts (CAFs), immune cells, endothelial cells and neurons. These non-neoplastic cells may account for more than 90% of all cells present in the pancreatic TME [32]. All activated fibroblast cells in the TME that

have a phenotype, function or location that are distinct from the quiescent fibroblasts are considered as CAFs. Two main subgroups of CAFs have been identified: myofibroblastic cancer-associated fibroblasts (myCAFs) and inflammatory cancer-associated fibroblasts (iCAFs). Recent studies have also suggested a third subtype of CAFs, the antigen-presenting cancer-associated fibroblasts (apCAFs) [30, 33]

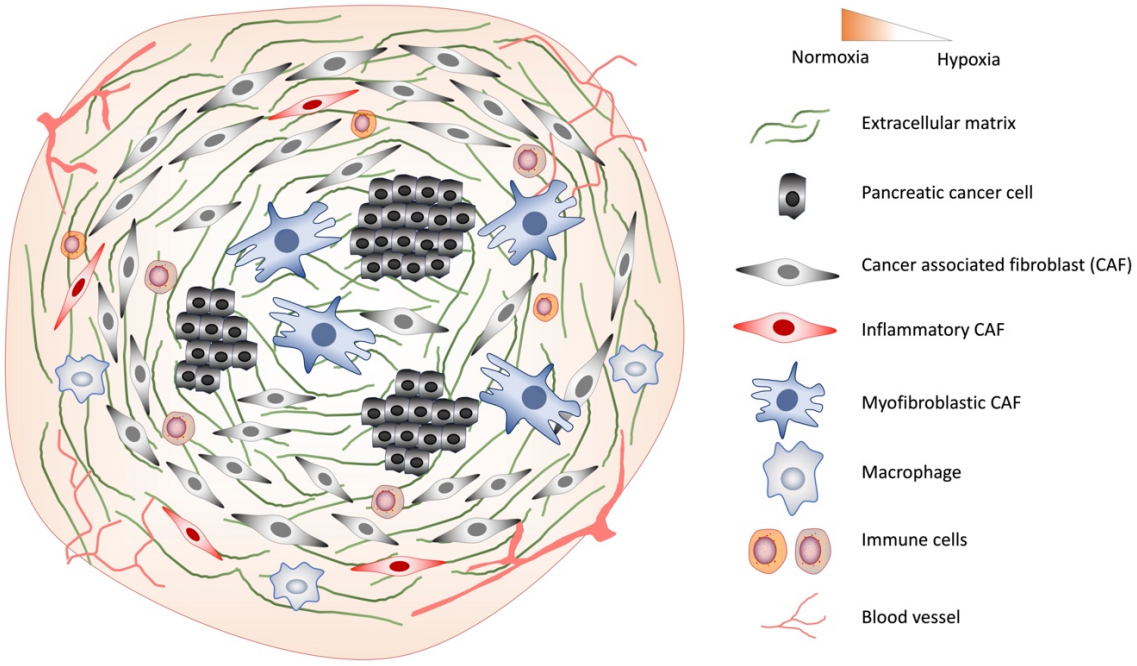

Figure 1.2. Overview of the pancreatic cancer tumor microenvironment. The stroma surrounding pancreatic cancer cells mainly consist of pancreatic stellate cells, immune cells, vasculature and extracellular matrix, which together create a hypoxic and nutrient-poor environment.

myCAFs are usually located closely around the malignant epithelial cells [32]. They are characterized by the upregulation of actin alpha 2 (*ACTA2*), leading to an increased α-smooth muscle actin (α-SMA) expression. myCAFs also display upregulation of collagen type I-, collagen type V- and collagen type VI alpha 1 chain (Col1a1, Col5a1 and Col6a1), leading to high levels of collagen deposition. TGF-β signaling from tumor cells is known to induce the formation of myCAFs [34, 35]. iCAFs are in contrast located more distantly from the cancer cells. They are characterized by higher expression of the inflammatory cytokines interleukin (IL) -1, -6 and -11, leukemia inhibitory factor (LIF) and granulocyte colony-stimulating factor (G-CSF). LIF and IL-6 have been reported to promote PDAC growth. IL-1 contributes to nuclear factor-κB (NF-κB) translocation to the nucleus, where it acts as a transcription factor for inflammatory genes driving the iCAF phenotype. iCAFs also exhibit a higher expression of

chemokines, including C-X-C motif chemokine ligand 1 and C-X-C motif chemokine ligand 2 [30, 34, 35].

Lastly, apCAFs are characterized by expression of major histocompatibility complex (MHC) class II-related genes such as H-2 class II histocompatibility antigen A beta chain (H2-Ab1) and cluster of differentiation 74 (CD74) [30, 32]. They are also found to activate T helper cells in an antigen-specific manner, indicating that they have the potential to modulate the immune response in PDAC [33]. The primary source of CAFs in PDAC is PSCs, which is the subject of this thesis [31]. At present, the term CAF and (activated) PSC are used interchangeably.

1.4.2 Heterogeneity

The presence of a high degree of molecular and genetic heterogeneity is observed both between different tumors (inter-tumor heterogeneity), but also within the same tumor (intra-tumor heterogeneity). Both forms of heterogeneity have been suggested to be obstacles to successful treatment of PDAC [36, 37]. This heterogeneity results from differences in composition, structural organization and functional properties of both the cancer cells and the stromal compartment. [36]. Erkan et al. proposed an activated stroma index which divided the area occupied by α-SMA, a marker of PSC activity, on the area occupied by collagen. In general, tumors with low collagen deposition and high stromal cell activity have the worst prognosis [38]. A high transcriptional and functional heterogeneity is also found in the CAFs, as distinct subpopulations are reported to produce complex effects on the progression and therapy responses in PDAC [33, 39-43].

1.5 Pancreatic stellate cells

1.5.1 Background

Pancreatic stellate cells make up for 4-7% of the human pancreas [44]. The existence of PSCs was first described in 1982 in the mouse pancreas by Watari et al. [45]. Sixteen years later, in 1998, PSCs were isolated and cultured from human and rodent pancreas by two independent research groups, M. V. Apte et al. and M. G. Bachem et al. [46, 47]. This opened up a new avenue in the field of pancreatic fibrogenesis.

In the healthy pancreas, the PSCs exist in a quiescent inactivated form, whereas upon injury or inflammation, the quiescent PSCs are transformed into their activated state. PSC activation is

promoted by several cytokines and transcription factors such as tumor necrosis factor-α (TNF-α), TGF-β, platelet-derived growth factor (PDGF), connective tissue growth factor (CTGF), hypoxia-inducible factor-1α (HIF-1α) and IL-1 [48]. Unlike other CAFs, PSCs can be reversed to a quiescent phenotype when the activating factor is stopped [32]. However, when subjected to repeated or sustained injury, PSCs may become permanently activated. Permanent or continuous activation of PSCs is usually the reason for the development of pathological fibrosis [32].

1.5.2 Phenotype

Quiescent PSCs are star-shaped cells with the ability to produce ECM proteins such as desmin, vimentin and matrix-degrading enzymes such as matrix metalloproteinases (MMPs). They also produce tissue inhibitors of metalloproteinases (TIMPs), which makes them able to maintain the balance between matrix formation and degradation. Quiescent PSCs store vitamin A-containing lipid droplets surrounding the nucleus in the cytosol. When filled with these lipids, they have a limited capacity to proliferate and migrate. Vitamin A inhibits the expression of α-SMA, collagen, fibronectin, and laminin. Therefore, the maintenance of a quiescent phenotype has been shown to be dependent on vitamin A levels [31, 49].

Upon activation, the quiescent PSCs lose their cytoplasmic lipid droplets and attain a myofibroblastic phenotype. They express high levels of α-SMA and reduce the production of desmin, vimentin and fibrillary acidic protein (GFAP). Activated PSCs secrete large amounts of ECM components such as collagen I and III, fibronectin, laminin, nestin, proteoglycans and matricellular proteins, and lose the balance between MMPs and TIMPs. In addition, the activated PSCs have an enlarged nucleus, increased secretion of cytokines, chemokines and growth factors, and enhanced migratory and proliferative potential. These characteristics contribute to the fibrosis and the hypoxic tumor microenvironment in PDAC [49, 50].

1.5.3 Markers

PSCs can be identified by immunostaining for selective markers. Markers for identifying the quiescent PSCs include GFAP, nestin, vimentin, neural cell adhesion molecule (NCAM), nerve growth factor (NGF) and synemin [31, 51]. In contrast, activated PSC can be identified by α-SMA, fibroblast activation protein-α (FAP-α) and fibroblast specific protein-1 (FSP-1) markers [51].

1.6 Cell metabolism

1.6.1 Metabolism

Metabolism is the total sum of chemical (biosynthetic) reactions taking place within each cell. This includes the breakdown of polymers such as proteins, polysaccharides and nucleic acids to obtain energy (catabolism) and the use of energy to synthesize macromolecules needed by the cell (anabolism). These chemical reactions are often coordinated in series termed metabolic pathways, in which the product of one reaction becomes the substrate of the next reaction [52].

1.6.2 Glucose metabolism

Under aerobic conditions, normal cells break down glucose into pyruvate in the cytosol through glycolysis. In the first phase of glycolysis, the "investment" phase, glucose is converted to glucose-6-phosphate (G6P) by hexokinase (HK) by using one adenosine triphosphate (ATP) molecule. This phosphorylation prevents glucose from leaving the cell. Glucose-6-phosphate isomerase (GPI) converts G6P into its isomer fructose-6-phosphate, which is further converted into fructose-1,6-bisphosphate by phosphofructokinase (PFK) using another ATP molecule. Fructose-1,6-bisphosphate is subsequently converted into dihydroxyacetone phosphate (DHAP) and glyceraldehyde 3-phosphate by fructose bisphosphate aldolase [53].

In the second phase of glycolysis, the "payoff" phase, glyceraldehyde-3-phosphate is oxidized into 1,3-bisphosphoglycerate by glyceraldehyde 3-phosphate dehydrogenase (GAPDH) with the reduction of an oxidized nicotinamide adenine dinucleotide (NAD+) molecule to reduced nicotinamide adenine dinucleotide (NADH) and H^+. Subsequently, 1,3-bisphosphoglycerate is converted into 3-phosphoglycerate by phosphoglycerate kinase (PGK1), producing the first ATP molecule from glycolysis. Phosphoglycerate mutase (PGM) then converts 3-phosphoglycerate into 2-phosphoglycerate, which in turn is converted to phosphoenolpyruvate (PEP) by enolase, with the release of one H_2O molecule. Due to the unstable state of PEP, pyruvate kinase will convert PEP to pyruvate with the release of the second ATP molecule [53].

Pyruvate travels to the mitochondria, where it is further broken down to carbon dioxide in the tricarboxylic acid cycle (TCA cycle). The TCA cycle generates reduced NADH and dihydroflavine-adenine dinucleotide ($FADH_2$) that can be used to transfer electrons in the electron transport chain (ETC). In the presence of oxygen, the ETC generates ATP through

oxidative phosphorylation (OXPHOS). ATP is an energy-carrying molecule that can be stored or used to fuel cellular processes. The breakdown of one glucose molecule gives two ATP from glycolysis, two ATP from the TCA cycle and 34 ATP from OXPHOS, gaining a total of 38 ATPs from aerobic respiration, as illustrated in Figure 1.3. Under anaerobic (hypoxic) conditions, cells are limited to use glycolysis only. The pyruvate generated by glycolysis is then reduced to lactate and secreted out of the cell [6, 52-55].

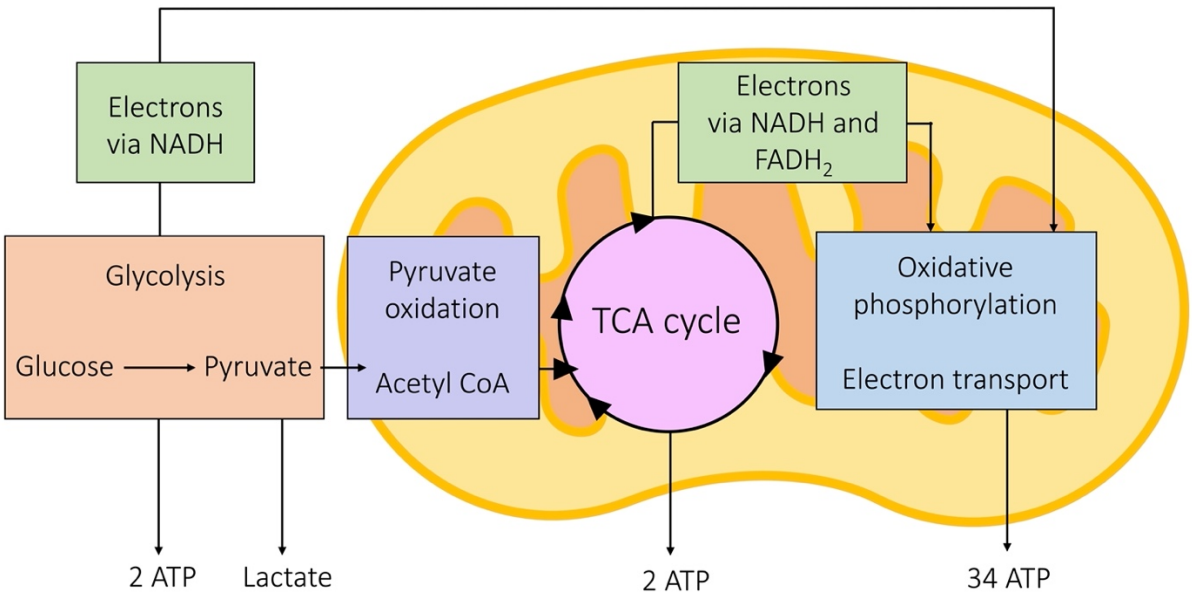

Figure 1.3. Schematic figure of cellular respiration, including glucose metabolism and energy production in the cell. Aerobic breakdown of glucose through glycolysis and the citric acid cycle, further fuels oxidative phosphorylation and produces the energy-carrying molecule ATP.

1.7 Cancer metabolism

One of the hallmarks of cancer is the reprogramming of metabolic activities in cancer cells compared to normal cells, which supports the acquisition and maintenance of malignant properties [56]. Six common changes in cancer cells compared to non-malignant cells include deregulated uptake of glucose and amino acids, increased demand for nitrogen, use of glycolysis/TCA cycle intermediates for biosynthesis and reduced nicotinamide adenine dinucleotide phosphate (NADPH) production, use of opportunistic modes of nutrient acquisition, alterations in metabolite-driven gene regulation, and metabolic interactions with the microenvironment. Few tumors display all six, but most tumors display several of them [57].

1.7.1 Warburg effect

A classic example of reprogrammed metabolism in cancer cells is the Warburg effect [56]. Otto Warburg discovered that many cancer cells largely rely on glycolysis, with the breakdown of glucose into lactate even during aerobic conditions. This makes no sense energetically as one glucose molecule only gives two ATP molecules through glycolysis, while it gives 34 ATP molecules if pyruvate is further broken down. This tendency of cancer cells to limit themselves to glycolysis even when provided with enough oxygen is called the Warburg effect. As the cancer cells metabolize glucose inefficiently, they have to compensate by importing enormous amounts of glucose. Therefore, they often express elevated levels of glucose transporters, particularly glucose transporter 1 (GLUT1), which span the plasma membrane and drive the high rates of glucose transport by these cells [6].

1.8 Pancreatic cancer metabolism

1.8.1 Overview

The major metabolic change in pancreatic cancer is altered glycolysis [58]. Oncogenic *KRAS*, which is the dominant genetic aberration in PDAC, has been shown to induce the transcription of GLUT1 and multiple glycolysis enzymes such as HK1 and -2, PFK-1, and lactate dehydrogenase (LDH) [58]. The phosphoinositide 3-kinase (PI3K) pathway is also known to regulate multiple steps in glucose metabolism. PI3K can activate Rac that remodels the actin cytoskeleton to actin-bound aldolase A, which catalyzes one of the steps in glycolysis [59]. Glycolysis activation is also promoted by the hypoxic environment in PDAC [59].

Several critical metabolic pathways depart from glycolysis, such as the TCA cycle, and anabolic pathways including pentose phosphate pathway (PPP), hexosamine biosynthesis pathway (HBP) and serine biosynthesis. The increased glycolysis found in PDAC cells also leads to increased flux of glycolysis intermediates through these pathways. Increased activity in these pathways promotes PDAC progression by providing energy (glycolysis and TCA cycle), new biomass support (PPP and serine biosynthesis), ROS maintenance (glutamine metabolism and TCA cycle), signal modulation (HBP) and DNA methylation (serine biosynthesis) [34, 58]. Increased flux through the non-oxidative arm of PPP also leads to an increase in pyrimidine nucleotide synthesis. This in turn, leads to accumulation of dCTP, which causes competitive inhibition of gemcitabine activity, thereby promoting gemcitabine resistance [60].

PDAC metabolism is also shown to be largely glutamine-dependent [61-63]. The enzyme for glutamine biosynthesis, glutamate ammonia ligase (GLUL), is overexpressed in PDAC [34]. Glutamine acts as a major carbon source and supports the synthesis of large amounts of metabolites, which is essential for highly proliferating cells such as pancreatic cancer cells (PCCs). PCCs also rely on the use of glutamine together with cytosolic malic enzyme (ME1) to generate NADPH for tumor growth and to maintain their ROS homeostasis [34].

1.8.2 Metabolic interactions between PSCs and cancer cells

The metabolic interactions between PSCs and cancer cells, illustrated in Figure 1.4, are considered a consequence of genetic mutations combined with a comprehensive paracrine signaling network [31]. Activated PSCs have been shown to act as an alternative energy source and to promote proliferation, invasiveness, metastasis, and chemoresistance in PCCs [31].

Some of the metabolic interactions between PSCs and PCCs are mediated by KRAS-dependent pathways [64, 65]. *KRAS* regulates sonic hedgehog secretion from PCCs, which causes activation of PSCs and induces secretion of various cytokines such as insulin-like growth factor-1 (IGF-1), growth arrest-specific 6 (GAS6), and granulocyte-macrophage colony-stimulating factor (GM-CSF). PSC-secreted IGF-1 activates the receptor tyrosine kinases insulin-like growth factor 1 receptor (IGF1R) and AXL, which leads to further activation of downstream PI3K-Akt phosphorylation in PCCs. This phosphorylation results in increased mitochondrial respiratory capacity in PCCs and subsequently elevated oxygen availability under hypoxia [66-69].

PSCs promote PCC progression by secretion of alanine and other non-essential amino acids (NEAAs), exosomes, lipids and growth factors [31]. The NEAAs, such as alanine, lead to metabolic reprogramming in PCCs. Autophagy-induced alanine serves as an alternative carbon source and is outcompeting glucose and glutamine in the TCA cycle to produce NEAAS and lipids. Moreover, the growth factors and exosomes secreted by PSCs play an important role in the metabolic balance of PCCs. Oncogenic Ras also contributes to the upregulation of macropinocytosis in PCCs, enabling them to take up more of the extracellular proteins secreted from PSCs to support their growth [31, 70, 71].

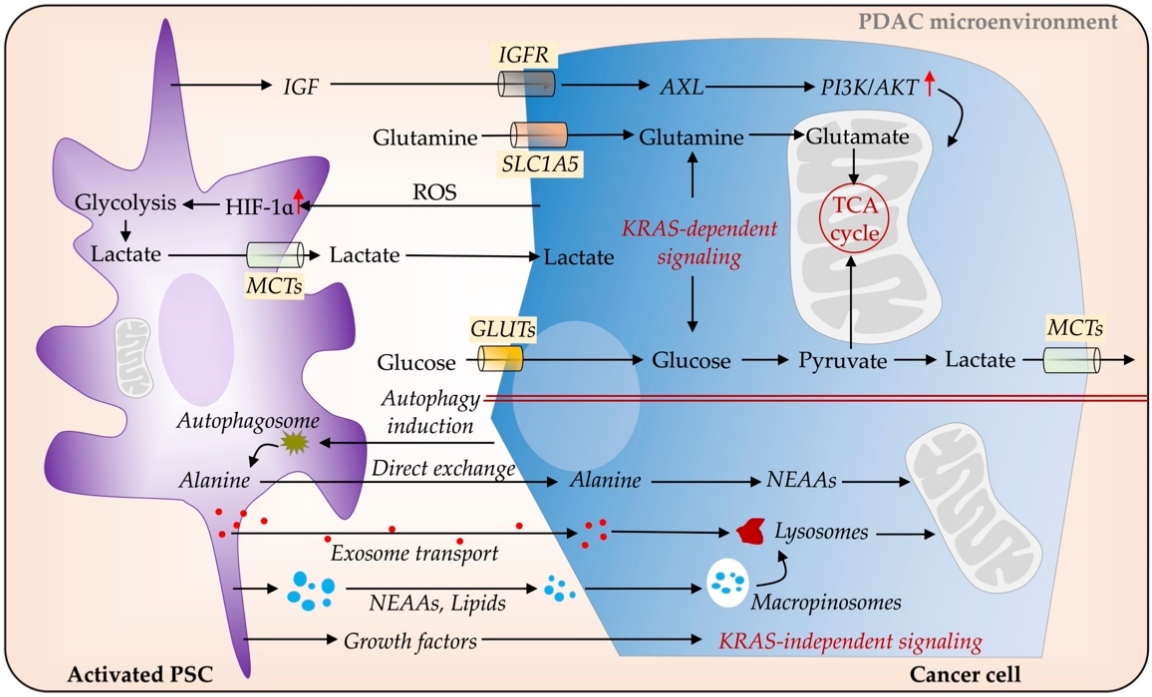

Figure 1.4. Interactions between pancreatic cancer cells (PCCs) and pancreatic stellate cells (PSCs). Activated PSCs facilitate metabolic reprogramming, act as an alternative energy source and promote proliferation, invasiveness, metastasis and chemoresistance in PCCs. PCCs secrete reactive oxygen species (ROS), which induce glycolysis in PSCs. Several cytokines and signaling pathways mediate the metabolic interactions between PSCs and PCCs via KRAS-dependent pathways. Figure adapted from reference [31].

1.8.3 Reverse Warburg effect

In 2009, the reverse Warburg effect was proposed [72]. The reverse Warburg effect suggests that cancer cells secrete reactive oxygen species (ROS) in the TME. This induces oxidative stress and stabilizes the HIF-1α in the surrounding PSCs, which triggers aerobic glycolysis [31, 73]. As a result of aerobic glycolysis, PSCs secrete energy metabolites such as lactate and pyruvate. The cancer cells use these energy metabolites in the TCA cycle, leading to an increase in OXPHOS generation of ATP. In this way, cancer cells that limit themselves to glycolysis (Warburg effect), get more energy by taking up energy metabolites from surrounding PSCs and by metabolizing them through the TCA cycle and OXPHOS. (Reverse Warburg effect) [31, 55, 72, 74].

1.9 Chemosensitivity

1.9.1 Gemcitabine

Gemcitabine, also known as 2′,2′-difluoro deoxycytidine (dFdC), is a nucleoside analog of deoxycytidine. Since 1997, when Burris et al. showed that gemcitabine was superior to fluorouracil (5-FU) with respect to overall survival, performance status and pain control, gemcitabine has become a standard treatment choice for PDAC [75, 76]. Although PCCs are more susceptible to gemcitabine than other anticancer agents, most patients develop chemoresistance within weeks of treatment initiation [76].

Gemcitabine is taken up and transported intracellularly mainly by human equilibrative nucleoside transporter 1 (hENT1) and human concentrative nucleoside transporter (hCNT) 1 and 3 [77]. Once inside the cell, most of it is inactivated by cytidine deaminase (CDA) and secreted into the extracellular space. The remaining gemcitabine is phosphorylated, mainly by deoxycytidine kinase (DCK), to dFdC monophosphate (dFdCMP), dFdC diphosphate (dFdCDP) and dFdC triphosphate (dFdCTP). dFdCTP competes with the substrate for DNA synthesis and induces cell death by apoptosis [76].

DCK and the nucleoside transporters hENT1, hCNT1 and hCNT3 lead to increased chemoresistance to gemcitabine when downregulated. In contrast, CDA, ribonucleotide reductase catalyzing the generation of dCTP, and thymidylate synthase catalyzing the generation of 2′-deoxythymidine-5′-monophosphate (dTMP), which is essential for DNA synthesis, lead to increased chemoresistance when upregulated [31, 76, 78-84]. Upregulated glycolysis in PCCs has also been demonstrated to promote chemoresistance as it feeds the non-oxidative arm of PPP, which leads to an increase in dCTP generation [60].

1.9.2 PSC-promoted chemoresistance

PSCs promotes chemoresistance to gemcitabine through multiple mechanisms, as illustrated in Figure 1.5. PSCs are intrinsically resistant to the cytotoxic actions of gemcitabine, partly due to the low expression of hENT1 and DCK [85]. Gemcitabine uptake by PSCs and intracellular entrapment of dFdCTP, reduces the availability of gemcitabine to PCCs. PSCs are also a source of cysteine-rich angiogenic inducer 61 (CYR61), which downregulates the nucleoside transporters hENT1 and hCNT3 [86]. Moreover, PSCs secrete deoxycytidine, which competes with gemcitabine processing by DCK in PCCs [87].

Several studies have revealed that PSCs also secretes several factors that promote chemoresistance in PCCs. These include nitric oxide, the ECM proteins fibronectin and collagen-1, and the growth factors IGF-1 and -2, IL-1β, IL-6 and hepatocyte growth factor (HGF) [31, 67, 88-95]. Moreover, extracellular vesicles (exosomes) secreted by PSCs have been shown to promote chemoresistance in PCCs. Richards et al. reported that PSCs exposed to gemcitabine increased their exosome release, which subsequently increased the expression of the transcription factor Snail, which is a known chemoresistance-inducing factor [96]. While Fang et al. revealed that PSC-derived exosome miRNA (miR-106b) also contributes to gemcitabine resistance in PDAC [97].

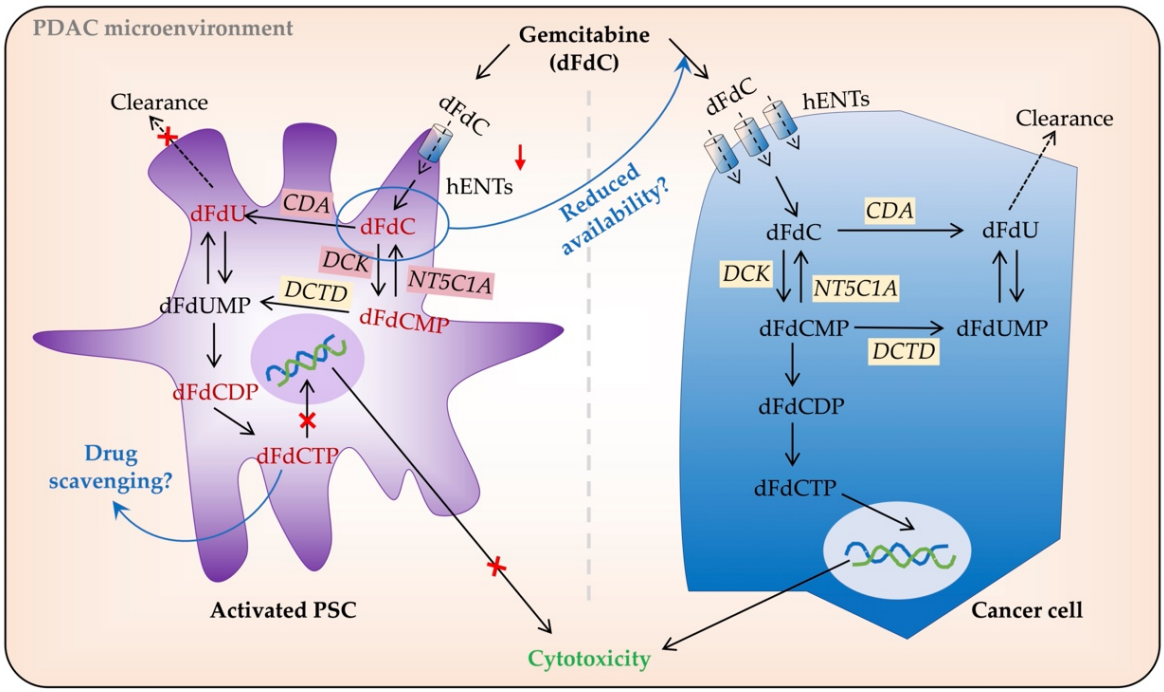

Figure 1.5. Gemcitabine (dFdC) processing in pancreatic cancer cells and pancreatic stellate cells. Most of the dFdC entering PCCs is inactivated by cytidine deaminase (CDA) and cleared into the extracellular space. The remaining dFdC is phosphorylated to its active form dFdCTP, which competes with DNA synthesis substrates and induces cell death by apoptosis. PSCs are resistant to the cytotoxic actions of gemcitabine. Gemcitabine uptake by PSCs and intracellular entrapment of dFdCTP reduce the availability of gemcitabine to PCCs. Figure adapted from reference [31].

As described above, increasing evidence suggests that PSCs play a pivotal role in the regulation of gemcitabine chemoresistance in PDAC. In addition, the PSCs also contribute to the reprogrammed metabolism in PDAC and act as a major energy source for cancer cells to fulfill their high energy demands in the challenging PDAC microenvironment. The predominance of

glycolysis is a major metabolic alteration in PDAC. Thus, it is of utmost importance to understand whether and how PSCs contribute to the glycolysis regulation, in addition to promoting chemoresistance in PDAC. Moreover, investigations into PSC-induced metabolic alteration in PDAC and its impact on chemosensitivity in PDAC have the potential to provide novel and better treatment strategies.

2 Aim of the study

PDAC has a poor prognosis with a 5-year survival rate of less than 8%. Surgical resection combined with adjuvant chemotherapy is usually the preferred treatment option for PDAC. Although chemotherapeutic agents such as gemcitabine can improve the prognosis of PDAC, the development of chemoresistance drastically reduces this potential benefit. PSCs, which constitute the main stromal cell population, contribute to an altered metabolism that supports tumor growth and chemoresistance in PDAC. Investigation that focuses on PSC-induced metabolic alterations and chemoresistance has the potential to enable the development of novel and better treatment strategies. Altered glycolysis is a key metabolic change observed in PDAC. However, the contribution of the PSCs to this process is not clearly understood. The aim of this study is to investigate the PSC-induced changes in glucose metabolism and chemosensitivity in human PCCs.

3 Materials and methods

3.1 Aseptic conditions

To avoid contamination by microorganisms such as bacteria, fungi or viruses, the cell culture work was always performed under aseptic conditions. All work with cell cultures was performed inside a laminar flow hood to prevent contamination from airborne particles and aerosols. The hood workbench and all equipment used inside the hood were sprayed with 70% ethanol before and after use. 70% ethanol kills bacteria, fungi and many viruses by denaturing their proteins and dissolving their lipids. The hood was also cleaned regularly. Moreover, gloves sprayed with 70% ethanol, were always used during experiments to protect the cell cultures from human contamination. Lastly, all reagents that were not provided sterile were either autoclaved or sterilized using a 0.22 µm syringe filter, depending on the amount of reagent.

3.2 Cells

3.2.1. Pancreatic cancer cell lines

Three commercially available and commonly used pancreatic cancer cell (PCC) lines, namely Capan-2 (#HTB-80™), HPAF-II (#CRL-1997™) and Mia PaCa-2 (#CRL-1420™) obtained from American Type Culture Collection (ATCC) (Manassas, VA, USA), were used in this study. Aliquots of the cells were stored in a liquid nitrogen vapor container until further use. Table 1 provides information on cell line characteristics, including key data on the patients from whose cancers these cells were originally derived [98, 99]. Additional information about these cell lines can be found at ATCC.

Table 1: Overview of cell lines. Donor information and characteristics [98].

Cell Line	Age	Gender	Derivation	Metastasis	Proliferation	Differentiation
Capan-2	56	Male	Primary tumor	No	96 hrs	Well
HPAF-II	44	Male	Ascites	Yes	41 hrs	Moderate
MIA-PaCa-2	65	Male	Primary tumor	-	40 hrs	Poor

3.2.2. Pancreatic stellate cell cultures

Human PDAC-derived primary PSC cultures, named PSC-1 and PSC-2, were obtained from two individual tumor biopsies (3.5 mm^2) from two different patients. The PSC cultures were isolated and propagated by the outgrowth method, developed by Bachem et al. [47, 100]. The PSC-1 cells were isolated from the tumor of a treatment-naive patient, whereas PSC-2 cells were isolated from the tumor of a patient, who was treated neoadjuvantly with 4-cycles of FOLFIRINOX before surgery.

Human Pancreatic Stellate Cells (HPaSteC), purchased from ScienCell Research Laboratories (San Diego, CA, USA), were isolated from the human pancreas of a 22-week-old, fetal, non-diseased, male donor, followed by purification and cryopreservation [100]. The HPaSteC cells are delivered frozen at passage one. Each cryovial contains 1 ml with a cell concentration of $>5.0 \times 10^5$. Cells are, upon delivery, directly transferred and stored into a liquid N_2 vapor container until further use. HPaSteC cells were cultured and maintained by other laboratory colleagues according to the supplier's protocol [100]. All three PSC cultures were used to obtain conditional medium (CM) as described in section 3.3.4.

3.3 Cell culture medium

3.3.1. Complete growth medium

The complete growth medium used during cell culture contains nutrients, growth factors, hormones and antibiotics. The growth medium was made of Dulbecco's modified Eagle's medium (DMEM) GlutaMAX™ 4.5 g/l glucose (#31966021) with the addition of sterile filtered amphotericin B (#15290026), penicillin-streptomycin (#15140122) and fetal bovine serum (FBS) (#16000044), all purchased from Thermo Fisher Scientific (Waltham, MA, USA). FBS is added to DMEM as a supplement for cell growth, while antibiotics are added to avoid infection. To prepare the complete growth medium, 50 ml FBS (10%), 5 ml amphotericin B (1%) and 5 ml (1%) penicillin-streptomycin were first pre-warmed in a water bath (37℃). Subsequently, FBS and the antibiotics were added to the DMEM bottle, which was shaken gently to mix.

3.3.2. Serum-free medium (SFM)

Depending on the experimental settings, either DMEM without the addition of FBS or antibiotics (i.e., plain DMEM), or low glucose DMEM (Sigma-Aldrich (Saint-Louis, MO, USA), #D6046) with the addition of 0.1% FBS, 1% amphotericin B and 1% penicillin-streptomycin, was used for serum-free conditions.

3.3.3. Freezing medium

Freezing medium was used to cryopreserve cells in liquid N_2 vapor containers for long-term storage. To obtain a freezing medium, 10% dimethyl sulfoxide (DMSO) (Sigma-Aldrich, #D5879) and 10% FBS were added to complete growth medium. DMSO acts as a cryoprotective agent by reducing the freezing point and preventing the formation of ice crystals, while FBS reduces oxidative stress.

3.3.4. Pancreatic stellate cell conditioned medium (PSC-CM)

PSCs were cultured in 100-mm petri-dishes (Fisher Scientific, #10212951) using complete growth medium. The complete growth medium was removed from the plate when the cells were sub-confluent. The plate was washed four times with PBS (Sigma-Aldrich, #P4417), following which 15 ml plain DMEM was added to the plate. The plate was incubated at 37°C for 48 hours. The medium was collected in a 15 ml tube and centrifuged at 5000 revolutions per minute (rpm) for five minutes. The supernatant containing proteins secreted by the PSCs was poured into a new 15 ml tube, and the pellet was discarded. This supernatant was referred to as the PSC-CM. PSC-CMs were stored at -20°C until further use.

3.4 Cell culturing process

3.4.1. Thawing

Prior to picking up from the liquid N_2 vapor tank the vials containing the cells, complete growth medium was warmed in a water bath to 37°C. Then the vials with the cells were warmed in a 37°C water bath until the sides of the vials thawed, but the center remained frozen. Approximately 10 ml complete growth medium was added to a 100-mm tissue culture plate and the cells were poured in. The plate was swirled gently and placed in a 37°C incubator overnight. The following day, the cells were observed under the light microscope for cell adherence, and the medium was changed to a fresh complete growth medium to get rid of

DMSO (from freezing medium) and dead/non-adherent cells. All cell lines used in this study were adherent cells.

3.4.2. Trypsinization

Trypsinization was used to detach the adherent cells from the plate before seeding them for experiments or further passaging. Firstly, the complete growth medium was removed from the plate. Thereafter, the plates were washed twice by adding 1 ml PBS to the side of the plate followed by gentle swirling of the plate. This washing step is important to remove any residual FBS from the complete growth medium, as it contains protease inhibitors that inhibit trypsin activity. Approximately 500 µl trypsin (Thermo Fisher Scientific, #BE17-161E) were added directly to the cells, and the plate was swirled and incubated for 3-5 minutes at 37°C. The trypsin protease cleaves the amino acids lysine and arginine at their c-terminal end, thereby breaking down the adhesion proteins that anchor the cells to the plate surface. The trypsin solution also contains ethylene diamine tetraacetic acid (EDTA), which acts as a metal chelator, removing calcium ions from the cell surface, enhancing the trypsin activity and contributing to the removal of cell-cell adhesions.

The cells were examined in a microscope to see if they were detached. When most of the cells were detached, 3 ml complete growth medium was added to stop the trypsinization process. The cell mixture was transferred to a 15 ml centrifuge tube and centrifuged at 1000 rpm for three minutes. The supernatant was discarded, and the cells were resuspended in sufficient complete growth medium or freezing medium depending on the next activity.

3.4.3. Counting

Cells were counted using Invitrogen Countess II automated cell counters. Equal volumes of cell mixture and trypan blue (Sigma-Aldrich, #T8154) were mixed, and 10 µl of this mixture were loaded onto a disposable Countess cell counting chamber slide (Thermo Fisher Scientific, #C10283). Trypan blue was used to stain dead cells as the stain can only pass through the porous cell membranes of dead cells. The slide was inserted into the machine, and the number of cells per ml was counted.

3.4.4. Passaging and seeding

For appropriate growth of cells, all cell lines were maintained in an incubator with 37°C and 5% CO_2. The growth medium was changed every 3-4 days. Cells were examined in a light microscope to inspect growth. When cells were approximately 80% confluent, they were split. During cell splitting, the cells were trypsinized (see section 3.4.2 for further details) and either seeded to a new plate with 10 ml complete growth medium for further passaging or counted and seeded for experiments in one of the different culture plates listed in Table 2.

Table 2. Overview of the different culture plates used and the cell seeding density.

Plate	Size	Plating volume	Seeding density	Cells at confluency
96 - well plate	0.3 cm^2	100 µl	0.01 x 10^6	0.05 x 10^6
6 - well plate	10 cm^2	2 ml	0.3 x 10^6	1.2 x 10^6
100 mm dish	60 cm^2	15 ml	5 x 10^6	20 x 10^6

3.4.5. Cryopreservation

Cryopreservation is a useful method for long-term storage of cells that maintains the cell viability. This is very useful when doing several experiments on the same cell line, as it minimizes mutations and genetic changes so that the cells retain the same characteristics regardless of when you want to use them. For cryopreservation, cells were trypsinized (see section 3.4.2 for further details) and resuspended in freezing medium. The resuspended cell mixture was aliquoted into cryovials (1 ml per vial) and frozen overnight at -80°C. Thereafter, these vials were transferred to a liquid N_2 tank (-196°C) for indefinite storage.

3.5 Experiments

3.5.1 Interactions between cancer cells and stellate cells.

For morphology, viability, proliferation, glucose metabolism and chemosensitivity experiments, a common experimental setup was used to investigate the impact of PSC-CM on PCCs. Approximately 5 000-10 000 cells/well were seeded in 100 µl/well DMEM in a 96-well plate and incubated overnight at 37°C. The following day, the plates were washed twice with PBS. The cells were incubated with 100 µl low-glucose DMEM (LGM) for two hours at 37°C to acclimatize the cells to a starving state. The cells were then again washed twice with PBS and 100 µl fresh medium, either SFM (plain DMEM or LGM) or one of the following PSC-

CMs: PSC-1, PSC-2 or HPaSteC were added. The cells were incubated with these media for 24, 48 or 72 hours at 37°C.

3.5.2 Hematoxylin & eosin staining

Hematoxylin & eosin (H&E) staining is a staining technique commonly used to recognize different types of cells, tissues and their morphological changes. Hematoxylin stains the nucleus with a dark blue color, while eosin stains the amino acids in the cytoplasm with a pink color.

For H&E staining, the cell culture medium was carefully removed, and cells were washed once with PBS to get rid of any remnants of the culture medium. To achieve fixation, the cells were incubated with 100 µl/well of 4% formaldehyde solution (ChemCruz™, #sc-281692) at 4°C for 15 minutes. Following fixation, the cells were washed three times with a wash buffer containing 0.1% Triton x-100 (Sigma-Aldrich, #T-9284) in 1X PBS, each wash for 3-5 minutes. Thereafter, cells were incubated with 100 µl/well hematoxylin solution (Abcam, Cambridge, Great Britain; #ab220365) for five minutes at room temperature to stain the nucleus. Hematoxylin was removed carefully, and the cells were washed three times with tap water, each wash for 3-5 minutes. Thereafter, cells were incubated with an acidified solution containing 0.1% acetic acid in distilled water for 1-2 seconds and then washed one time with tap water (100 µl/well). After acidification, cells were incubated with 100 µl/well eosin solution (Abcam, #ab246824) for <1 minute to obtain a cytoplasmic stain. Following cytoplasmic staining, cells were washed three times with tap water, each wash for 3-5 minutes and one time with distilled water (100 µl/well). Lastly, 100 µl distilled water was added to each well. The plates were stored at 4°C until further use (maximum one week).

3.5.3 Morphology assessment

The H&E-stained cells were examined and pictures were captured using a light microscope (Zeiss) using a 10X ocular lens and a 40X objective lens. The cells were counted manually, and ImageJ was used to measure the percentage of area covered by the cells.

3.5.4 MTT cell viability assay

Thiazolyl blue tetrazolium bromide (MTT) is a water-soluble yellow tetrazolium salt that in actively respiring cells is converted by the mitochondria into insoluble purple formazan

crystals. The MTT assay is based on measuring the concentration of formazan to indicate the number of viable cells [101].

A mixture of plain DMEM and MTT (Sigma-Aldrich, #M2128) labeling reagent, 5 µl MTT per 100 µl (ratio 1:20), was prepared. The culture medium was replaced with 100 µl of the MTT/DMEM mix per well, and the plate was incubated for four hours at 37 °C. One set of wells with MTT but no cells were included as a negative control. Violet colored formazan crystals were observed under the light microscope. The MTT/DMEM mix was then carefully removed and 100 µl DMSO was added to solubilize the purple formazan crystals. Finally, the absorbance was read at 570 nm by using a spectrophotometer. A flowchart describing the MTT cell viability assay is illustrated in Figure 3.1.

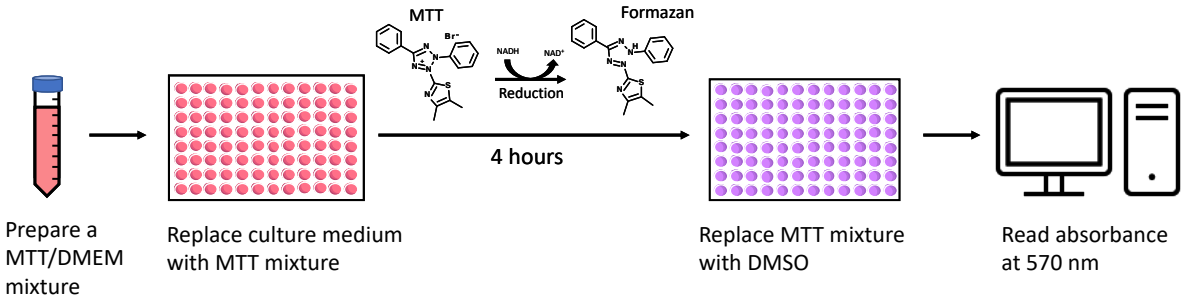

Figure 3.1. MTT assay flowchart. Culture medium is replaced by a mixture of MTT and plain DMEM (ratio 1:20). After four hours, the MTT mixture is replaced by DMSO, and the absorbance is read at 570 nm using a spectrophotometer. Compound models are illustrated using PubChem Sketcher V2.4.

3.5.5 BrdU cell proliferation assay

Bromodeoxyuridine (BrdU) is a pyrimidine analog which is incorporated instead of thymidine into newly synthesized DNA of proliferating cells. The BrdU cell proliferation assay is based on detecting the amount of BrdU that is incorporated during cell proliferation, using a BrdU mouse antibody. An anti-mouse antibody linked with horseradish peroxidase (HRP) is then used to recognize the bound detection antibody. HRP substrate 3,3′,5,5′-tetramethylbenzidine (TMB) is used to develop a color that can be read by a spectrophotometer.

The “BrdU Cell Proliferation ELISA Kit (colorimetric)” (Abcam, #ab126556) was used. All reagents used were prepared according to the manual for this kit. Approximately 20 000 cells/well were seeded in 100 µl/well complete growth medium in a 96-well plate. The plate

was incubated overnight at 37°C followed by incubations with SFM or PSC-CM for 24 and 72 hours as described in section 3.5.1. After incubation, the medium was removed and replaced with 100 µl of BrdU diluted in DMEM in each well, followed by an overnight incubation. The following day, cells were incubated with 200 µl fixing solution at room temperature for 30 minutes. Following fixation, the plates were washed three times with 100 µl 1X wash buffer. Thereafter, 100 µl/well anti-BrdU monoclonal detector antibody was added, and the plates were incubated for one hour at room temperature.

The wells were then washed three times with 1X wash buffer. After washing, the cells were incubated with 100 µl/well 1X peroxidase goat anti-mouse IgG conjugate for 30 minutes at room temperature, followed by three washes with 1X wash buffer. A final water wash was performed by flooding the entire plate with distilled water. The plate was gently hit against absorbent paper towels to dry. Then followed a final incubation with 100 µl/well TMB peroxidase substrate for 30 minutes at room temperature in the dark. Positive wells are labeled with a blue color, the intensity of which is proportional to the amount of BrdU incorporated in the proliferating cells. The reaction was stopped by adding 100 µl of stop solution to each well. A color change from blue to bright yellow can be seen in positive wells. The plate was read at 450 nm by using a spectrophotometer.

3.5.6 Glucose transport assay

[^{3}H]-2-deoxy-D-glucose ([^{3}H]2-DG) is transported into the cells with the same transporters as glucose but contains a hydroxyl group which prevents it from further breakdown in the glycolysis. Inside the cells, [^{3}H]2-DG is phosphorylated, which prevents it from leaving the cell. The ionizing radiation from [^{3}H]2-DG encounters crystals in the scintillation solution, which emits light. The number of photons in the emitted light is directly proportional to the number of ionizing particles (radioactivity), in this case, radiolabeled glucose. This signal is read by the liquid scintillation analyzer (PACKARD, TRI-CARB 2300TR).

The plate was washed twice with PBS before adding 100 µl Krebs Ringer HEPES (KRH) buffer containing 50 mM HEPES (Sigma-Aldrich, #H3375), 137 mM NaCl (Sigma-Aldrich, #31434-M), 4.7 mM KCl (Sigma-Aldrich, #P9541), 1.85 mM $CaCl_2$ (Sigma-Aldrich, #223506), 1.3 mM $MgSO_4$ (Sigma-Aldrich, #105886), 0.1% bovine serum albumin (BSA) (Sigma-Aldrich, #A4503) adjusted to pH: 7.4 with NaOH. Then 10 µl of start solution, containing [^{3}H]2-DG

(Perkin Elmer (Waltham, MA, USA), #NET238C001MC), 2-deoxy-DG (Sigma-Aldrich, #D8375-1G) and PBS, was added to each well. The plate was incubated for 24 hours at 37°C. The next day, cells were incubated with a stop solution consisting of phloretin (Sigma-Aldrich, #P7912), methanol (Sigma-Aldrich, #34860), and PBS for 10 minutes to stop the glucose transport. Phloretin stops glucose transport by inhibiting the glucose transporters. The plate was thereafter washed three times with ice-cold PBS. The plate was either frozen down, or cells were lysed by incubation with 100 µl 0.2 M NaOH for 10 minutes. 50 µl each of these cell lysates was transferred to a scintillation tube along with 4 ml Opti-Fluor (Perkin Elmer, #6013199). A scintillation analyzer was used to measure the amount of radioactive glucose from the cell lysates. The amount of [^{3}H]2-DG taken up by the cells is directly proportional to the radioactivity.

3.5.7 Glycolysis assay (Lactate secretion)

This assay is based on the principle of anaerobic glycolysis which produces lactate that is secreted by the cells. Lactate dehydrogenase (LDH) is an enzyme that functions by converting lactate and NAD+ to pyruvate and NADH in the medium. NADH is reducing a tetrazolium salt in the reaction solution to a colored formazan which absorbs light between 490 nm and 520 nm. The amount of formazan present is directly proportional to the amount of lactate in the medium, which makes it an indirect measure of glycolysis activity.

To measure glycolysis or lactate content in the medium, a “Glycolysis Cell-Based Assay” kit (Cayman Chemical Ann Arbor, MI, USA, #600450) was used according to the manufacturer's instructions. Briefly, a standard dilution range from 0 to 10 mM was prepared by mixing the L-lactate stock (10 mM) with a diluent (culture medium), as shown in Table 3. The supernatant from PSC-CM treated PCCs and duplicates of the standards and blanks were added to a 96-well plate together with an assay buffer. Then a reaction solution containing enzyme, substrate and cofactor was added to each well. The plate was incubated for 30 minutes on a see-saw rocker before reading absorbance at 490 nm using a spectrophotometer.

Table 3. Dilution scheme for standard dilution range of L-Lactate.

Vial	Volume of diluent (µl)	Volume and source of L-Lactate (µl)	Final L-Lactate concentration
A	0	300 of stock	10 mM
B	100	100 of vial A	5 mM
C	100	100 of vial B	2.5 mM
D	100	100 of vial C	1.25 mM
E	100	100 of vial D	625 µM
F	100	100 of vial E	313 µM
G	100	100 of vial F	156 µM
H	200	0	0 µM

3.5.8 Measurement of protein concentration

Bradford protein assay was used to measure protein concentrations to account for differences in cell numbers. The Bradford reagent contains a Coomassie dye which in an acidic environment is converted from a red color (absorbance maximum 465 nm) observed when no proteins are bound, to a blue color (absorbance maximum 610 nm) when proteins are bound. The intensity of the blue color is directly proportional to the protein concentration.

A standard dilution range with known concentrations was prepared by mixing BSA stock (2000 µg/ml) with a diluent (PBS) as shown in Table 4. 10 µl of the standards (31.25, 62.5, 125, 250, 500, 1000 and 2000 µg/ml) and a blank were added in duplicates to the two first columns of a 96-well plate. 5 µl or 10 µl of the samples, depending on the content, were added to the remaining wells. 200 µl Bradford reagent (Sigma-Aldrich) was added to each well containing either standard or sample. Finally, the protein concentration was read on a spectrophotometer at 595 nm, which is where the differences between both dyes are greatest.

Table 4. Dilution scheme for standard dilution range of BSA.

Vial	Volume of diluent (µl)	Volume and source of BSA (µl)	Final BSA concentration (µg/ml)
A	0	1000 of stock	2000
B	325	325 of vial A	1000
C	325	325 of vial B	500
D	325	325 of vial C	250
E	325	325 of vial D	125
F	325	325 of vial E	62.5
G	325	325 of vial F	31.25
H	650	0	0

3.5.9 NV-5440 dose-response curve

As glycolysis is the primary pathway for energy production in PDAC, the inhibition of glycolytic enzymes has been suggested as therapeutic targets [58, 102]. NV-5440 is a recently discovered GLUT inhibitor with GLUT1, a commonly overexpressed glucose transporter in PDAC, as its main target [103-105]. To determine the optimal concentration of NV-5440 for blocking glucose transport in Mia PaCa-2 cells, a dose-response curve was used. Approximately 10 000 cells per well were seeded in 100 µl/well complete growth medium in a 96-well plate and incubated overnight. The following day, the medium was replaced with plain DMEM containing various concentrations of NV-5440 (from 0.01 µM to 10 µM) or 0.1% DMSO as control. The cells were incubated for four hours at 37°C. Then the glucose transport was determined using [^{3}H]2-DG (see section 3.5.6 for further details).

3.5.10 Gemcitabine chemosensitivity assessment

MTT assay was used to investigate the impact of different PSC-CMs on the chemosensitivity of PCCs. For this purpose, the PDAC cell lines Capan-2, HPAF-II and Mia PaCa-2 were exposed for 72 hours to PSC-CM from PSC-1, PSC-2 and HPaSteC. Thereafter, the cells were incubated with 10 µM gemcitabine (Sigma-Aldrich, #G6423) or without gemcitabine (control) for 48 hours, before cell viability was measured using a MTT assay (see section 3.5.4 for further details)

3.5.11 Preparation of protein lysates

Protein lysates were prepared for use in western blot analysis. This procedure was performed when the plate was almost fully confluent (minimum 70%). The wells were washed with PBS three times with subsequent addition of 150 µl lysis buffer (Laemmli buffer containing 4% SDS, 20% glycerol, and 120 mM Tris-HCl pH 6.8) to each well. Bromophenol blue (BPB) (Sigma-Aldrich, #B0126) (5% of total lysis buffer) was added to 1.5 ml tubes. BPB is used as a tracking dye by binding to the proteins in the sample. The plate was swirled lightly, and the formation of a viscous substance was observed. The plate was rested for five minutes, and then the wells were scraped completely, and the viscous substance was collected in a corresponding 1.5 ml tube. Two replicates were collected in the same tube. 2-mercaptoethanol (Sigma-Aldrich, #M3148) (10% of the total volume of lysis buffer) was added (inside a fume hood) to each 1.5 ml tube. 2-mercaptoethanol is used to cleave disulfide bonds, ensuring that the protein subunits become separated. The tubes were heated for five minutes at 95°C on a heating block.

During heating, the pressure from the tube was expelled by opening the lid of the tube halfway into the incubation time. Tubes were stored at -20°C until needed.

3.5.12 Western blot

Sodium dodecyl sulfate–polyacrylamide gel electrophoresis (SDS-PAGE) with 10% polyacrylamide gels was used to separate aliquots of protein from the protein lysates. A semi-dry transfer system (Bio-Rad) was used to transfer the proteins to nitro-cellulose membranes. The nitro-cellulose membranes were then blocked in Tris-buffered saline containing 0.1% Tween 20 (TBST) with 5% non-fat dry milk solution and incubated with the primary antibodies as indicated (in TBST with 5% non-fat dry milk or BSA) overnight at 4°C. The blots were then washed three times in TBST and incubated with HRP-conjugated secondary antibodies at room temperature for one hour. LumiGLO® (KPL, Gaithersburg, MD, USA) was used to visualize the blots, and the densitometric analysis of the immunoblots was performed using Labworks Software (UVP, Cambridge, UK).

3.5.13 Secretome analysis

The secretome is the set of proteins that are secreted into the extracellular space. Liquid chromatography with tandem mass spectrometry (LC-MS/MS) is one of the techniques used for secretome measurements. The analysis of the secretome is known as secretomics, which is one type of proteomics. Secretory proteins play important roles in the crosstalk between cells, and secretomics is therefore a useful technique to understand the molecular basis of pathogenesis. A flowchart describing the secretome analysis is illustrated in Figure 3.2.

The PSC-CM samples from PSC-1, PSC-2 and HPaSteC (5 ml in triplicate for each culture) were subjected to the proteomics-based secretome analysis as described previously [100]. The PSC-CM samples (collected as described in section 3.3.4) were concentrated down to 5% of the original volume (5 ml was reduced to 450 µl) using 10 kDa cut off Amicon Ultra centrifugal filter devices. Peptides are easier to fractionate by LC and ionize and fragment more efficiently than whole proteins, resulting in a spectrum that is easier to interpret for protein identification. The proteins were therefore alkylated, reduced and in-solution digested with trypsin (Promega) overnight at 37°C. Alkylation modifies cysteine SH-groups, to prevent them from forming unwanted novel disulfide bonds [106]. Trypsin cleaves lysine and arginine residues in the proteins yielding peptides of more appropriate molecular weights for mass spectrometry. The

peptides were further concentrated, followed by de-salting, to remove salts which can decrease the signal-to-noise ratio in MS [107]. The samples were then subjected to MS at the Proteomics Core Facility (University of Oslo, Norway). MS was performed using the STAGE-TIP method with a C18 resin disk (3M Empore). Each peptide mixture was analyzed by nEASY-LC coupled to QExactive Plus (ThermoElectron, Bremen, Germany) with EASY Spray PepMap®RSLC column (C18, 2 µm, 100Å, 75 µm x 50 cm).

Proteome Discoverer 2.1 (Thermo Fisher Scientific) and Mascot 2.6 (Matrix Science, London, UK) were used on the MS raw files for protein identification. For the Mascot searches, the following criteria were used: trypsin digestion with two missed cleavages allowed, carbamidomethyl (C) as fixed modification and Acetyl (N-term), Gln->pyro-Glu (N-term Q), Oxidation (M) as dynamic modifications. The parent mass tolerance was set to 10 ppm and MS/MS tolerance 0.1 Da. For the database searches, the Swiss-Prot database for human entries supplemented with known contaminants provided by MaxQuant was used. All of the reported protein identifications were statistically significant ($p<0.05$) in Mascot and filtered in Proteome Discoverer for at least medium confidence identifications. The list of identified proteins was subjected to the Kyoto Encyclopedia of Genes and Genomes (KEGG) database for pathway analysis, and Gene Ontology (GO) analysis was conducted using the DAVID Bioinformatics Database. [108-110].

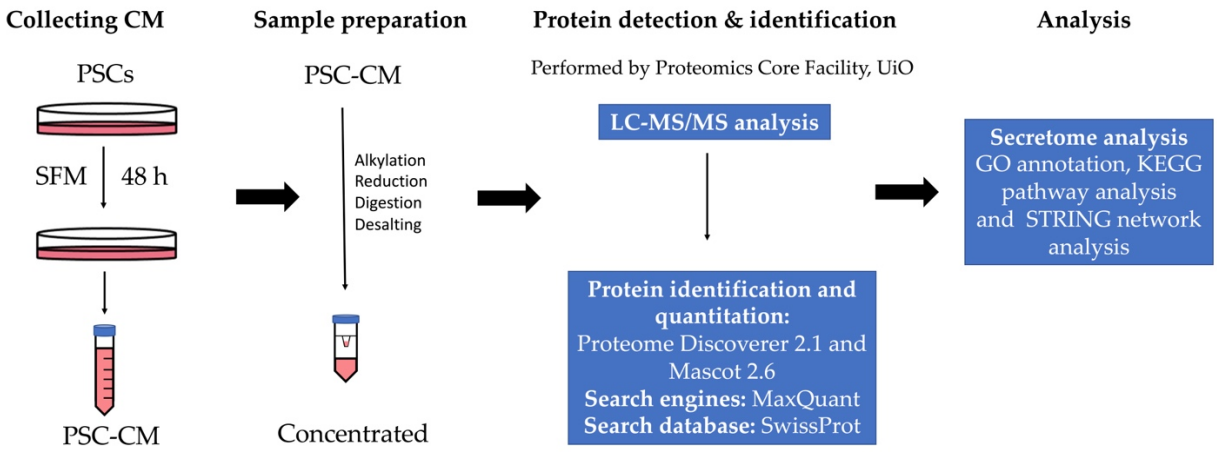

Figure 3.2. Secretome analysis flowchart. Conditional medium from PSC-1, PSC-2 and HPaSteC were collected and concentrated down to 5% of the original volume. The proteins were alkylated, reduced and digested with trypsin overnight at 37°C. The remaining peptides were further concentrated and desalted before mass spectrometry was performed using the STAGE-TIP method with a C18 resin disk. Proteome Discoverer 2.1 and Mascot 2.6 were used on the MS raw files for protein identification.

3.5.14 Statistical analysis

All values are presented as mean ± standard error of mean (SEM). Statistical analysis was performed by a two-tailed unpaired student's t-test for comparison of two groups. P-values of 0.05 or less were considered to be statistically significant.

4 Results

4.1 H&E Staining

The first step in this study was to investigate the impact of three different PSC-CMs on the phenotype of PCCs. For this purpose, three different PDAC cell lines Capan-2, HPAF-II and Mia PaCa-2 were exposed to CM from PSC-1, PSC-2 and HPaSteC for 24 and 72 hours. Thereafter, H&E staining was performed to study the impact of PSC-CM on the morphology and the growth of PCCs. Pictures captured from the H&E staining are presented in Figure 4.1.

4.1.1 Morphology

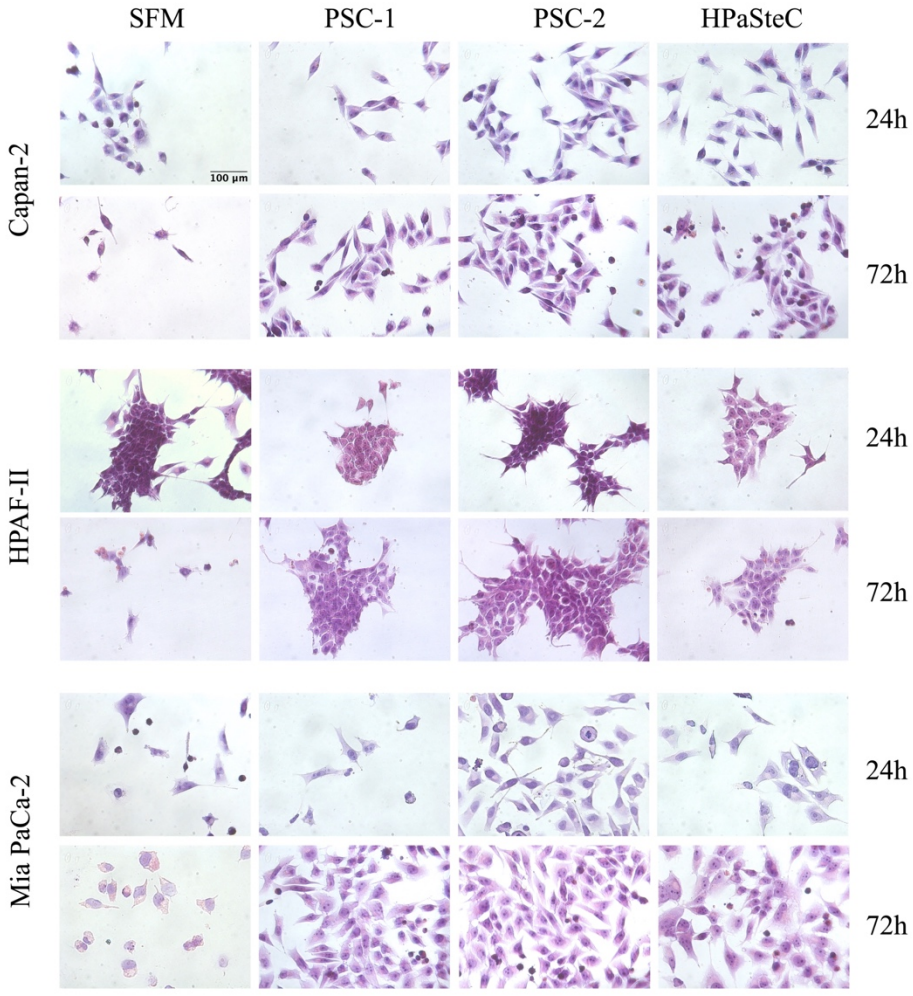

Figure 4.1. Morphology assessment. Approximately 5000 cells/well of the cell lines Capan-2, HPAF-II and Mia PaCa-2 were seeded in a 96-well plate and incubated overnight. Thereafter, cells were treated with SFM or PSC-CM for 24 and 72 hours, and the cells were stained using H&E staining. Pictures were taken with a 10X ocular lens and a 40X objective lens. Scale bar = 100 µm. *SFM, serum-free DMEM; PSC, pancreatic stellate cell; PSC-CM, PSC-conditioned medium; H&E, hematoxylin and eosin*.

As indicated in Figure 4.1, all three PCC lines showed a somewhat elongated shape at baseline. In general, the shape did not seem to be affected by the PSC-CM when incubated for 24 hours. When incubated for 72 hours, the SFM treated PCCs displayed a somewhat more rounded shape. In general, HPAF-II cells were growing in clusters, while Mia PaCa-2 and Capan-2 cells were growing more separately. In most cases, the PSC-CM treated cells showed more growth than the SFM treated cells.

4.1.2 Cell growth

The H&E-stained images represented in Figure 4.1 were analyzed in two different aspects, cell number (Figure 4.2 left panel) and growth area (Figure 4.2 right panel). Cell numbers were counted manually, while the growth area was found by calculating the percentage of area which was covered by cell growth using the software ImageJ.

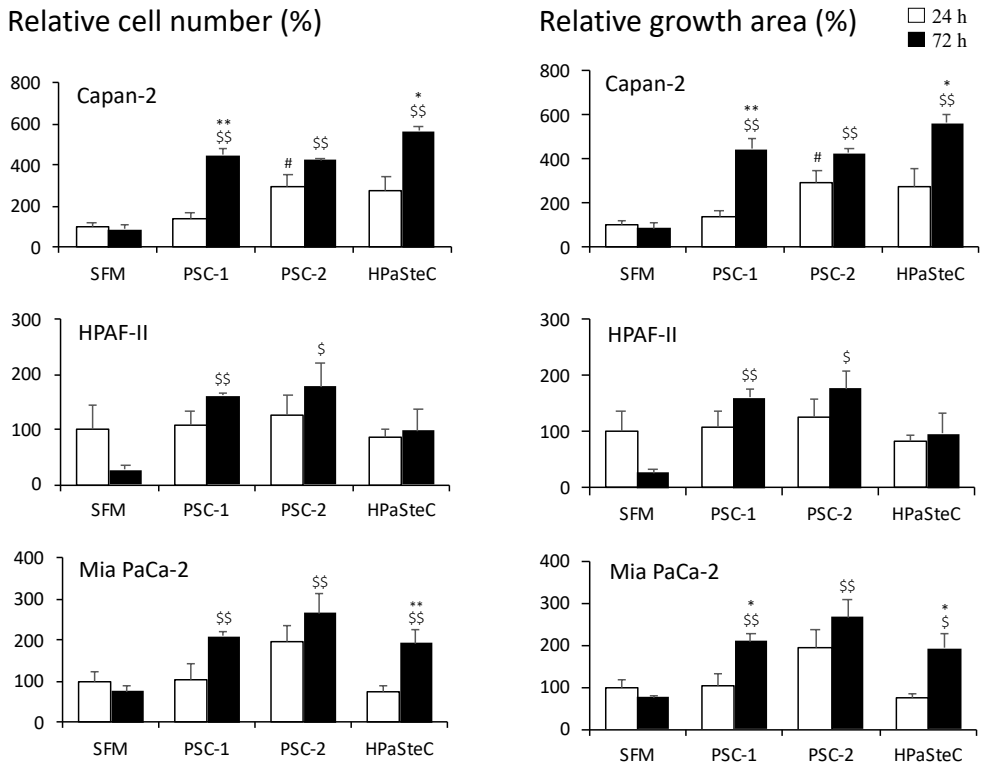

Figure 4.2. Cell growth assessment. The pictures from the H&E staining (represented in Figure 4.1) were used to examine the cell growth of PCCs treated with three different PSC-CM, as indicated. Cell numbers were counted manually, and ImageJ was used to calculate the percentage of area that was covered by cell growth. The area covered by cells and the cell number are presented as percentage change from basal line (cells treated with SFM for 24 hours, set to 100). The error bars are calculated as the standard error of the mean. *p<0.05, **p<0.01 comparing 24 to 72 hours for SFM or PSC-CM, #p<0.05, ##p<0.01 comparing SFM vs PSC-CM at 24 hours, $p<0.05, $$p<0.01 comparing SFM vs PSC-CM at 72 hours. *H&E, hematoxylin and eosin; PCC, pancreatic cancer cell; PSC, pancreatic stellate cell; PSC-CM, PSC-conditioned medium; SFM, serum-free DMEM.*

Except for the increase observed in PSC-2 treated Capan-2 cells at 24 hours, none of the other PSC-CMs induced any change in cell growth in any of the three PCC lines at 24 hours compared to SFM. Whereas for 72 hours, both cell number and growth area were higher in all PCC lines and all PSC-CMs, the only exception being HPAF-II exposed to HPaSteC-derived CM. None of the PCC lines treated with SFM displayed a statistically significant difference in cell number or growth comparing 24 and 72 hours, although a decreasing trend was observed in HPAF-II.

When comparing the changes induced by PSC-CM at 24 versus 72 hours, CM from PSC-1 induced an increase in growth area for Mia PaCa-2, and an increase in both the cell number and growth area for Capan-2 from 24 to 72 hours. While CM from HPaSteC induced an increase in both the cell number and growth area for both Mia PaCa-2 and Capan-2 from 24 to 72 hours. Interestingly, the CM from PSC-2 showed no time-dependent change in any of the PCCs. None of the PSC-CMs showed any change in cell number or growth area from 24 to 72 hours in HPAF-II. Among the PSC-CMs, HPaSteC at 72 hours displayed the highest increase in both cell number and growth area compared to other PSCs in Capan-2, whereas it was the case for PSC-2 for HPAF-II and Mia PaCa-2. Among the PCCs, Capan-2 was most influenced by the PSC-CMs, followed by Mia PaCa-2 and, lastly, HPAF-II.

4.2 Cell viability

MTT assay was used to investigate the impact of different PSC-CMs on the cell viability of PCCs. For this purpose, the PDAC cell lines Capan-2, HPAF-II and Mia PaCa-2 were exposed to PSC-CM from PSC-1, PSC-2 and HPaSteC for 24 and 72 hours. Thereafter, an MTT assay was performed. As MTT is converted to purple formazan crystals by the mitochondria, the concentration of formazan is used as an indication of the number of viable cells. The results from the MTT assay are presented as relative cell viability in Figure 4.3.

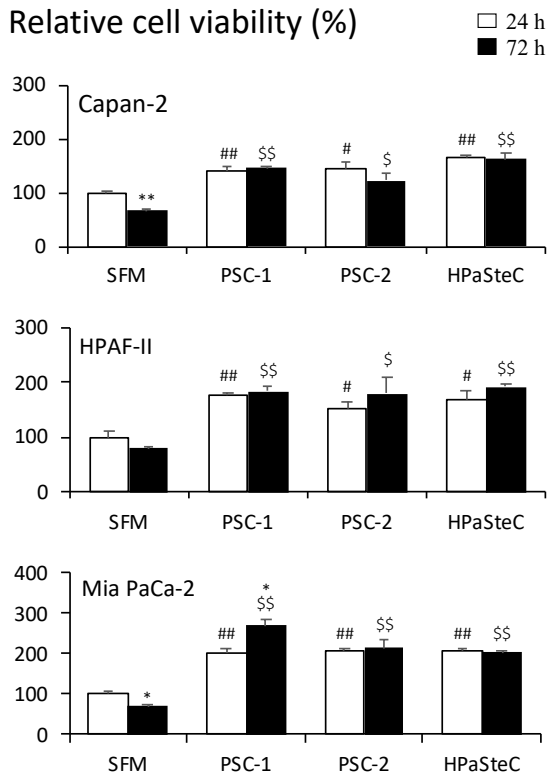

Figure 4.3 MTT based cell viability assessment. The PCCs were seeded in 96-well plates and incubated with SFM and PSC-CM for 24 and 72 hours. After incubation, MTT cell viability assay was performed and the absorbance at 570 nm was measured using a spectrophotometer. Cell viability is presented as a percentage change in the number of viable cells compared with the basal condition (SFM 24 hours). The error bars are calculated as the standard error of the mean. *p<0.05, **p<0.01 comparing 24 to 72 hours for SFM or PSC-CM, #p<0.05, ##p<0.01 comparing SFM vs PSC-CM at 24 hours, $p<0.05, $$p<0.01 comparing SFM vs PSC-CM at 72 hours. *MTT, thiazolyl blue tetrazolium bromide; PCC, pancreatic cancer cell; SFM, serum-free DMEM; PSC, pancreatic stellate cell; PSC-CM, PSC-conditioned medium.*

Compared with the SFM treated cells, PSC-CM treated cells show a significant increase in cell viability both for 24- and 72-hour incubations for all three cell lines. SFM treated Capan-2 and Mia PaCa-2 cells show a decrease in cell viability from 24 to 72 hours. Whereas, for the PSC-CM treated cells, the cell viability in general does not seem to be changing much from 24 to 72 hours, with the only significant change being an increase for Mia PaCa-2 cells treated with CM from PSC-1.

Figure 4.3 also shows that there is not much variation in the impact of the different PSC-CMs on the viability of the cell lines. For both Capan-2 and HPAF-II, 24-hour PSC-CM incubated cells display a 1.5 to 2-fold increase, and 72-hour PSC-CM incubated cells display a 2 to 2.5-fold increase in cell viability compared with SFM treated cells. A slightly larger variation was found for Mia Paca-2 cells, where the cells incubated with CM from PSC-1 for 72 hours displayed a 4-fold increase, while the cells incubated with CM from PSC-2 and HPaSteC for 72 hours only displayed a 3-fold increase compared with SFM treated cells.

4.3 Cell proliferation

BrdU cell proliferation assay was used to investigate the impact of three different PSC-CMs on the proliferation of PCCs. For this purpose, the PDAC cell lines Capan-2, HPAF-II and Mia PaCa-2 were exposed to PSC-CM from PSC-1, PSC-2 and HPaSteC for 24 and 72 hours. Then the cells were treated with BrdU, which is incorporated into newly synthesized DNA in proliferating cells. Antibodies are used to attach a color substrate, which gives a blue color for positive wells. The intensity is proportional to the amount of BrdU incorporated in the proliferating cells. The results from the BrdU assay are presented as relative cell proliferation in Figure 4.4.

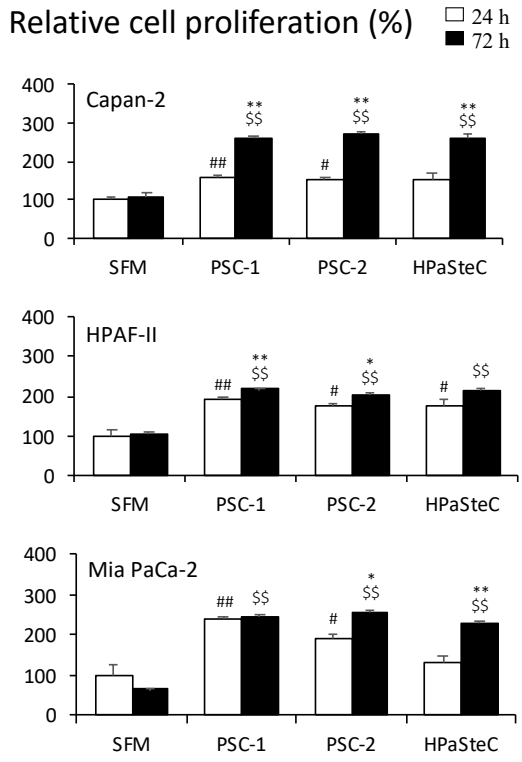

Figure 4.4. BrdU based cell proliferation assessment. The PCCs were seeded in 96-well plates and incubated with SFM and PSC-CM for 24 and 72 hours. After incubation, BrdU cell proliferation assay was performed, and the results were measured as absorbance at 450 nm using a spectrophotometer. Cell proliferation is presented as a percentage change in the number of proliferating cells compared with the base line (SFM 24 hours). The error bars are calculated as the standard error of the mean. *p<0.05, **p<0.01 comparing 24 to 72 hours for SFM or PSC-CM, #p<0.05, ##p<0.01 comparing SFM vs PSC-CM at 24 hours, $p<0.05, $$p<0.01 comparing SFM vs PSC-CM at 72 hours. *BrdU, Bromodeoxyuridine; PCC, pancreatic cancer cell, SFM, serum-free DMEM; PSC, pancreatic stellate cell; PSC-CM, PSC-conditioned medium.*

Comparing PSC-CM with SFM, all three cell lines exhibited a significant increase in cell proliferation when treated with PSC-1 and PSC-2, and HPAF-II also showed a significant increase when treated with HPaSteC for the 24-hour incubation. Whereas for the 72-hour incubation, all PSC-CMs give a significant increase in cell proliferation in all cell lines, compared with SFM treated cells. Comparing the change in cell proliferation from 24 to 72 hours, SFM treated cells show no significant change, while all three PSC-CMs give a significant increase for the Capan-2 cell line, PSC-1 and PSC-2 give a significant increase for the HPAF-II cell line, and PSC-2 and HPaSteC give a significant increase for Mia PaCa-2.

Figure 4.4 also shows that there is no large variation in the impact of the different PSC-CMs on the proliferation of Capan-2 and HPAF-II. For Capan-2, 24-hour PSC-CM incubated cells displayed a 1.5-fold increase, and 72-hour PSC-CM incubated cells displayed a 2 to 2.5-fold increase in cell proliferation compared with SFM treated cells. For HPAF-II, all PSC-CM incubated cells displayed about a 2-fold increase in cell proliferation for both 24 and 72 hours, compared with SFM treated cells. Mia Paca-2 cells showed a slightly larger variation in the impact of the different PSC-CMs for the 24-hour incubation, whereby CM from PSC-1, PSC-2 and HPaSteC caused a 2.5-, 2- and 1.5-fold increase in cell proliferation, respectively. However, at 72 hours, the impact of the PSC-CMs was more similar, ranging from a 3.5- to a 4-fold increase in cell proliferation.

4.4 Glucose transport

[^{3}H]2-DG was used to investigate the basal glucose transport and the impact of different PSC-CMs on the ability of PCCs to transport glucose. The PDAC cell lines Capan-2, HPAF-II and Mia PaCa-2 were used. For basal glucose transport, the cells were treated with [^{3}H]2-DG for 8, 24 and 72 hours. For PSC-CM exposed glucose transport, cells were first incubated with CM from PSC-1, PSC-2 and HPaSteC for 24 and 72 hours, and thereafter with [^{3}H]2-DG for 24 hours. The ionizing radiation from [^{3}H]2-DG encounters crystals in a scintillation solution that emits light that is read by a liquid scintillation analyzer. To account for differences in cell number, the protein concentration was measured using Bradford protein assay. The basal glucose transport of the three cell lines is presented in Figure 4.5.

4.4.1 Basal glucose transport in PCCs

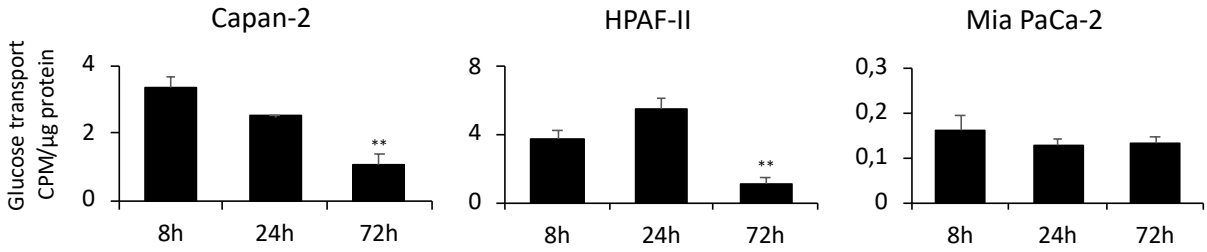

Figure 4.5. Measurement of basal glucose transport. The PCCs were seeded in 96-well plates and incubated overnight with SFM. The cells were then incubated with [^{3}H]2-DG for 8, 24 or 72 hours, following which the ionizing radiation was measured using a scintillation counter. Glucose transport is presented as CPM/µg protein. The error bars are calculated as the standard error of the mean. *p<0.05, **p<0.01 comparing change in glucose transport for 24- and 72-hour incubations vs the 8-hour incubation. *PCC, pancreatic cancer cell; SFM, serum free DMEM; [^{3}H]2-DG, [^{3}H]-2-deoxy-D-glucose; CPM, Counts per minute.*

As observed in Figure 4.5, there was no significant change in glucose transport comparing the 8- and 24-hour incubations for any of the cell lines. Comparing the 8- and 72-hour incubations, both Capan-2 and HPAF-II exhibited a significant 3-fold decrease in glucose transport after 72 hours. Capan-2 and HPAF-II showed around the same amount of intracellular [^{3}H]2-DG with approximately 3.5 CPM/µg following 8-hour incubation and 1 CPM/µg following 72-hour incubation. However, whereas Capan-2 exhibited a decreasing trend in glucose transport to 2.5 CPM/µg after 24 hours, HPAF-II showed an increasing trend to 5.5 CPM/µg. Mia PaCa-2, on the other hand, showed a much lower glucose transport, ranging from 0.13 to 0.16 CPM/µg. It is noteworthy that the basal glucose transport in Mia PaCa-2 cells was >20-fold lower compared to both Capan-2 and HPAF-II. Mia PaCa-2 also showed a slightly decreasing trend from 8 to 72 hours, but no significant change in relation to the time-dependent transport.

4.4.2 PSC-CM-induced glucose transport in PCCs

The relative glucose transport of the three PDAC cell lines exposed to PSC-CM is presented in Figure 4.6.

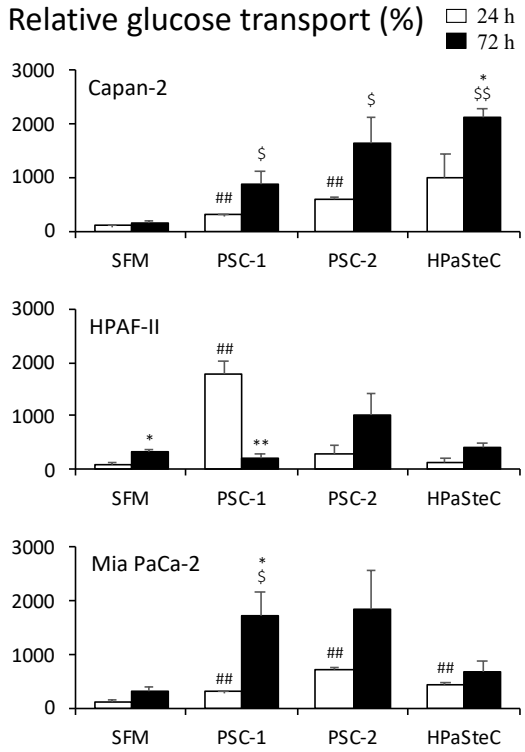

Figure 4.6. Glucose transport assessment. The PCCs were seeded in 96-well plates and incubated with SFM and PSC-CM for 24 and 72 hours. Thereafter, cells were incubated with [^{3}H]2-DG for 24 hours, before the ionizing radiation was measured using a scintillation counter. Glucose transport is presented as CPM/µg protein. The error bars are calculated as the standard error of the mean *p<0.05, **p<0.01 comparing 24 to 72 hours for SFM or PSC-CM, #p<0.05, ##p<0.01 comparing SFM vs PSC-CM at 24 hours, $p<0.05, $$p<0.01 comparing SFM vs PSC-CM at 72 hours. *PCC, pancreatic cancer cell; SFM, serum free DMEM; PSC, pancreatic stellate cell; PSC-CM, PSC-conditioned medium; [^{3}H]2-DG, [^{3}H]-2-deoxy-D-glucose; CPM, Counts per minute.*

Comparing PSC-CM with SFM for the 24-hour incubation, CM from PSC-1 resulted in a significant increase in glucose transport in all three cell lines, CM from PSC-2 caused a

significant increase in Capan-2 and Mia PaCa-2, and CM from HPaSteC gave a significant increase in Mia PaCa-2 only. Interestingly, for the 72-hour incubation, CM from PSC-1 gave a significant increase in both Capan-2 and Mia PaCa-2, while PSC-2 and HPaSteC only gave a significant increase in Capan-2. Comparing the change between the 24- and 72-hour incubations for SFM treated cells, only HPAF-II showed a significant change, with a 3-fold increase after 72 hours. For the PSC-CMs, all three cell lines showed an increasing trend for all three conditional media, except for HPAF-II cells treated with PSC-1, which, interestingly, showed a significant decrease from 24 to 72 hours. The only significant increase from 24 to 72 hours was found for Capan-2 cells exposed to CM from HPaSteC and Mia PaCa-2 cells exposed to CM from PSC-1.

Figure 4.6 also shows that the different PSC-CMs have a highly variable impact on the different cell lines. PSC-1 caused a significant increase for all the cell lines at 24 hours and also after 72 hours for Capan-2 and Mia PaCa-2. The effect of PSC-1 derived CM was largest in HPAF-II cells at 24 hours. CM from PSC-2 caused a significant increase at both 24 and 72 hours for Capan-2, and at 24 hours for Mia PaCa-2. While CM from HPaSteC only showed a significant increase at 24 hours for Mia PaCa-2 and 72 hours for Capan-2. Comparing the different cell lines, the CMs had the highest impact on Capan-2 cells, which showed a significantly increased glucose transport for all CMs, except for CM from HPaSteC-CM at 24 hours. Mia PaCa-2 cells seemed to be more affected by a 24-hour incubation when all PSC-CMs had a significant effect, while at 72 hours, only PSC-1 had a significant effect. Lastly, HPAF-II was only affected by CM from PSC-1 after 24-hour incubation.

4.5 Lactate secretion

A Glycolysis Cell-Based Assay Kit was used to investigate the impact of three different PSC-CMs on the lactate secretion of PCCs. For this purpose, the PDAC cell lines Capan-2, HPAF-II and Mia PaCa-2 were exposed to the PSC-CM obtained from PSC-1, PSC-2 and HPaSteC for 24 and 72 hours. The cell culture supernatant collected during glycolysis assay was added to a 96-well plate together with an assay buffer and an enzyme mixture. Lactate dehydrogenase converts lactate and NAD+ to pyruvate and NADH in the medium. NADH reduces a tetrazolium salt in the reaction solution, which creates a cyan color. The absorbance at 490 nm indicates the amount of lactate in the medium. The relative lactate secretion measured from the glycolysis cell-based assay is presented in Figure 4.7.

4.5.1 PSC-CM-induced lactate secretion in PCCs

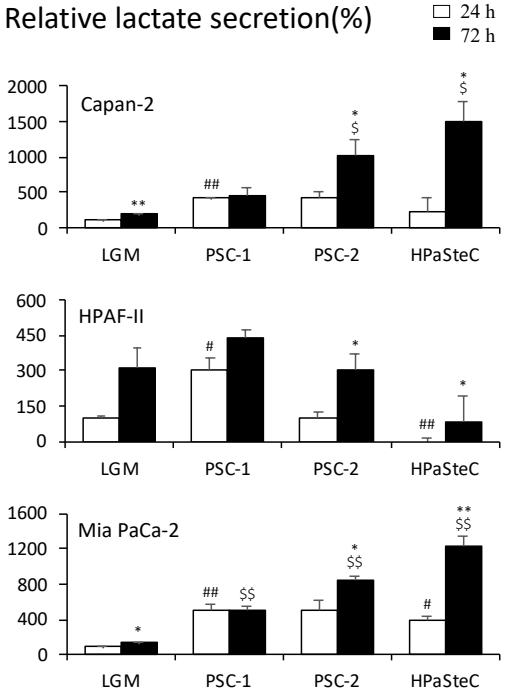

Figure 4.7. Measurement of lactate secretion. The PCCs were seeded in 96-well plates and incubated with low glucose DMEM medium (LGM) and PSC-CM for 24 and 72 hours. Subsequently a Glycolysis Cell-Based Assay kit was used to measure lactate secretion. Lactate secretion is presented as a percentage change in the amount of lactate (mM) compared with the basal condition (LGM 24 hours). The error bars are calculated as the standard error of the mean. *p<0.05, **p<0.01 comparing 24 to 72 hours for LGM or PSC-CM, #p<0.05, ##p<0.01 comparing LGM vs PSC-CM at 24 hours, $p<0.05, $$p<0.01 comparing LGM vs PSC-CM at 72 hours. *PCC, pancreatic cancer cell; LGM, low glucose medium; PSC, pancreatic stellate cell; PSC-CM, PSC-conditioned medium.*

Comparing PSC-CM with LGM for the 24-hour incubation, CM from PSC-1 caused a significant increase in lactate secretion in all three cell lines, while CM from HPaSteC resulted in a significant increase in Mia PaCa-2 and a significant decrease in HPAF-II cells. CM from PSC-2 showed no change in lactate secretion in any of the cell lines at 24 hours compared with LGM. When incubated for 72 hours, CM from both PSC-2 and HPaSteC caused an increase in lactate secretion in both Capan-2 and Mia Paca-2, but not in HPAF-II, while CM from PSC-1 resulted in an increase in Mia PaCa-2 only.

All three cell lines showed an increasing trend in lactate secretion from 24 to 72 hours for LGM treated cells. However, the change was only significant for the Capan-2 and Mia PaCa-2 cell lines. CM from PSC-2 and HPaSteC gave a significant increase in lactate secretion in all three cell lines from 24 to 72 hours. Capan-2 and Mia PaCa-2 were influenced strongest by PSC-CMs, and they both showed the same trend after 72 hours, with the highest lactate secretion caused by CM from HPaSteC, followed by that from PSC-2 and PSC-1. HPAF-II showed an opposite trend, but the changes were not statistically significant.

4.5.2 Lactate secretion under nutrient-poor conditions

In this experiment, the lactate secretion of the PCCs was measured under nutrient-poor conditions. PCCs pre-exposed to SFM or PSC-CM for 24 hours were further incubated with LGM for 24 to 48 hours, and the relative lactate secretion was measured using the glycolysis cell-based assay. Results are presented in Figure 4.8.

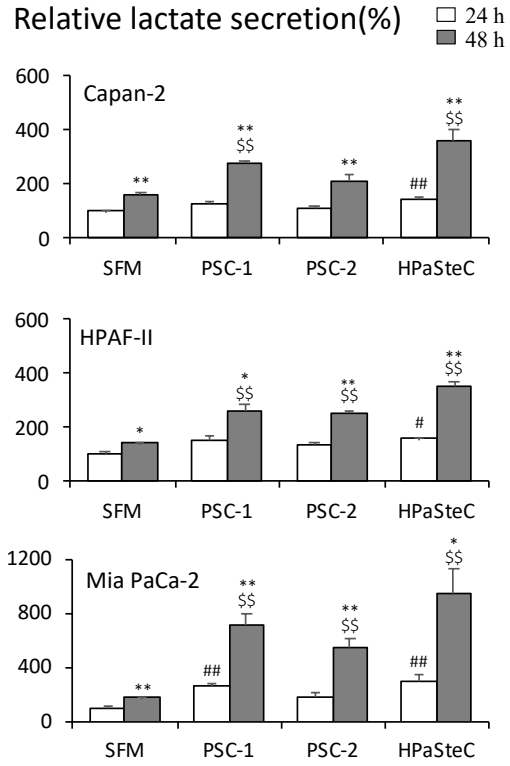

Figure 4.8. Measurement of lactate secretion. The PCCs were seeded in 96-well plates and incubated with SFM or PSC-CM for 24 hours, followed by a 24- or 48-hour incubation with low glucose DMEM medium (LGM). Subsequently, a Glycolysis Cell-Based Assay kit was used to measure lactate secretion. Lactate secretion is presented as a percentage change in the amount of lactate (mM) compared with the basal condition (SFM 24 hours). The error bars are calculated as the standard error of the mean. *p<0.05, **p<0.01 comparing 24 to 48 hours for SFM or PSC-CM, #p<0.05, ##p<0.01 comparing SFM vs PSC-CM at 24 hours, $p<0.05, $$p<0.01 comparing SFM vs PSC-CM at 48 hours. *PCC, pancreatic cancer cell; SFM, serum free DMEM; PSC, pancreatic stellate cell; PSC-CM, PSC-conditioned medium.*

Compared with SFM treated cells, the cells incubated with CM from PSC-1 caused a significant increase in lactate secretion in Mia PaCa-2 only, while CM from HPaSteC resulted in a significant increase in all three cell lines after 24 hours in nutrient-poor medium. Notably, none of PSC-2 incubated PCCs shows a significant change in lactate secretion after 24 hours. After 48 hours in nutrient-poor medium, all PSC-CMs incubated cells displayed an increase in lactate secretion in all three cell lines, except for Capan-2 incubated with CM from PSC-2, where the increase was not statistically significant. For both SFM and PSC-CM, all three cell lines showed increased lactate secretion after the 48 hours compared with 24 hours in nutrient-poor medium. The effect of the different PSC-CMs followed the same pattern for all three cell lines after both 24 and 48 hours, with HPaSteC-derived CM giving the highest increase, followed in descending order by CM from PSC-1 and PSC-2.

4.6 Impact of PSC-CM on chemosensitivity

4.6.1 Gemcitabine sensitivity

Gemcitabine is a standard of care for PDAC treatment. MTT-based cell viability assay was used to investigate the impact of different PSC-CMs on the gemcitabine sensitivity in PCCs. For this purpose, the PDAC cell lines Capan-2, HPAF-II and Mia PaCa-2 were first exposed to SFM or PSC-CM from PSC-1, PSC-2 and HPaSteC for 72 hours and then treated with or without 10 µM gemcitabine for 48 hours. Thereafter, gemcitabine-induced cytotoxicity was determined by assessing the reduction in cell viability using an MTT assay. The results are presented as relative cell viability in Figure 4.9.

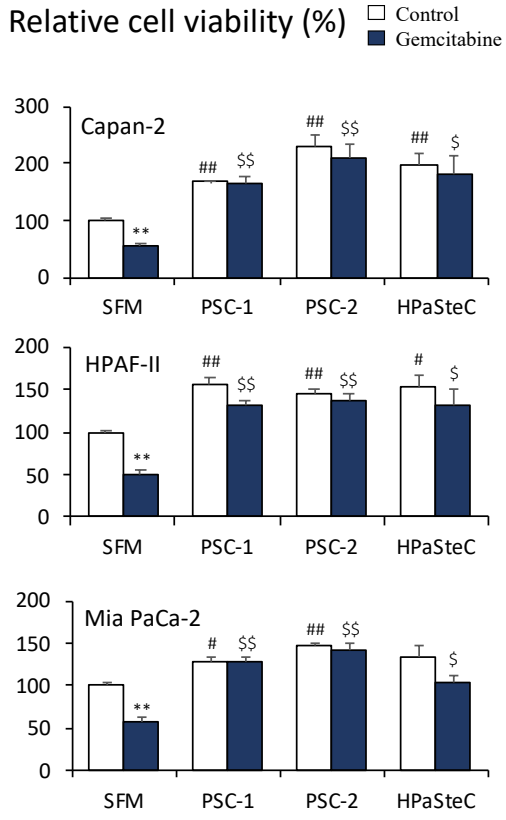

Figure 4.9 Gemcitabine sensitivity. The PCCs were seeded in 96-well plates and incubated with SFM and PSC-CM for 72 hours. Subsequently, the cells were incubated with gemcitabine (10 µM) for 48 hours. Following incubation, MTT cell viability assay was performed and the absorbance at 570 nm was measured using a spectrophotometer. Cell viability is presented as a percentage change in the number of viable cells compared with the basal condition (SFM treated control cells). The error bars are calculated as the standard error of the mean. *p<0.05, **p<0.01 comparing gemcitabine treated cells with the control, #p<0.05, ##p<0.01 comparing SFM vs PSC-CM for control cells, $p<0.05, $$p<0.01 comparing SFM vs PSC-CM for gemcitabine treated cells. *PCC, pancreatic cancer cell; SFM, serum-free DMEM; PSC, pancreatic stellate cell; PSC-CM, PSC-conditioned medium.*

When comparing SFM incubated cells, the cells treated with gemcitabine displayed a significant decrease in cell viability compared with the untreated cells. At a 10 µM concentration, gemcitabine significantly reduced the cell viability in all three cell lines, although at a variable level. However, comparing the PSC-CM treated cells, no significant change in viability was observed between the cells treated with gemcitabine compared with the untreated cells. This suggests that all three PSC-CMs induced significant resistance to gemcitabine-induced cytotoxicity in the three PCCs.

4.6.2 NV-5440 dose-response Curve

[^{3}H]2-DG was used to investigate the impact of the glucose transporter inhibitor NV-5440 on glucose transport in Mia PaCa-2 cells. The cells were incubated with NV-5440 in different concentrations ranging from 0 to 10 μM for four hours, followed by a 24-hour incubation with [^{3}H]2-DG. The intracellular [^{3}H]2-DG amount was measured using a liquid scintillation counter, and the data was normalized using protein concentration. Figure 4.10 presents the amount of glucose transport at different concentrations of NV-5440.

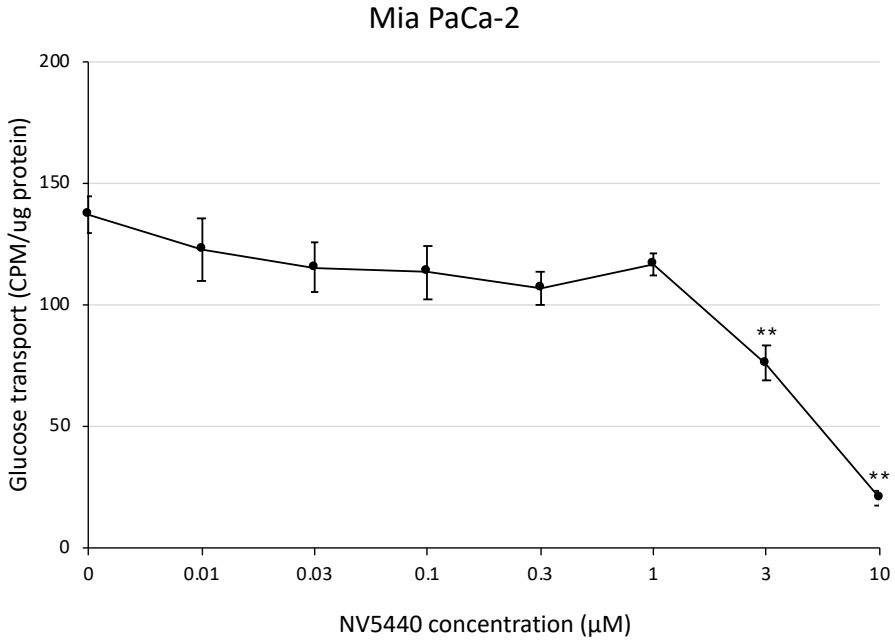

Figure 4.10. NV-5440 dose response curve. Mia PaCa-2 cells were seeded in a 96-well plate and incubated with various concentrations of GLUT1 inhibitor - NV-5440, for four hours. Subsequently, the cells were incubated with [^{3}H]2-DG for 24 hours, before the ionizing radiation was measured using a scintillation counter. Glucose transport is presented as CPM/μg protein. The error bars are calculated as the standard error of the mean. *p<0.05, **p<0.01 comparing NV-5440 with control (DMEM with 0.1% DMSO). *PCC, pancreatic cancer cell; [^{3}H]2-DG, [^{3}H]-2-deoxy-D-glucose; CPM, Counts per minute.*

As shown in the figure, there was no significant change in glucose transport observed between 0 and 1 μM of NV-5440. The first significant decrease was found for cells treated with 3 μM, where the glucose transport was decreased by 45% compared with the control cells. A further significant reduction was seen for cells treated with 10 μM NV-5440, when the glucose transport was reduced by 75% compared with the control cells.

4.6.3 Impact of NV-5440 and Gemcitabine on glucose transport in PCCs

The PDAC cell lines Capan-2, HPAF-II and Mia PaCa-2 were incubated with SFM or PSC-CM for 72 hours, followed by a 4-hour incubation with NV-5440 or gemcitabine. Subsequently, the cells were treated with [^{3}H]2-DG for 24 hours, and glucose transport was determined.

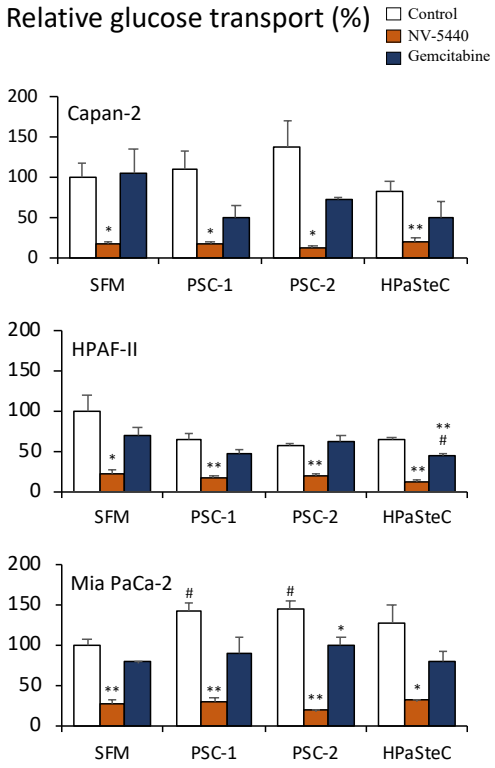

Figure 4.11. Assessment of glucose transport. The PCCs were seeded in 96-well plates and incubated with SFM and PSC-CM for 72 hours, followed by a 4-hour incubation with NV-5440, gemcitabine or SFM (control). Subsequently, they were incubated with [^{3}H]2-DG during 24 hours for assessment of glucose transport. The results are presented as the relative change in glucose transport comparing NV-5440 and gemcitabine-treated cells with non-treated controls. The error bars are calculated as the standard error of the mean. *p<0.05, **p<0.01 comparing NV-5440 or Gemcitabine with the control, #p<0.05, comparing SFM vs PSC-CM. *PCC, pancreatic cancer cell; SFM, serum free DMEM; [^{3}H]2-DG, [^{3}H]-2-deoxy-D-glucose; PSC, pancreatic stellate cell; PSC-CM, PSC-conditioned medium; CPM, Counts per minute.*

As observed in Figure 4.11, comparing the NV-5440 treated cells with the control cells, a significant decrease in glucose transport was seen for all three cell lines incubated with SFM or PSC-CM. In contrast, the only significant changes found for gemcitabine treated cells compared with the control cells was a significant decrease in HPAF-II cells treated with HPaSteC and Mia PaCa-2 treated with PSC-2. No significant change was seen when comparing SFM with PSC-CM for the NV-5440 treated cells. For the control cells, an increase in glucose transport was observed for Mia PaCa-2 control cells treated with CM from PSC-1 and PSC-2, whereas for the gemcitabine treated cells, a reduction in glucose transport was seen for HPAF-II cells treated with HPaSteC compared with SFM.

4.7 Western blot

To investigate the protein expression of glucose metabolism-related proteins in the three PDAC cell lines Capan-2, Mia PaCa-2 and HPAF-II, western blotting was performed. Figure 4.12 shows the results from western blotting of 13 different metabolic regulatory proteins with GAPDH or vinculin as loading controls. GAPDH is a housekeeping protein, while vinculin is one of the major components of cell-cell and cell-matrix adjunctions, both abundantly present in cells.

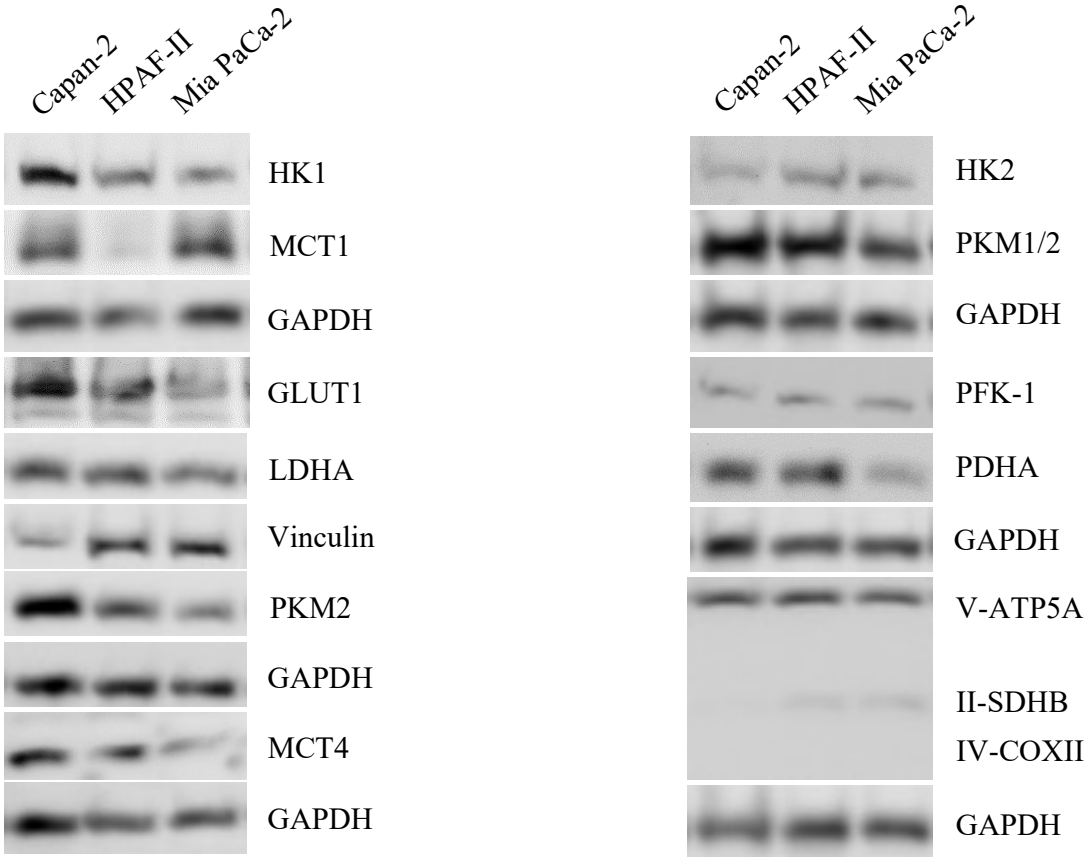

Figure 4.12. Western blot based protein expression analysis. The proteins from protein lysates of human PCCs - Capan-2, HPAF-II and Mia PaCa-2 - were subjected to SDS-PAGE and subsequently transferred using semi-dry transfer, followed by incubation with respective primary antibodies and secondary antibodies. LumiGLO® was used to visualize the blots, and the densitometric analysis of the immunoblots was performed using Labworks Software. *SDS-PAGE, Sodium dodecyl sulphate–polyacrylamide gel electrophoresis; HK1, Hexokinase 1; MCT1, Monocarboxylate transporter 1; GLUT1, Glucose transporter 1; LDHA, Lactate dehydrogenase A; PKM2, Pyruvate kinase M2 isoform; MCT4, Monocarboxylate transporter 4; HK2, Hexokinase 2; PKM1/2, Pyruvate kinase M1 and M2 isoforms; PFK-1, Phosphofructokinase-1; PDHA, pyruvate dehydrogenase E1 component subunit alpha; OXPHOS, oxidative phosphorylatio*n; V-ATP5A, *complex V - ATP synthase subunit alpha; II-SDHB, complex-II succinate dehydrogenase iron-sulfur subunit; IV-COXII, complex IV cytochrome c oxidase II.*

As seen in Figure 4.12, GLUT1, which is responsible for glucose transport into the cell, was expressed at a lower level in Mia PaCA-2 as compared with Capan-2 and HPAF-II. Considering the expression of hexokinases, responsible for phosphorylation of glucose to G6P, Capan-2 showed a stronger expression of HK1, and a slightly weaker expression of HK2 compared with the other two cell lines. In HPAF-II and Mia PaCa-2 expression of HK1 and HK2 was similar. All three cell lines showed a similar expression of PFK-1, which catalyzes the conversion of fructose 6-phosphate to fructose 1,6-bisphosphate, and LDHA, a catalyst for the conversion of lactate to pyruvate.

In the blot showing the combined detection of PKM1 and -2, both of which catalyze the conversion of phosphoenolpyruvate to pyruvate, Mia PaCa-2 displayed a slightly lower expression compared with the other two cell lines. In the blot in which only PKM2 was detected, Capan-2 displayed a stronger expression than the two other cell lines. PDHA, a catalyst of the conversion of pyruvate to acetyl-CoA and CO_2, was expressed at a lower level in Mia PaCa-2 compared with the other two cell lines.

Looking at the proton-coupled monocarboxylate transporters MCT1 and MCT4, which catalyze the transport of monocarboxylates such as lactate and pyruvate, MCT1 was very weakly expressed in HPAF-II cells, while MCT4 was weakly expressed in Mia PaCa-2 cells. Regarding the mitochondrial complex proteins, ATP synthase subunit alpha (ATP5A), which belongs to complex V, was the only protein for which all three cell lines showed a strong, clear band. For succinate dehydrogenase iron-sulfur subunit (SDHB), which belongs to complex II, a weak band was seen in HPAF-II and Mia PaCa-2, while there was no detectable expression of cytochrome c oxidase II (COXII), which belongs to complex IV.

4.8 Secretome analysis

Conditioned medium from PSC-1, PSC-2 and HPaSteC was analyzed by MS. Proteome Discoverer 2.1 and Mascot 2.6 were used on the MS raw files for protein identification. Figure 4.13 shows the number of proteins detected in the conditioned medium from PSC-1, PSC-2 and HPaSteC.

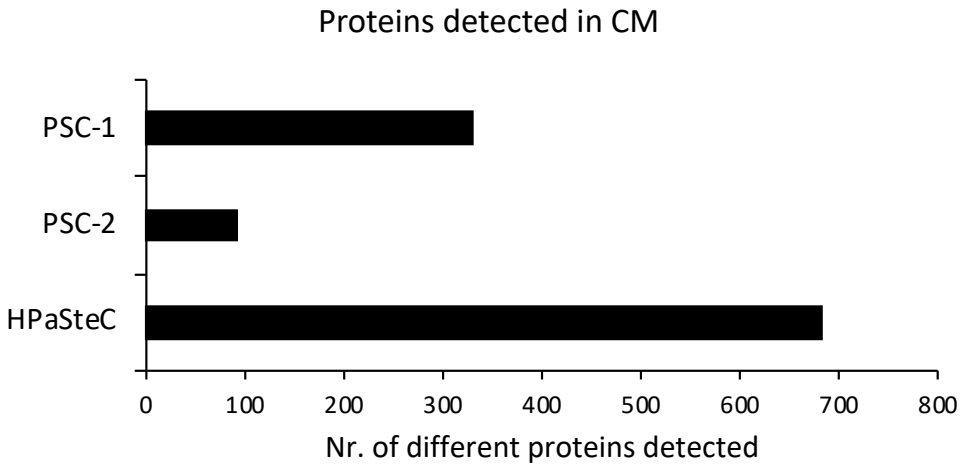

Figure 4.13. Number of proteins detected/identified by LC-MS/MS. CM from PSC-1, PSC-2 and HPaSteC was analyzed for protein content using LC-MS/MS. *LC-MS/MS, Liquid Chromatography with tandem mass spectrometry; PSC, pancreatic stellate cell; PSC-CM, PSC-conditioned medium.*

A total of 685 different proteins (*Homo sapiens*) were identified in CM from PSC-1, PSC-2 and HPaSteC. The number of proteins detected was highest in CM from HPaSteC with a total of 684 proteins. About half the number of proteins were detected in CM from PSC-1 with a total of 332 proteins. In comparison, only a total of 93 proteins were detected in CM from PSC-2, which is about a third of the number found in CM from PSC-1. The proteins detected by MS were subject to KEGG pathway analysis using the DAVID bioinformatics tool. The top pathways identified based on protein count, using the KEGG pathway analysis, are presented in Table 5.

Table 5. Top pathways identified using KEGG pathway analysis. The proteins detected in the CM from PSC-1, PSC-2 and HPaSteC by LC-MS/MS were subjected to KEGG pathway analysis using the DAVID bioinformatics tool. *CM, conditional medium; LC-MS/MS, Liquid Chromatography with tandem mass spectrometry.*

Pathway ID	Pathway Description	Nr. of proteins detected (% of total proteins)		
		PSC-1	PSC-2	HPaSteC
1100	Metabolic pathways	41 (12.3%)	6 (6.5%)	78 (11.4%)
4510	Focal adhesion	28 (8.4%)	19 (20.4%)	40 (5.8%)
4151	PI3K-Akt signaling pathway	26 (7.8%)	15 (16.1%)	36 (5.3%)
1200	Carbon metabolism	17 (5.1%)	4 (4.3%)	25 (3.7%)
4512	ECM-receptor interaction	23 (6.9%)	17 (18.3%)	24 (3.5%)

The category including most of the proteins for PSC-1 and HPaSteC were metabolic pathways, with as much as 12.3% and 11.4% of total proteins, respectively. Of the proteins associated with metabolic pathways, 5.1% and 3.7% were involved in carbon metabolism for PSC-1 and HPaSteC, respectively. For PSC-2 the largest fraction of proteins was associated with focal adhesion, with as much as 20.4% of the proteins. The proteins from the three different CMs were also associated with ECM-receptor interaction and PI3K-Akt signaling.

A list of the carbon metabolism-related proteins found in the KEGG pathway analysis, including their label-free quantification (LFQ) intensity for the different PSC-CMs was compiled (presented in Table 6). The LFQ intensity is a measure of protein intensity which is normalized to exclude outliers and used to compare samples. The carbon metabolism-related proteins from the KEGG pathway analysis were further analyzed with the STRING database. In Figure 4.14, the proteins are further grouped according to their function and interactions.

Table 6. List of carbon metabolism pathway proteins identified. The LFQ intensity is presented as the mean of the three replicates for each PCS-CM. *LFQ, Label-free quantification; PSC, pancreatic stellate cell; PSC-CM, PSC-conditioned medium.*

Gene ID	Protein name	LFQ intensity PSC1	LFQ intensity PSC2	LFQ intensity HPaSteC
ACAT2	Acetyl-CoA acetyltransferase, cytosolic	0	0	2345533
ADH5	Alcohol dehydrogenase 5 (class-3)	0	0	3522467
ALDOA	Aldolase, fructose-bisphosphate A	11710333	217240	57659333
ALDOC	Aldolase, fructose-bisphosphate C	3510667	0	13404000
ENO1	Alpha-enolase	14796333	0	125526667
ENO2	Gamma-enolase	457867	0	2179400
FH	Fumarate hydratase	0	0	8269567
GPI	Glucose-6-phosphate isomerase	17987000	0	25241667
GOT1	Glutamic-oxaloacetic transaminase 1	0	0	8651333
GOT2	Glutamic-oxaloacetic transaminase 2	0	0	2104167
GAPDH	Glyceraldehyde-3-phosphate dehydrogenase	1875567	0	31769667
IDH1	Isocitrate dehydrogenase [NADP] cytoplasmic	1015453	0	18379300
MDH1	Malate dehydrogenase 1	2371140	0	17835600
MDH2	Malate dehydrogenase 2	2281833	0	17741833
ME1	Malic enzyme 1	0	0	2103333
PGD	Phosphogluconate dehydrogenase	0	0	8200467
PGK1	Phosphoglycerate kinase 1	3370433	0	12019000
PGAM1	Phosphoglycerate mutase 1	11395200	0	31554467
PGLS	6-phosphogluconolactonase	0	0	19464467
PSAT1	Phosphoserine aminotransferase 1	4136267	604700	22630000
PSPH	Phosphoserine phosphatase	1229167	0	6587100
PKM	Pyruvate kinase M1/2	5725500	954633	31850333
TALDO1	Transaldolase 1	1921200	0	12450167
TKT	Transketolase	1008847	0	48787000
TPI1	Triosephosphate isomerase 1	24008333	9429833	53959900

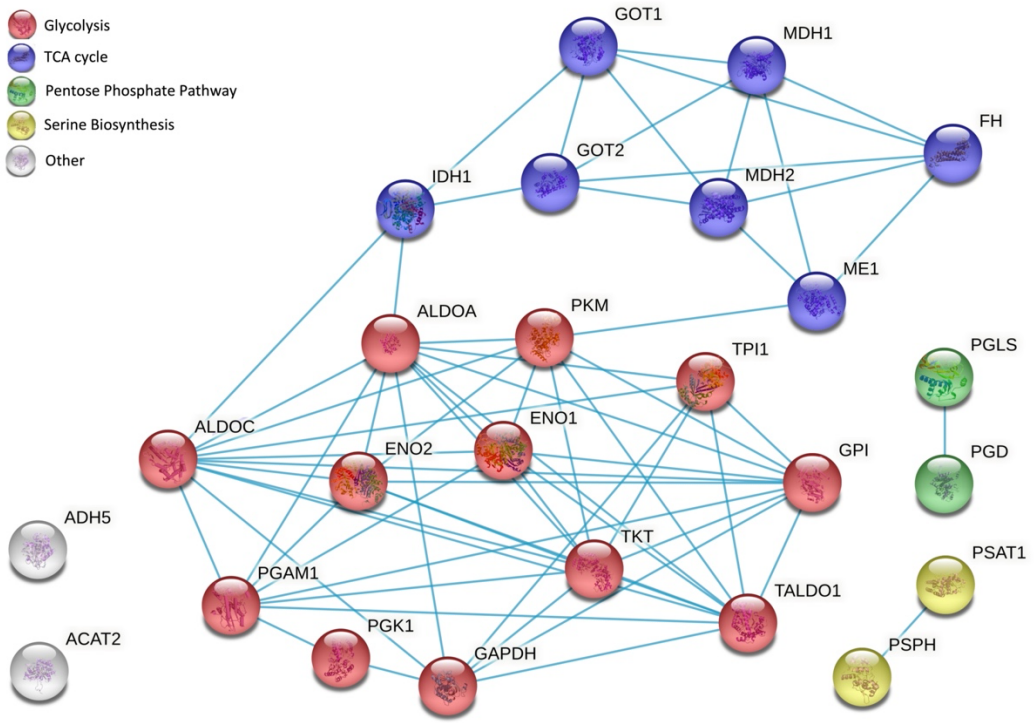

Figure 4.14. STRING network for carbon metabolism related proteins found in the PSC-CM. The list of carbon metabolism related proteins from the KEGG pathway analysis were further analyzed with the STRING database. The node coloring represents the type of cluster the protein belongs to. Red nodes: glycolysis, purple nodes: TCA cycle, yellow nodes: serine biosynthesis, green nodes: pentose phosphate pathway. The blue lines represent known interactions from curated databases. *ACAT2, Acetyl-CoA acetyltransferase 2; ADH5, Alcohol dehydrogenase 5 (class 3); ALDOA, Aldolase, fructose-bisphosphate A; ALDOC, Aldolase, fructose-bisphosphate C; ENO1, Alpha-enolase; ENO2, Gamma-enolase; FH, Fumarate hydratase; GPI, Glucose-6-phosphate isomerase; GOT1, Glutamic-oxaloacetic transaminase 1; GOT2, Glutamic-oxaloacetic transaminase 2; GAPDH, Glyceraldehyde-3-phosphate dehydrogenase; IDH1, Isocitrate dehydrogenase [NADP] cytoplasmic; MDH1, Malate dehydrogenase 1; MDH2, Malate dehydrogenase 2; ME1, Malic enzyme 1; PGD, Phosphogluconate dehydrogenase; PGK1, Phosphoglycerate kinase 1; PGAM1, Phosphoglycerate mutase 1; PGLS, 6-phosphogluconolactonase; PSAT1, Phosphoserine aminotransferase 1; PSPH, Phosphoserine phosphatase; PKM, Pyruvate kinase M1/2; TALDO1, Transaldolase 1; TKT, Transketolase; TPI1, Triosephosphate isomerase 1.*

Seventeen carbon metabolism-related proteins were found in the CM from PSC-1, whereas all 25 carbon metabolism proteins were detected in the CM from HPaSteC. All of the proteins found in CM from both PSC-1 and HPaSteC showed a higher LFQ intensity for HPaSteC. The glycolysis proteins ALDOA, PKM and TPI1 and the pentose phosphate pathway protein PSAT1 were the only carbon metabolism proteins detected in all three PSC-CMs. In CM from HPaSteC, the by far highest LFQ intensity was found for ENO1, which was 2.5-fold higher than the second highest LFQ intensities that were found for ALDOA, TKT and TPI1. In CM

from both PSC-1 and PSC-2, the highest LFQ intensities were found for TPI1. For PSC-1, the LFQ intensity for TPI1 was 1.5-fold higher than the second highest LFQ intensity, which was for GPI. In CM from PSC-2, the LFQ intensity for the three other carbon metabolism-related proteins was relatively low, with the second highest LFQ intensity found for PKM being 10-fold lower than for TPI1.

Of the 25 carbon metabolism-related proteins detected (shown as a STRING protein-protein interaction network in Figure 4.14), 12 were involved in glycolysis, seven were involved in the TCA cycle, two were involved in serine biosynthesis and two were involved in the pentose phosphate pathway. The two last proteins, ADH5 and ACAT2, are involved in alcohol and aldehyde metabolism, and lipid metabolism, respectively. CM from PSC-1 and HPaSteC contained the same glycolysis and serine biosynthesis proteins. The CM from PSC-1 only contained three of the seven TCA proteins that were found in the CM from HPaSteC. The two pentose phosphate pathway proteins, and the two unclassified proteins ADH5 and ACAT2, were only found in CM from HPaSteC.

5 Discussion

PDAC is associated with profound chemoresistance, resulting in an extremely poor prognosis with a 5-year survival rate of less than 8% [111]. Currently, the only potential cure for PDAC is surgery. However, because PDAC causes few and non-specific symptoms, PDAC is often discovered at an advanced stage, such that only around 20% of all PDAC patients have surgically resectable disease [24]. Despite its modest clinical effects, gemcitabine has been the most commonly used chemotherapeutic drug for PDAC since 1997 [76]. While the profound metabolic reprogramming in PDAC is known to contribute to treatment resistance, the underlying mechanisms are yet to be fully understood [34, 60]. Increasing evidence also suggests that PSCs, the main cellular component of the TME, play a pivotal role in the acquired chemoresistance of PCCs [31, 112-114].

Several studies have explored how PSCs contribute to the acquired chemoresistance in PCCs, and several different mechanisms have been revealed [31, 112-114]. First of all, PSCs are the principal source of fibrosis, creating a dense TME which acts as a physical barrier for efficient drug delivery [48, 115]. As PSCs are intrinsically resistant to the cytotoxic actions of gemcitabine, PSCs also reduce the bioavailability of gemcitabine by intracellular entrapment. PSCs are also known to secrete CYR61, which downregulates the nucleoside transporters hENT1 and hCNT3, which are crucial mediators of gemcitabine uptake in PCCs. Moreover, PSCs have been shown to secrete deoxycytidine, which competes with gemcitabine processing by DCK in PCCs [87]. Some studies have also revealed that PSCs secretes several factors that promote PCC chemoresistance, including nitric oxide, exosomes, the ECM proteins fibronectin and collagen-1, and the growth factors IGF-1, IGF-2, IL-1β, IL-6 and HGF [33, 66, 85-94].

PSCs are also known to help PCCs to maintain their metabolic demands in the nutrient-poor, hypoxic PDAC environment through unconventional ways (metabolic rewiring). Metabolic rewiring in PCCs and stromal components of PDAC enables recycling of nutritional substrates and access to alternate fuel sources to sustain tumor growth and survival [64, 116, 117]. PCCs induce oxidative stress in PSCs, which triggers aerobic glycolysis and consequently an increased secretion of energy fuels such as lactate and pyruvate that can be taken up by the PCCs and used as fuel for the TCA cycle [31, 73]. PSCs are also known to supply the PCCs with NEAAs such as alanine, which also can be converted to pyruvate and used as fuel for the PCCs [31]. In addition, macropinocytosis is upregulated in PCCs, which leads to an increase in

the uptake of extracellular material to support their growth [31, 70, 71]. As PSCs provide substantial quantities of fuel to maintain the metabolic demands in PCCs, the PCCs usually limit themselves to glycolysis. The increased glycolysis in PCCs has been demonstrated to contribute to increased flux of glycolysis intermediates through metabolic pathways such as the PPP, HBP and serine biosynthesis [34, 58]. An increase in the non-oxidative arm of PPP has been shown to promote gemcitabine resistance by the increased generation of dCTP, which causes competitive inhibition of gemcitabine. Metabolic pathways have therefore been suggested as targets to overcome gemcitabine resistance in PDAC [60].

The contribution of PSCs to glycolysis regulation, the major metabolic alteration in PDAC, is yet to be fully understood [58]. Furthermore, increasing evidence indicates that gemcitabine resistance is related to the metabolism of glucose, amino acids, and lipids [31, 118]. If and how PSC-induced metabolic changes and chemoresistance in PCCs are interlinked is currently unknown. However, investigations into PSC-induced metabolic alteration and its impact on chemosensitivity in PDAC have the potential to reveal better treatment strategies. This study aimed to investigate the impact of PSCs on the regulation of glucose metabolism and the development of chemoresistance in PDAC.

To investigate the impact of PSC-secreted factors on PCCs, CM was collected from three different PSCs. First, the impact of these PSC-CMs on the phenotype of PCCs was investigated through assessments of morphology, growth, viability and proliferation. H&E staining (Figure 4.1) revealed that the HPAF-II cells grew very clustered, while growth in Mia PaCa-2 and Capan-2 was more segregated. However, no significant impact of PSC-CM on the morphology of the cells was observed. All three PCC lines displayed increased cell growth when incubated with PSC-CMs for 72 hours, compared with SFM treated cells, the only exception being HPAF-II cells exposed to CM from HPaSteC (Figure 4.2). This indicates that the PSCs used in this study secrete factors that support growth in PCCs.

An increase in cell viability and proliferation was also found for PSC-CM treated cells compared with SFM treated cells during both 24- and 72-hour incubations (Figure 4.3 & 4.4), indicating that the PSCs also secrete factors that support viability and proliferation in PCCs. All three PSC-CMs caused a time-dependent increase (24 to 72 hours) in cell proliferation, while for cell viability, the only time-dependent increase was found for Mia PaCa-2 treated with PSC-1. As all proliferating cells are viable, but not all viable cells are proliferating, an

opposite trend could be explained by an increased fraction of the viable cells being in a proliferating state. Of note, the findings of these two assays may not be directly comparable due to a significant difference in the principles of the assays that were used. The cell viability assay is based on the principle of conversion of MTT to formazan crystals by metabolically active cells, whereas the proliferation assay is based on the principle of incorporation of BrdU in active DNA synthesis. No significant time-dependent change in cell proliferation was seen for the SFM treated PCCs, whereas both SFM treated Capan-2 and Mia PaCa-2 showed a time-dependent decrease in cell viability. The decrease in cell viability under SFM-conditions could be partially explained by the lack of sufficient nutrients compared to PSC-CMs.

Even though the PSC-CMs lead to a significant increase in growth, viability and proliferation for PCCs in most cases, large variability in the degree of impact was seen between the PSC-CMs. Regarding cell proliferation, Capan-2 was the only cell line that showed a significant increase from 24 to 72 hours for all three PSC-CMs, while regards to cell viability, the only significant increase between 24 and 72 hours was found for Mia PaCa-2 incubated with CM from PSC-1. Interestingly, the CM from PSC-2 was the only CM that did not show any time-dependent change in cell growth. A likely explanation for this could be the fact that CM from PSC-2 contains a considerably lower number and amount of different secretory proteins that regulate the interactions between PSCs and PCCs as compared to the other PSC-CMs (Figure 4.13).

To investigate the impact of conditioned medium from PSCs on glucose metabolism in PCCs, measurements of glucose transport and lactate secretion were conducted. The transport of glucose across the plasma membrane is mediated by two classes of transporters, glucose transporters (GLUTs) which are facilitated transporters and sodium-glucose cotransporters (SGLTs), which are active transporters. The glucose transporter GLUT1 is commonly upregulated in PDAC. Higher levels of GLUT1 are also associated with worse prognosis and treatment response as compared to low levels [58, 119]. The measurement of basal glucose transport conducted in this study, revealed considerably lower glucose transport in Mia PaCa-2 compared to the other two cell lines (Figure 4.5). One explanation for this is the low level of GLUT1 expression in Mia PaCa-2 cells, revealed in the western blot, which also is in line with reports in the literature [120]. The basal glucose transport in Capan-2 and HPAF-II was decreased after 72 hours, while it remained unchanged in Mia PaCa-2.

By inhibiting glucose metabolism, 2-DG causes glycolytic deprivation-induced cytotoxic effects and cell death in PCC lines in a dose-dependent manner [121]. One explanation for the decreased glucose transport detected in Capan-2 and HPAF-II after 72 hours could therefore be that the cells have transported cytotoxic amounts of [^{3}H]2-DG, which causes cell death. Dead cells, and the [^{3}H]2-DG entrapped in them, are washed away before the samples are subject to the scintillation analyzer, and the 72-hour samples might therefore contain a lower cell number. Protein concentration is measured to account for such differences in cell numbers. However, as a higher protein concentration only gives an indication of higher amounts of viable cells and is not a direct measure, differences in cell number could still have some impact on the result. In addition, the cells can have taken up different amounts of [^{3}H]2-DG. It is then more likely that the cells that survived for 72 hours have transported lower amounts of [^{3}H]2-DG and have therefore not been killed by the cytotoxic effects. This could possibly explain the low number of [^{3}H]2-DG detected per µg protein after 72 hours. Mia PaCa-2 was the only cell line that did not show any significant decrease after 72 hours. One possible explanation for this is that the low levels of [^{3}H]2-DG, which is transported into Mia PaCa-2, is not enough to cause cytotoxic effects even after 72 hours.

When incubated with PSC-CMs, both Capan-2 and Mia PaCa-2 showed a significant increase in glucose transport for all three PSCs compared with SFM (Figure 4.6). PSC-1 was the only CM that led to an increase in glucose transport for all three cell lines. In HPAF-II, the increase in glucose transport when incubated with PSC-1 was only seen at 24 hours, not at 72 hours. Although some large variations were found when it comes to the effect of the different PSC-CMs on the different cell lines, the results indicate that the PSCs used in this study, especially PSC-1, do secrete factors that increase the glucose transport in PCCs. Some of the heterogeneity found in this experiment could probably be explained by the heterogeneity between the cell lines in general, as observed in the western blot (Figure 4.12). Most relevant for this experiment is the expression of GLUT1. Although Mia PaCa-2 showed a lower expression of GLUT1, the relative increase in glucose transport was quite similar to what was found for Capan-2. This indicates that the PSC-CM secreted factors induce glucose transport for cells with both low and high basal expression of GLUT1.

The glucose entering PCCs tends to be broken down to lactate through glycolysis, regardless of the oxygen availability (Warburg effect) [31]. PCCs are also known to import lactate secreted from nearby PSCs. To account for this excessive amount of lactate, PCCs also tend to increase

their expression of MCT1 and MCT4 on the plasma membrane to accelerate the lactate flux [118, 122-124]. The lactate secretion experiments performed in this study aimed to investigate the impact of PSC-CM on the tumor cell lactate secretion in the three different PCC lines.

The first lactate secretion experiment (Figure 4.7) showed a large variation between both the different PCC lines and the different PSC-CMs. Compared with LGM treated cells, the lactate secretion was increased in all three cell lines when incubated with CM from PSC-1 for 24 hours. When incubated for 72 hours, the lactate secretion was increased in both Mia PaCa-2 and Capan-2 when incubated with CM from PSC-2 and HPaSteC compared with LGM. Mia PaCa-2 was influenced the most by the PSC-CMs, displaying a significant increase in lactate secretion for all three PSC-CMs compared with LGM, with the only exception being 24-hour exposure to CM from PSC-2.

In the experiment investigating lactate secretion of the cells during nutrient-poor conditions, all three cell lines displayed a significantly higher lactate secretion after incubation in nutrient-poor conditions for 48 hours compared with 24 hours (Figure 4.8). This indicates that all three PCC lines increase glycolysis when the nutrient availability is low. Unlike the first lactate secretion experiment, this experiment showed similar trends for the effect of all three PSC-CMs. After the 48-hour incubation, all three PCC lines displayed a significant increase in lactate secretion following incubation with PSC-CM as compared to SFM, except for Capan-2 exposed to CM from PSC-2. Similarly, all three PCC lines showed the highest lactate secretion when incubated with CM from HPaSteC, followed by PSC-1 and PSC-2. One possible explanation for this finding could be that the highest number of secretory proteins that can effectuate this process were found in HPaSteC, followed in descending order by PSC-1 and PSC-2 (Figure 4.13).

The increase in lactate secretion seen for PSC-CM treated cells compared with SFM treated cells indicates the contribution of secretory proteins in the PSC-CM. This could partly be due to the increase in glucose transport, as shown in Figure 4.6, which leads to an increase in lactate production through glycolysis. However, it could also be due to several other mechanisms involved in glycolysis regulation. The higher amount of lactate secreted by PSC-CM incubated cells compared with SFM incubated cells after 48 hours in nutrient-poor conditions indicates that the PSC-CM induces metabolic reprogramming so that the increased glycolysis also remains after the PSC-CM is removed.

As glycolysis is the primary pathway for energy production in PDAC and the inhibition of key glycolytic genes has been shown to inhibit the tumorigenic activity of PDAC cells, glycolytic enzymes have been suggested as therapeutic targets [58, 102]. The first rate-limiting step of glycolysis is glucose transport, mediated by glucose transporters such as GLUT1, which is commonly overexpressed in PDAC [103-105]. Several GLUT inhibitors have been developed to treat cancer, but none of them has been advanced to clinical studies [103]. NV-5440, recently discovered by Kang et al., has been shown to inhibit the uptake of [^{3}H]2-DG by inhibiting GLUT1 transporters [103, 125].

Enhanced GLUT1 expression is demonstrated to lead to a glucose-dependent increase in mammalian target of rapamycin complex 1 (mTORC1) activity. mTORC1 regulates cell growth based on nutrient availability. When nutrients are available, mTORC1 is switched on and promotes the conversion of nutrients and energy into macromolecules, while it suppresses the autophagic recycling of macromolecules [126]. Overactivation of mTORC1 contributes to cancer progression by promoting an increase in cell size and proliferation, and mTORC1 is therefore also a therapeutic target in cancer [125, 127, 128]. As a consequence of the inhibition of GLUT1, NV-5440 has also been shown to selectively inhibit mTORC1 through glucose depletion [103, 129].

In this study, [^{3}H]2-DG was used to investigate the effect of NV-5440 and gemcitabine on glucose transport in Capan-2, HPAF-II and Mia PaCa-2 cells and to explore whether PSC-CM impacts the inhibiting effect of NV-5440 (Figure 4.11). The dose-response curve for NV-5440 in Mia PaCa-2 cells revealed that the minimum concentration required for significant inhibition of glucose transport was 3 μM, which resulted in a 45% reduction in glucose transport compared with the control cells (Figure 4.10). An increase to 10 μM NV-5440 showed a further decrease in glucose transport with a reduction of 75%, compared with control cells. Hence this concentration was chosen for further experiments.

Compared with the control cells, a significant decrease in glucose transport was seen for NV-5440 treated cells in all three PCC lines, both when incubated with SFM and PSC-CM. This indicates that NV-5440 is able to block glucose transport in all three cell lines, which was as expected. Comparing NV-5440 treatment between the cells incubated with SFM and PSC-CM revealed no significant change, indicating that the PSC-CM secretome does not affect the actions of NV-5440. The only gemcitabine treated cells that showed a significant decrease in

glucose transport compared with the control cells, was Mia PaCa-2 cells exposed to CM from PSC-2, and HPAF-II cells exposed to CM from HPaSteC. Except this, the glucose transport in most cells was not significantly affected by gemcitabine, but a decreasing trend was seen. One possible explanation for the reduced glucose transport for some of the gemcitabine treated cells could be that the uptake of both [^{3}H]2-DG and gemcitabine, which both have cytotoxic effects on cells, are more likely to induce cell death, compared with the uptake of [^{3}H]2-DG only. The cells which have taken up a larger amount of both [^{3}H]2-DG and gemcitabine are more likely to die, and the remaining cells are therefore more likely to be the cells that have taken up less [^{3}H]2-DG.

The effect of PSC-CMs on gemcitabine chemosensitivity of PCCs was investigated using an MTT-based cell viability assay (Figure 4.9). The cells incubated with SFM displayed a significant 40-50% reduction in cell viability when treated with gemcitabine compared with untreated cells for all three PCC lines. This indicates that the PCCs are sensitive to gemcitabine. For the PSC-CM exposed PCCs, no significant change in cell viability was observed between the gemcitabine treated cells and control cells. This indicates that all three PSC-CMs used in this study contain factors that protect the PCCs from gemcitabine-induced cytotoxicity, thereby promoting chemoresistance. This is in line with the results from several other studies suggesting that PSC-secreted factors induce resistance to gemcitabine in PCCs [86, 87, 112, 130]. PSC-CM treated cells did also show significantly higher cell viability compared with the SFM treated cells for both gemcitabine treated and untreated cells, with Mia PaCa-2 exposed to CM from HPaSteC being the only exception. This also further confirms the findings shown in Figure 4.3, implicating that PSCs secrete factors that support PCC cell viability.

Western blot was used to explore the basal expression of glucose metabolism-related proteins in the three PCC lines used in this study (Figure 4.12). Glycolytic flux, which in this study was assessed through measurements of glucose transport and lactate secretion, is regulated by glucose transporters, rate-limiting enzymes, and the intermediates of glycolysis [131]. Considerable variations in glucose transport and lactate secretion were observed between the three cell lines used in this study. Further investigation into the expression of glucose metabolism-related proteins in the PCCs can improve our understanding of the differences in glycolytic flux found between the three PCCs.

Mutation in *KRAS*, which is present in all three PCC lines used in this study, has been shown to enhance the glycolytic pathway by up-regulating the expression of glucose transporters and rate-limiting enzymes of glycolysis such as GLUT1, HK2, PFK-1 and LDHA [58, 132]. As previously mentioned, when discussing basal glucose transport, expression of the glucose transporter GLUT1 is low in Mia PaCa-2 compared with the other cell lines. Hexokinase, the initial enzyme of glycolysis that catalyzes the phosphorylation of glucose to G6P, has several isoforms. In healthy adults, the HK1 isoform is highly expressed in most tissues, while the HK2 isoform is limited to adipose tissue, skeletal muscles and the heart. However, to support the increased metabolic demand, HK2 is often expressed in high levels in cancer cells [133]. The western blot results revealed that HK2 was expressed together with HK1 in all three PCC lines used in this study, with Capan-2 showing a slightly stronger expression of HK1 and a slightly weaker expression of HK2 compared with the other two cell lines.

No significant differences were found between the cell lines when it comes to the expression of LDHA, which catalyzes the conversion from lactate to pyruvate and back, and PFK-1, the catalyst of the rate-limiting step of glycolysis, namely the phosphorylation of fructose-6-phosphate [53]. However, the PFK-1 bands were relatively weak compared with the other glycolytic enzymes. Pyruvate kinase isozymes M1 and M2 (PKM1 and PKM2) are also important glycolytic enzymes, as they catalyze the conversion of phosphoenolpyruvate to pyruvate [53]. The expression of PKM2, which is known to be oncogenic and overexpressed in PDAC, was variable between the three PCCs with the highest expression in Capan-2 and lowest in Mia PaCa-2 cells [134]. The total PKM expression, including both PKM1 and PKM2, was stronger in Capan-2 and HPAF-II than in Mia PaCa-2.

The proton-coupled monocarboxylate transporters MCT1 and MCT4 mediate most of the lactate transport across the plasma membrane. Although they are bidirectional transporters, MCT1 has a high and MCT4 has a low affinity for lactate, making MCT1 mainly responsible for the influx of lactate, and MCT4 primarily responsible for the efflux of lactate [123]. The western blot showed a lower expression of MCT1 in HPAF-II and a lower expression of MCT4 in Mia PaCa-2 compared with the other cell lines. This indicates that HPAF-II has a lower influx capacity, and Mia PaCa-2 has a lower efflux capacity of lactate compared with the other cell lines.

Lastly, the expression of the OXPHOS proteins, SDHB and COXII, ATP5A, which belong to mitochondrial complex II, IV and V, respectively, were investigated. The expression of OXPHOS related proteins has been demonstrated to be highly heterogeneous between individual tumors [135]. Among the OXPHOS related proteins investigated in this study, ATP5A, which in the presence of a proton gradient produces ATP from ADP, was the only protein expressed in all three cell lines. For SDHB, which transfers electrons from succinate to ubiquinone, only a weak band was detected in HPAF-II and Mia PaCa-2. COXII, which is the last enzyme in the ETC and catalyzes the reduction of O_2 to H_2O, showed no detectable expression in any of the cell lines. The low expression of OXPHOS proteins indicates a low OXPHOS rate in the cell lines used in this study, which have also previously been reported for the Mia PaCa-2 and Capan-2 cell lines [135].

Overall, the western blot results further confirm the heterogeneity found between the three cell lines, which also reflects the heterogeneity found in PDAC in general. Comparing the cell lines, Capan-2 expressed all the same proteins as HPAF-II and Mia PaCa-2, except for the OXPHOS protein SDHB, while HPAF-II exhibited a very weak expression of MCT1, indicating a lower influx capacity of lactate. Notably, Mia PaCa-2, which showed the highest increase in lactate secretion when incubated with PSC-CMs (Figure 4.7 and 4.8), was also found to have a lower basal expression of two lactate secretion regulation enzymes PKM2 and MCT4, compared with the other cell lines. However, further investigations are required to find out if PSC-CMs have any influence on the expression or activity of both enzymes.

In this study, and in accordance with previous studies, PSC-CMs are shown to affect cancer cell behavior through a variety of different molecular mechanisms, suggesting that PSC-secreted factors promote tumor progression [31, 100, 136-139]. Analysis of the secretome from PSCs provides valuable information which can be used to further explore which of the secreted factors promote tumor progression in PCCs and the molecular mechanisms behind this. A secretome-based analysis of PSC-1, PSC-2 and HPaSteC was performed to investigate which secreted factors are present in the PSC-CMs used in this study and what their molecular functions are.

A total of 685 different proteins were identified in CM from PSC-1, PSC-2 and HPaSteC. However, the results revealed large differences in the number of proteins secreted by the three PSCs (Figure 4.13). Most proteins were detected in CM from HPaSteC with 684 different

proteins, followed by CM from PSC-1 with 332 proteins. For CM from PSC-2, which is derived from a neoadjuvantly treated patient, only 93 different proteins were detected. Moreover, a large difference was also seen in the intensity of individual proteins detected in the three PSC-CMs. This large difference in the amount and expression of proteins detected is probably the reason for some of the observed variation in the effect of the PSC-CMs on PCCs.

To determine the functional role of the secreted proteins, a GO analysis was performed using the DAVID bioinformatics resource tool (Table 5). Some of the top pathways from the GO analysis were focal adhesion and ECM receptor interactions. Proteins associated with focal adhesion constituted 8.4% of PSC-1, 20.4% of PSC-2 and 5.8% of HPaSteC secreted proteins, while 6.9% of PSC-1, 18.3% of PSC-2 and 3.5% of HPaSteC secreted proteins were associated with ECM receptor interactions. Both of these pathways include ECM structural proteins such as collagens and cell adhesion proteins such as laminins and fibronectin. High expression of collagen has been shown to correlate with drug resistance in ovarian and breast cancer, and collagen-1 has been shown to promote chemoresistance in PDAC [31, 140-142]. PSC-secreted fibronectin has also been reported to play a key role in the development of resistance to gemcitabine. The same study also showed that, compared to fibronectin alone, the PSC-CM induced a significantly higher chemoresistance in the PCC, suggesting that other components of the PSC-secretome may also contribute to the induction of chemoresistance [112].

Moreover, 7.8% of PSC-1, 16.1% of PSC-2 and 5.3% of HPaSteC secreted proteins were associated with PI3K-Akt signaling. PI3K-Akt signaling is one of the most commonly deregulated signaling pathways in cancer. It is estimated that in at least 60% of PDAC patients, the PI3K-Akt signaling pathway is deregulated in their tumor [143, 144]. It has also previously been shown that PSCs activate the c-Met/PI3K/Akt pathway in PCCs, inhibiting cancer cell apoptosis, thus enhancing chemoresistance to gemcitabine in PCCs [95]. From a metabolic perspective, Akt has been shown to increase glucose uptake through activation of GLUT1 and to stimulate glycolysis by phosphorylation of HK2 [145, 146].

Finally, the pathways including the highest number of proteins identified from the PSC-1 and HPaSteC secretome were metabolic pathways, including 12.3% of PSC-1, 6.5% of PSC-2 and 11.4% of HPaSteC secreted proteins. Also, previous reports indicate that the largest fraction of PSC-secreted proteins relates to metabolic pathways [112, 147]. In contrast to PSC-secreted proteins related to PI3K-Akt signaling and the ECM, which have already been reported to

contribute to enhanced chemoresistance, it is currently unknown if PSC-secreted proteins associated with metabolic pathways have any impact on chemoresistance in PDAC.

In total, 78 different metabolism-related proteins were found in the PSC-CMs in this study, and 25 of them were related to carbon metabolism. Further investigations into the carbon metabolism-related proteins revealed that half of them were involved in glycolysis, seven were involved in the TCA cycle, while serine biosynthesis and PPP accounted for two proteins each (Figure 4.14). The remaining two were ADH5 and ACAT2, which are involved in alcohol and aldehyde metabolism, and lipid metabolism, respectively [148, 149]. However, while the role of these carbon metabolism-related enzymes is well known when located intracellularly, it remains unclear why they are secreted by PSCs, and which function they have at the extracellular level in PDAC.

Several studies have explored the extracellular presence of glycolytic enzymes, and some of the enzymes were shown to have structural and regulatory functions and to play a role in cell-cell communication [150-152]. Glycolytic enzymes found in secreted exosomes are also believed to form temporary structural-functional complexes within the exosome, which are referred to as metabolons [153]. The secreted metabolic proteins can also be taken up by PCCs through macropinocytosis and be used as fuel [70]. However, to find out the role of the metabolic proteins secreted from PSCs and to figure out if they have any impact on chemoresistance in PCCs, requires further investigation.

Comparing the carbon metabolism related proteins between the three PSC-CMs, eight proteins were found in HPaSteC CM exclusively, 17 were found in both PSC-1 and HPaSteC, while ALDOA, PKM, TPI1 and PSAT1 were the only carbon metabolism-related proteins found in all three secretomes (Table 6). High expression of both ALDOA and PKM2 has been shown to correlate with poor prognosis in PDAC patients [154, 155]. TPI1, which displayed the highest LFQ intensity among the carbon metabolism-related proteins detected in CM from PSC-1 and PSC-2, was shown to be one of the most abundant proteins in serum from PDAC patients with poor survival before and after chemotherapy. Its levels have also been shown to gradually increase as the disease progresses [156, 157]. Less is known about PSAT1 in PDAC, but it has been shown to contribute to cell proliferation and cancer development and is found to be overexpressed in breast and lung cancer [158]. However, as all these enzymes are known to play an important role either in PDAC or other cancers, their impact when secreted out of the

cell has not been investigated much. How they influence PCCs, when secreted from PSCs, is also yet to be understood.

The glycolysis enzyme alpha-enolase (ENO1) was the carbon metabolism-related protein with the highest LFQ intensity in the HPaSteC secretome and also among the proteins with the highest LFQ intensity in PSC-1. ENO1 is shown to have a multifunctional role in PDAC depending on its location [159]. Outside the cell, it acts as a plasminogen receptor, which enhances the ability of PDAC cells to degrade ECM and may thus promote tumor invasion and metastasis [156, 159-162].

The secretome analysis performed in this study provides an overview of metabolic proteins secreted by PSCs that originated from a healthy human (HPaSteC), a neoadjuvant treated PDAC with four cycles of FOLFIRINOX (PSC-2), and an untreated PDAC (PSC-1). Considerable differences in proteins secreted between the different PSC-CMs were found. Some of these differences could be explained by the different origins of the PSCs. HPaSteC originates from the stroma of a fetal pancreas, which is considerably different from the stroma in a grown-up pancreas. The different composition of secreted proteins found for HPaSteC compared with the other two cell lines could be reflected by the different ECM composition and function the fetal stroma has compared with adult stroma. One possible explanation for the significantly larger number of proteins secreted by HPaSteC compared with the other PSCs could be that the fetal stroma contributes to the further development of the organ and thereby needs to secrete a large number of proteins and factors required.

Regards to PSC-2, the number of secreted proteins was significantly lower compared with HPaSteC and PSC-1. The source tumor from which PSC-2 was isolated from was neoadjuvantly treated, and therefore, it is possible that the chemotherapy has caused a decrease in the secretion activity of the PSCs. Another possible explanation could be that these PSCs come from areas where much of the cancer had regressed under treatment and that the PSCs therefore become less active. Further investigations are needed to understand the differences between the different PSC lines. However, these results indicate that it is important to keep in mind that the origin of the PSCs used in experiments should be considered, as the differences in function and composition of PSCs from different origins also could impact the results. To further investigate the impact of PSCs on the PCCs, a PSC line originating from untreated cancer, such as PSC-1 will probably lead to the most relevant results. More studies are required

to understand the role of the PSC-secreted metabolic proteins in the context of gemcitabine chemoresistance and metabolic rewiring of PDAC.

To summarize, a general trend of increased viability, proliferation, glucose transport, glycolysis and reduced chemosensitivity was seen in PCCs exposed to PSC-CM compared to PCCs incubated with SFM. Therefore, this study provides further evidence delineating the role of PSCs as an extracellular factor supporting the cancer cells through various mechanisms. Moreover, considerable variations were found both between the three different PCC lines and the three different PSC-CMs, indicating strong inter-tumor heterogeneity, a hallmark of PDAC. The western blot analysis revealed considerable differences in the expression of different metabolic proteins between the three PCC lines, while the secretome analysis revealed large variations in the number of proteins and the intensity of the proteins detected between the three different PSC-CMs. The heterogeneity found in this study at multiple levels further confirms that metabolic rewiring in PDAC is far from a uniform phenomenon, which makes it challenging to investigate. The secretome analysis also revealed that a large fraction of the proteins detected in the secretome of PSCs is metabolic proteins. However, the PSC-secreted metabolic proteins have to be further investigated to figure out whether they impact the tumor-stroma crosstalk and if they play a role in chemosensitivity in PDAC.

Some of the limitations of this study includes the selection of PCCs and PSCs. For further experiments, it could be useful to select PCC lines based on metabolic profiles found in recent literature and potentially include a cell line without KRAS mutation. It could also be useful to include more than one PSC line per condition (neoadjuvantly treated and untreated) to be able to tell if the differences detected are common for the condition of the source tumor or if it only applies to that single PSC line. Regards to the experimental setup, it would be useful to perform such experiments in hypoxic conditions to make it even more similar to the actual TME in PDAC.

6 Conclusion

In conclusion, the work conducted in this study revealed a general trend of increased viability, proliferation, glucose transport, glycolysis and reduced chemosensitivity in PCCs exposed to PSC-CM compared to PCCs incubated with SFM. This further confirms the impact of PSC-secreted factors on chemoresistance and implies that PSC-secreted factors also influence the metabolic rewiring in PDAC. A large fraction of the proteins detected in the secretome of PSCs is involved in metabolic pathways inside the cells. However, what their role is when secreted out of the cell, and if and how they influence PCCs, needs to be further investigated. Inter-patient heterogeneity poses a major challenge in the treatment of PDAC. This heterogeneity was also reflected in this study by the considerable variation in results between both the PSCs and PCCs. Further investigations into the molecular mechanisms underlying the PSC-CM induced changes in glucose metabolism and chemosensitivity in PCCs are needed to enable the development of more effective treatment strategies.

References

1. Leung, P.S., *Overview of the pancreas.* Adv Exp Med Biol, 2010. **690**: p. 3-12.
2. Zhou, Q. and D.A. Melton, *Pancreas regeneration.* Nature, 2018. **557**(7705): p. 351-358.
3. Hegyi, P., et al., *Pancreatic ductal bicarbonate secretion: challenge of the acinar Acid load.* Front Physiol, 2011. **2**: p. 36.
4. Pandol, S.J., in *The Exocrine Pancreas*. 2010: San Rafael (CA).
5. J. Gordon Betts, K.A.Y., James A. Wise, Eddie Johnson, Brandon Poe, Dean H. Kruse, Oksana Korol, Jody E. Johnson, Mark Womble, Peter DeSaix, *Anatomy and Physiology*. 2013, OpenStax: cnx.org/content/col11496/1.6.
6. Weinberg, R., *Biology of Cancer*. 2 ed. 2014, New York: Garland Publishing Inc.
7. Shyr, D. and Q. Liu, *Next generation sequencing in cancer research and clinical application.* Biol Proced Online, 2013. **15**(1): p. 4.
8. Jun, S.Y. and S.M. Hong, *Nonductal Pancreatic Cancers.* Surg Pathol Clin, 2016. **9**(4): p. 581-593.
9. McGuigan, A., et al., *Pancreatic cancer: A review of clinical diagnosis, epidemiology, treatment and outcomes.* World J Gastroenterol, 2018. **24**(43): p. 4846-4861.
10. Vareedayah, A.A., S. Alkaade, and J.R. Taylor, *Pancreatic Adenocarcinoma.* Mo Med, 2018. **115**(3): p. 230-235.
11. Rahib, L., et al., *Projecting cancer incidence and deaths to 2030: the unexpected burden of thyroid, liver, and pancreas cancers in the United States.* Cancer Res, 2014. **74**(11): p. 2913-21.
12. Sung, H., et al., *Global cancer statistics 2020: GLOBOCAN estimates of incidence and mortality worldwide for 36 cancers in 185 countries.* CA Cancer J Clin, 2021.
13. Ferlay J, E.M., Lam F, Colombet M, Mery L, Piñeros M, Znaor A, Soerjomataram I, Bray F. *Global Cancer Observatory: Cancer Today*. [cited 2021 12/2]; Available from: https://gco.iarc.fr/today.
14. Norway, C.R.o., *Cancer in Norway 2019- Cancer incidence, mortality, survival and prevalence in Norway*. 2020, Cancer Registry of Norway: Oslo.
15. Rawla, P., T. Sunkara, and V. Gaduputi, *Epidemiology of Pancreatic Cancer: Global Trends, Etiology and Risk Factors.* World J Oncol, 2019. **10**(1): p. 10-27.
16. Kreftforeningen. *Bukspyttkjertelkreft*. 2021; Available from: https://kreftforeningen.no/om-kreft/kreftformer/bukspyttkjertelkreft/.
17. Alberts B, J.A., Lewis J, et al., *Molecular Biology of the Cell*. 2002, Garland Science: New York.
18. Christenson, E.S., E. Jaffee, and N.S. Azad, *Current and emerging therapies for patients with advanced pancreatic ductal adenocarcinoma: a bright future.* Lancet Oncol, 2020. **21**(3): p. e135-e145.
19. Waters, A.M. and C.J. Der, *KRAS: The Critical Driver and Therapeutic Target for Pancreatic Cancer.* Cold Spring Harb Perspect Med, 2018. **8**(9).
20. Zeitouni, D., et al., *KRAS Mutant Pancreatic Cancer: No Lone Path to an Effective Treatment.* Cancers (Basel), 2016. **8**(4).
21. Grant, T.J., K. Hua, and A. Singh, *Molecular Pathogenesis of Pancreatic Cancer.* Prog Mol Biol Transl Sci, 2016. **144**: p. 241-275.
22. Dardare, J., et al., *SMAD4 and the TGFbeta Pathway in Patients with Pancreatic Ductal Adenocarcinoma.* Int J Mol Sci, 2020. **21**(10).
23. Qian, Y., et al., *Molecular alterations and targeted therapy in pancreatic ductal adenocarcinoma.* J Hematol Oncol, 2020. **13**(1): p. 130.

24. Adamska, A., A. Domenichini, and M. Falasca, *Pancreatic Ductal Adenocarcinoma: Current and Evolving Therapies.* Int J Mol Sci, 2017. **18**(7).
25. Masiak-Segit, W., et al., *Surgical treatment of pancreatic cancer.* Pol Przegl Chir, 2018. **90**(2): p. 45-53.
26. Torphy, R.J., Y. Fujiwara, and R.D. Schulick, *Pancreatic cancer treatment: better, but a long way to go.* Surg Today, 2020. **50**(10): p. 1117-1125.
27. Pusceddu, S., et al., *Comparative Effectiveness of Gemcitabine plus Nab-Paclitaxel and FOLFIRINOX in the First-Line Setting of Metastatic Pancreatic Cancer: A Systematic Review and Meta-Analysis.* Cancers (Basel), 2019. **11**(4).
28. Amrutkar, M., et al., *Establishment and Characterization of Paired Primary Cultures of Human Pancreatic Cancer Cells and Stellate Cells Derived from the Same Tumor.* Cells, 2020. **9**(1).
29. Weniger, M., K.C. Honselmann, and A.S. Liss, *The Extracellular Matrix and Pancreatic Cancer: A Complex Relationship.* Cancers (Basel), 2018. **10**(9).
30. Hosein, A.N., R.A. Brekken, and A. Maitra, *Pancreatic cancer stroma: an update on therapeutic targeting strategies.* Nat Rev Gastroenterol Hepatol, 2020. **17**(8): p. 487-505.
31. Amrutkar, M. and I.P. Gladhaug, *Stellate Cells Aid Growth-Permissive Metabolic Reprogramming and Promote Gemcitabine Chemoresistance in Pancreatic Cancer.* Cancers (Basel), 2021. **13**(4).
32. Hessmann, E., et al., *Microenvironmental Determinants of Pancreatic Cancer.* Physiol Rev, 2020. **100**(4): p. 1707-1751.
33. Elyada, E., et al., *Cross-Species Single-Cell Analysis of Pancreatic Ductal Adenocarcinoma Reveals Antigen-Presenting Cancer-Associated Fibroblasts.* Cancer Discov, 2019. **9**(8): p. 1102-1123.
34. Yao, W., A. Maitra, and H. Ying, *Recent insights into the biology of pancreatic cancer.* EBioMedicine, 2020. **53**: p. 102655.
35. Sunami, Y., J. Haussler, and J. Kleeff, *Cellular Heterogeneity of Pancreatic Stellate Cells, Mesenchymal Stem Cells, and Cancer-Associated Fibroblasts in Pancreatic Cancer.* Cancers (Basel), 2020. **12**(12).
36. Cros, J., et al., *Tumor Heterogeneity in Pancreatic Adenocarcinoma.* Pathobiology, 2018. **85**(1-2): p. 64-71.
37. Heid, I., et al., *Co-clinical Assessment of Tumor Cellularity in Pancreatic Cancer.* Clin Cancer Res, 2017. **23**(6): p. 1461-1470.
38. Erkan, M., et al., *The activated stroma index is a novel and independent prognostic marker in pancreatic ductal adenocarcinoma.* Clin Gastroenterol Hepatol, 2008. **6**(10): p. 1155-61.
39. Ohlund, D., et al., *Distinct populations of inflammatory fibroblasts and myofibroblasts in pancreatic cancer.* J Exp Med, 2017. **214**(3): p. 579-596.
40. Neuzillet, C., et al., *Inter- and intra-tumoural heterogeneity in cancer-associated fibroblasts of human pancreatic ductal adenocarcinoma.* J Pathol, 2019. **248**(1): p. 51-65.
41. Yu, Y., et al., *Targeting Aggressive Fibroblasts to Enhance the Treatment of Pancreatic Cancer.* Expert Opin Ther Targets, 2021. **25**(1): p. 5-13.
42. Pereira, B.A., et al., *CAF Subpopulations: A New Reservoir of Stromal Targets in Pancreatic Cancer.* Trends Cancer, 2019. **5**(11): p. 724-741.
43. Helms, E., M.K. Onate, and M.H. Sherman, *Fibroblast Heterogeneity in the Pancreatic Tumor Microenvironment.* Cancer Discov, 2020. **10**(5): p. 648-656.
44. Ferdek, P.E. and M.A. Jakubowska, *Biology of pancreatic stellate cells-more than just pancreatic cancer.* Pflugers Arch, 2017. **469**(9): p. 1039-1050.

45. Watari, N., Y. Hotta, and Y. Mabuchi, *Morphological studies on a vitamin A-storing cell and its complex with macrophage observed in mouse pancreatic tissues following excess vitamin A administration.* Okajimas Folia Anat Jpn, 1982. **58**(4-6): p. 837-58.
46. Apte, M.V., et al., *Periacinar stellate shaped cells in rat pancreas: identification, isolation, and culture.* Gut, 1998. **43**(1): p. 128-33.
47. Bachem, M.G., et al., *Identification, culture, and characterization of pancreatic stellate cells in rats and humans.* Gastroenterology, 1998. **115**(2): p. 421-32.
48. Jin, G., et al., *Molecular Mechanism of Pancreatic Stellate Cells Activation in Chronic Pancreatitis and Pancreatic Cancer.* J Cancer, 2020. **11**(6): p. 1505-1515.
49. Thomas, D. and P. Radhakrishnan, *Pancreatic Stellate Cells: The Key Orchestrator of The Pancreatic Tumor Microenvironment.* Adv Exp Med Biol, 2020. **1234**: p. 57-70.
50. Zhou, Y., et al., *Pancreatic Stellate Cells: A Rising Translational Physiology Star as a Potential Stem Cell Type for Beta Cell Neogenesis.* Front Physiol, 2019. **10**: p. 218.
51. Mekapogu, A.R., et al., *Multifunctional role of pancreatic stellate cells in pancreatic cancer.* Annals of Pancreatic Cancer, 2019. **2**.
52. Judge, A. and M.S. Dodd, *Metabolism.* Essays Biochem, 2020. **64**(4): p. 607-647.
53. Chaudhry, R. and M. Varacallo, *Biochemistry, Glycolysis*, in *StatPearls*. 2021: Treasure Island (FL).
54. Zimmermann, F.K., *Glycolysis*, in *Encyclopedia of Genetics*. 2001, Academic Press. p. 885-888.
55. Martinez-Reyes, I. and N.S. Chandel, *Mitochondrial TCA cycle metabolites control physiology and disease.* Nat Commun, 2020. **11**(1): p. 102.
56. DeBerardinis, R.J. and N.S. Chandel, *Fundamentals of cancer metabolism.* Sci Adv, 2016. **2**(5): p. e1600200.
57. Pavlova, N.N. and C.B. Thompson, *The Emerging Hallmarks of Cancer Metabolism.* Cell Metab, 2016. **23**(1): p. 27-47.
58. Yan, L., et al., *Glucose Metabolism in Pancreatic Cancer.* Cancers (Basel), 2019. **11**(10).
59. Hu, H., et al., *Phosphoinositide 3-Kinase Regulates Glycolysis through Mobilization of Aldolase from the Actin Cytoskeleton.* Cell, 2016. **164**(3): p. 433-46.
60. Shukla, S.K., et al., *MUC1 and HIF-1alpha Signaling Crosstalk Induces Anabolic Glucose Metabolism to Impart Gemcitabine Resistance to Pancreatic Cancer.* Cancer Cell, 2017. **32**(1): p. 71-87 e7.
61. Perera, R.M. and N. Bardeesy, *Pancreatic Cancer Metabolism: Breaking It Down to Build It Back Up.* Cancer Discov, 2015. **5**(12): p. 1247-61.
62. Derle, A., et al., *The role of metabolic adaptation to nutrient stress in pancreatic cancer.* Cell Stress, 2018. **2**(12): p. 332-339.
63. Blum, R. and Y. Kloog, *Metabolism addiction in pancreatic cancer.* Cell Death Dis, 2014. **5**: p. e1065.
64. Halbrook, C.J. and C.A. Lyssiotis, *Employing Metabolism to Improve the Diagnosis and Treatment of Pancreatic Cancer.* Cancer Cell, 2017. **31**(1): p. 5-19.
65. Dunne, R.F. and A.F. Hezel, *Genetics and Biology of Pancreatic Ductal Adenocarcinoma.* Hematol Oncol Clin North Am, 2015. **29**(4): p. 595-608.
66. Tape, C.J., et al., *Oncogenic KRAS Regulates Tumor Cell Signaling via Stromal Reciprocation.* Cell, 2016. **165**(7): p. 1818.
67. Ireland, L., et al., *Chemoresistance in Pancreatic Cancer Is Driven by Stroma-Derived Insulin-Like Growth Factors.* Cancer Res, 2016. **76**(23): p. 6851-6863.
68. Li, X., et al., *Sonic hedgehog paracrine signaling activates stromal cells to promote perineural invasion in pancreatic cancer.* Clin Cancer Res, 2014. **20**(16): p. 4326-38.

69. Liu, J., et al., *Critical role of oncogenic KRAS in pancreatic cancer (Review).* Mol Med Rep, 2016. **13**(6): p. 4943-9.
70. Commisso, C., et al., *Macropinocytosis of protein is an amino acid supply route in Ras-transformed cells.* Nature, 2013. **497**(7451): p. 633-7.
71. Davidson, S.M., et al., *Direct evidence for cancer-cell-autonomous extracellular protein catabolism in pancreatic tumors.* Nat Med, 2017. **23**(2): p. 235-241.
72. Pavlides, S., et al., *The reverse Warburg effect: aerobic glycolysis in cancer associated fibroblasts and the tumor stroma.* Cell Cycle, 2009. **8**(23): p. 3984-4001.
73. Fu, Y., et al., *The reverse Warburg effect is likely to be an Achilles' heel of cancer that can be exploited for cancer therapy.* Oncotarget, 2017. **8**(34): p. 57813-57825.
74. Wilde, L., et al., *Metabolic coupling and the Reverse Warburg Effect in cancer: Implications for novel biomarker and anticancer agent development.* Semin Oncol, 2017. **44**(3): p. 198-203.
75. Binenbaum, Y., S. Na'ara, and Z. Gil, *Gemcitabine resistance in pancreatic ductal adenocarcinoma.* Drug Resist Updat, 2015. **23**: p. 55-68.
76. Amrutkar, M. and I.P. Gladhaug, *Pancreatic Cancer Chemoresistance to Gemcitabine.* Cancers (Basel), 2017. **9**(11).
77. Marechal, R., et al., *Human equilibrative nucleoside transporter 1 and human concentrative nucleoside transporter 3 predict survival after adjuvant gemcitabine therapy in resected pancreatic adenocarcinoma.* Clin Cancer Res, 2009. **15**(8): p. 2913-9.
78. Spratlin, J., et al., *The absence of human equilibrative nucleoside transporter 1 is associated with reduced survival in patients with gemcitabine-treated pancreas adenocarcinoma.* Clin Cancer Res, 2004. **10**(20): p. 6956-61.
79. Bhutia, Y.D., et al., *CNT1 expression influences proliferation and chemosensitivity in drug-resistant pancreatic cancer cells.* Cancer Res, 2011. **71**(5): p. 1825-35.
80. Saiki, Y., et al., *DCK is frequently inactivated in acquired gemcitabine-resistant human cancer cells.* Biochem Biophys Res Commun, 2012. **421**(1): p. 98-104.
81. Weizman, N., et al., *Macrophages mediate gemcitabine resistance of pancreatic adenocarcinoma by upregulating cytidine deaminase.* Oncogene, 2014. **33**(29): p. 3812-9.
82. Wang, C., et al., *Establishment of human pancreatic cancer gemcitabineresistant cell line with ribonucleotide reductase overexpression.* Oncol Rep, 2015. **33**(1): p. 383-90.
83. Rose, M.G., M.P. Farrell, and J.C. Schmitz, *Thymidylate synthase: a critical target for cancer chemotherapy.* Clin Colorectal Cancer, 2002. **1**(4): p. 220-9.
84. Rejiba, S., et al., *Gemcitabine-based chemogene therapy for pancreatic cancer using Ad-dCK::UMK GDEPT and TS/RR siRNA strategies.* Neoplasia, 2009. **11**(7): p. 637-50.
85. Amrutkar, M., et al., *Differential Gemcitabine Sensitivity in Primary Human Pancreatic Cancer Cells and Paired Stellate Cells Is Driven by Heterogenous Drug Uptake and Processing.* Cancers (Basel), 2020. **12**(12).
86. Hesler, R.A., et al., *TGF-beta-induced stromal CYR61 promotes resistance to gemcitabine in pancreatic ductal adenocarcinoma through downregulation of the nucleoside transporters hENT1 and hCNT3.* Carcinogenesis, 2016. **37**(11): p. 1041-1051.
87. Dalin, S., et al., *Deoxycytidine Release from Pancreatic Stellate Cells Promotes Gemcitabine Resistance.* Cancer Res, 2019. **79**(22): p. 5723-5733.
88. Erkan, M., et al., *Periostin creates a tumor-supportive microenvironment in the pancreas by sustaining fibrogenic stellate cell activity.* Gastroenterology, 2007. **132**(4): p. 1447-64.

89. Haqq, J., et al., *Pancreatic stellate cells and pancreas cancer: current perspectives and future strategies.* Eur J Cancer, 2014. **50**(15): p. 2570-82.
90. Muerkoster, S., et al., *Tumor stroma interactions induce chemoresistance in pancreatic ductal carcinoma cells involving increased secretion and paracrine effects of nitric oxide and interleukin-1beta.* Cancer Res, 2004. **64**(4): p. 1331-7.
91. Armstrong, T., et al., *Type I collagen promotes the malignant phenotype of pancreatic ductal adenocarcinoma.* Clin Cancer Res, 2004. **10**(21): p. 7427-37.
92. Neumann, C.C.M., et al., *Tumor-stromal cross-talk modulating the therapeutic response in pancreatic cancer.* Hepatobiliary Pancreat Dis Int, 2018. **17**(5): p. 461-472.
93. Long, K.B., et al., *IL6 Receptor Blockade Enhances Chemotherapy Efficacy in Pancreatic Ductal Adenocarcinoma.* Mol Cancer Ther, 2017. **16**(9): p. 1898-1908.
94. Duluc, C., et al., *Pharmacological targeting of the protein synthesis mTOR/4E-BP1 pathway in cancer-associated fibroblasts abrogates pancreatic tumour chemoresistance.* EMBO Mol Med, 2015. **7**(6): p. 735-53.
95. Xu, J., et al., *Paracrine HGF promotes EMT and mediates the effects of PSC on chemoresistance by activating c-Met/PI3K/Akt signaling in pancreatic cancer in vitro.* Life Sci, 2020. **263**: p. 118523.
96. Richards, K.E., et al., *Cancer-associated fibroblast exosomes regulate survival and proliferation of pancreatic cancer cells.* Oncogene, 2017. **36**(13): p. 1770-1778.
97. Fang, Y., et al., *Exosomal miRNA-106b from cancer-associated fibroblast promotes gemcitabine resistance in pancreatic cancer.* Exp Cell Res, 2019. **383**(1): p. 111543.
98. Deer, E.L., et al., *Phenotype and genotype of pancreatic cancer cell lines.* Pancreas, 2010. **39**(4): p. 425-35.
99. *ATCC*. [cited 2021; Available from: https://www.lgcstandards-atcc.org/?geo_country=no.
100. Lenggenhager, D., et al., *Commonly Used Pancreatic Stellate Cell Cultures Differ Phenotypically and in Their Interactions with Pancreatic Cancer Cells.* Cells, 2019. **8**(1).
101. Kumar, P., A. Nagarajan, and P.D. Uchil, *Analysis of Cell Viability by the MTT Assay.* Cold Spring Harb Protoc, 2018. **2018**(6).
102. Cao, L., et al., *Glycometabolic rearrangements--aerobic glycolysis in pancreatic cancer: causes, characteristics and clinical applications.* J Exp Clin Cancer Res, 2020. **39**(1): p. 267.
103. Reckzeh, E.S. and H. Waldmann, *Small-Molecule Inhibition of Glucose Transporters GLUT-1-4.* Chembiochem, 2020. **21**(1-2): p. 45-52.
104. Rai, V. and S. Agrawal, *Targets (Metabolic Mediators) of Therapeutic Importance in Pancreatic Ductal Adenocarcinoma.* International Journal of Molecular Sciences, 2020. **21**(22): p. 8502.
105. Ito, H., et al., *Glucose transporter-1 gene expression is associated with pancreatic cancer invasiveness and MMP-2 activity.* Surgery, 2004. **136**(3): p. 548-56.
106. Muller, T. and D. Winter, *Systematic Evaluation of Protein Reduction and Alkylation Reveals Massive Unspecific Side Effects by Iodine-containing Reagents.* Mol Cell Proteomics, 2017. **16**(7): p. 1173-1187.
107. Morris, R.M. and B.L. Nunn, *Sample preparation and processing for planktonic microbial community proteomics.* Methods Enzymol, 2013. **531**: p. 271-87.
108. Dennis, G., Jr., et al., *DAVID: Database for Annotation, Visualization, and Integrated Discovery.* Genome Biol, 2003. **4**(5): p. P3.
109. Huang da, W., B.T. Sherman, and R.A. Lempicki, *Systematic and integrative analysis of large gene lists using DAVID bioinformatics resources.* Nat Protoc, 2009. **4**(1): p. 44-57.

110. Kanehisa, M. and S. Goto, *KEGG: kyoto encyclopedia of genes and genomes.* Nucleic Acids Res, 2000. **28**(1): p. 27-30.
111. Orth, M., et al., *Pancreatic ductal adenocarcinoma: biological hallmarks, current status, and future perspectives of combined modality treatment approaches.* Radiat Oncol, 2019. **14**(1): p. 141.
112. Amrutkar, M., et al., *Secretion of fibronectin by human pancreatic stellate cells promotes chemoresistance to gemcitabine in pancreatic cancer cells.* BMC Cancer, 2019. **19**(1): p. 596.
113. McCarroll, J.A., et al., *Role of pancreatic stellate cells in chemoresistance in pancreatic cancer.* Front Physiol, 2014. **5**: p. 141.
114. Sherman, M.H., et al., *Stromal cues regulate the pancreatic cancer epigenome and metabolome.* Proc Natl Acad Sci U S A, 2017. **114**(5): p. 1129-1134.
115. Fu, Y., et al., *The critical roles of activated stellate cells-mediated paracrine signaling, metabolism and onco-immunology in pancreatic ductal adenocarcinoma.* Mol Cancer, 2018. **17**(1): p. 62.
116. Cohen, R., et al., *Targeting cancer cell metabolism in pancreatic adenocarcinoma.* Oncotarget, 2015. **6**(19): p. 16832-47.
117. Olivares, O. and S. Vasseur, *Metabolic rewiring of pancreatic ductal adenocarcinoma: New routes to follow within the maze.* Int J Cancer, 2016. **138**(4): p. 787-96.
118. Qin, C., et al., *Metabolism of pancreatic cancer: paving the way to better anticancer strategies.* Mol Cancer, 2020. **19**(1): p. 50.
119. Cameron, M.E., A. Yakovenko, and J.G. Trevino, *Glucose and Lactate Transport in Pancreatic Cancer: Glycolytic Metabolism Revisited.* J Oncol, 2018. **2018**: p. 6214838.
120. Isayev, O., et al., *Inhibition of glucose turnover by 3-bromopyruvate counteracts pancreatic cancer stem cell features and sensitizes cells to gemcitabine.* Oncotarget, 2014. **5**(13): p. 5177-89.
121. Coleman, M.C., et al., *2-deoxy-D-glucose causes cytotoxicity, oxidative stress, and radiosensitization in pancreatic cancer.* Free Radic Biol Med, 2008. **44**(3): p. 322-31.
122. Wu, D.H., et al., *miR-124 Suppresses Pancreatic Ductal Adenocarcinoma Growth by Regulating Monocarboxylate Transporter 1-Mediated Cancer Lactate Metabolism.* Cell Physiol Biochem, 2018. **50**(3): p. 924-935.
123. Kong, S.C., et al., *Monocarboxylate Transporters MCT1 and MCT4 Regulate Migration and Invasion of Pancreatic Ductal Adenocarcinoma Cells.* Pancreas, 2016. **45**(7): p. 1036-47.
124. Schneiderhan, W., et al., *CD147 silencing inhibits lactate transport and reduces malignant potential of pancreatic cancer cells in in vivo and in vitro models.* Gut, 2009. **58**(10): p. 1391-8.
125. Kang, S.A., et al., *Discovery of Small-Molecule Selective mTORC1 Inhibitors via Direct Inhibition of Glucose Transporters.* Cell Chem Biol, 2019. **26**(9): p. 1203-1213 e13.
126. Valvezan, A.J. and B.D. Manning, *Molecular logic of mTORC1 signalling as a metabolic rheostat.* Nat Metab, 2019. **1**(3): p. 321-333.
127. Kim, L.C., R.S. Cook, and J. Chen, *mTORC1 and mTORC2 in cancer and the tumor microenvironment.* Oncogene, 2017. **36**(16): p. 2191-2201.
128. de la Cruz Lopez, K.G., et al., *mTORC1 as a Regulator of Mitochondrial Functions and a Therapeutic Target in Cancer.* Front Oncol, 2019. **9**: p. 1373.
129. Buller, C.L., C.W. Heilig, and F.C. Brosius, 3rd, *GLUT1 enhances mTOR activity independently of TSC2 and AMPK.* Am J Physiol Renal Physiol, 2011. **301**(3): p. F588-96.
130. Liu, Y., et al., *Periostin promotes the chemotherapy resistance to gemcitabine in pancreatic cancer.* Tumour Biol, 2016. **37**(11): p. 15283-15291.

131. TeSlaa, T. and M.A. Teitell, *Techniques to monitor glycolysis.* Methods Enzymol, 2014. **542**: p. 91-114.
132. Institute, N.C., *RAS Cell Lines*. 2018.
133. Patra, K.C. and N. Hay, *Hexokinase 2 as oncotarget.* Oncotarget, 2013. **4**(11): p. 1862-3.
134. James, A.D., et al., *Cutting off the fuel supply to calcium pumps in pancreatic cancer cells: role of pyruvate kinase-M2 (PKM2).* British Journal of Cancer, 2020. **122**(2): p. 266-278.
135. Masoud, R., et al., *Targeting Mitochondrial Complex I Overcomes Chemoresistance in High OXPHOS Pancreatic Cancer.* Cell Rep Med, 2020. **1**(8): p. 100143.
136. Hwang, R.F., et al., *Cancer-associated stromal fibroblasts promote pancreatic tumor progression.* Cancer Res, 2008. **68**(3): p. 918-26.
137. Gao, Z., et al., *Pancreatic stellate cells increase the invasion of human pancreatic cancer cells through the stromal cell-derived factor-1/CXCR4 axis.* Pancreatology, 2010. **10**(2-3): p. 186-93.
138. Tjomsland, V., et al., *Functional heterogeneity in tumor-derived human pancreatic stellate cells: Differential expression of HGF and implications for mitogenic signaling and migration in pancreatic cancer cells.* Oncotarget, 2017. **8**(42): p. 71672-71684.
139. Bachem, M.G., et al., *Pancreatic stellate cells--role in pancreas cancer.* Langenbecks Arch Surg, 2008. **393**(6): p. 891-900.
140. Shields, M.A., et al., *Biochemical role of the collagen-rich tumour microenvironment in pancreatic cancer progression.* Biochem J, 2012. **441**(2): p. 541-52.
141. Januchowski, R., et al., *Increased Expression of Several Collagen Genes is Associated with Drug Resistance in Ovarian Cancer Cell Lines.* J Cancer, 2016. **7**(10): p. 1295-310.
142. Iseri, O.D., et al., *Gene expression analysis of drug-resistant MCF-7 cells: implications for relation to extracellular matrix proteins.* Cancer Chemother Pharmacol, 2010. **65**(3): p. 447-55.
143. Baer, R., et al., *Implication of PI3K/Akt pathway in pancreatic cancer: When PI3K isoforms matter?* Adv Biol Regul, 2015. **59**: p. 19-35.
144. Murthy, D., K.S. Attri, and P.K. Singh, *Phosphoinositide 3-Kinase Signaling Pathway in Pancreatic Ductal Adenocarcinoma Progression, Pathogenesis, and Therapeutics.* Front Physiol, 2018. **9**: p. 335.
145. Koundouros, N. and G. Poulogiannis, *Phosphoinositide 3-Kinase/Akt Signaling and Redox Metabolism in Cancer.* Front Oncol, 2018. **8**: p. 160.
146. Fruman, D.A., et al., *The PI3K Pathway in Human Disease.* Cell, 2017. **170**(4): p. 605-635.
147. Wehr, A.Y., et al., *Analysis of the human pancreatic stellate cell secreted proteome.* Pancreas, 2011. **40**(4): p. 557-66.
148. Wu, K., et al., *A novel suppressive effect of alcohol dehydrogenase 5 in neuronal differentiation.* J Biol Chem, 2014. **289**(29): p. 20193-9.
149. Zhao, Z., et al., *Prognostic significance of two lipid metabolism enzymes, HADHA and ACAT2, in clear cell renal cell carcinoma.* Tumour Biol, 2016. **37**(6): p. 8121-30.
150. Miura, N., et al., *Tracing putative trafficking of the glycolytic enzyme enolase via SNARE-driven unconventional secretion.* Eukaryot Cell, 2012. **11**(8): p. 1075-82.
151. Chiellini, C., et al., *Characterization of human mesenchymal stem cell secretome at early steps of adipocyte and osteoblast differentiation.* BMC Mol Biol, 2008. **9**: p. 26.
152. Brandi, J., et al., *Secretome protein signature of human pancreatic cancer stem-like cells.* J Proteomics, 2016. **136**: p. 1-12.

153. Goran Ronquist, K., *Extracellular vesicles and energy metabolism.* Clin Chim Acta, 2019. **488**: p. 116-121.
154. Ji, S., et al., *ALDOA functions as an oncogene in the highly metastatic pancreatic cancer.* Cancer Lett, 2016. **374**(1): p. 127-135.
155. Mohammad, G.H., et al., *Targeting Pyruvate Kinase M2 and Lactate Dehydrogenase A Is an Effective Combination Strategy for the Treatment of Pancreatic Cancer.* Cancers (Basel), 2019. **11**(9).
156. de Oliveira, G., et al., *An Integrated Meta-Analysis of Secretome and Proteome Identify Potential Biomarkers of Pancreatic Ductal Adenocarcinoma.* Cancers (Basel), 2020. **12**(3).
157. Follia, L., et al., *Integrative Analysis of Novel Metabolic Subtypes in Pancreatic Cancer Fosters New Prognostic Biomarkers.* Front Oncol, 2019. **9**: p. 115.
158. Wang, H., et al., *Overexpression of PSAT1 regulated by G9A sustains cell proliferation in colorectal cancer.* Signal Transduct Target Ther, 2020. **5**(1): p. 47.
159. Principe, M., et al., *Alpha-enolase (ENO1) controls alpha v/beta 3 integrin expression and regulates pancreatic cancer adhesion, invasion, and metastasis.* J Hematol Oncol, 2017. **10**(1): p. 16.
160. Principe, M., et al., *Targeting of surface alpha-enolase inhibits the invasiveness of pancreatic cancer cells.* Oncotarget, 2015. **6**(13): p. 11098-113.
161. Lopez-Alemany, R., et al., *Inhibition of cell surface mediated plasminogen activation by a monoclonal antibody against alpha-Enolase.* Am J Hematol, 2003. **72**(4): p. 234-42.
162. Miles, L.A., et al., *Role of cell-surface lysines in plasminogen binding to cells: identification of alpha-enolase as a candidate plasminogen receptor.* Biochemistry, 1991. **30**(6): p. 1682-91.

Appendix

Abbreviations

[^{3}H]2-DG	[^{3}H]-2-deoxy-D-glucose
ACAT2	Acetyl-CoA acetyltransferase 2
ADH5	Alcohol dehydrogenase 5(class 3)
Akt	Protein kinase B
ALDOA	Aldolase fructose-bisphosphate A
ALDOC	Aldolase fructose-bisphosphate C
APC	Adenomatous polyposis coli
apCAFs	Antigen presenting cancer-associated fibroblasts
ATCC	American Type Culture Collection
ATP	Adenosine triphosphate
BRCA2	Breast Cancer gene 2
BrdU	Bromodeoxyuridine
BSA	Bovine serum albumin
CAF	Cancer-associated fibroblasts
CD74	Cluster of differentiation 74
CDA	Cytidine deaminase
CDKN2A	Cyclin-dependent kinase inhibitor 2A
CM	Conditional medium
CPM	Counts per minute
CT	Computed tomography
CTGF	Connective tissue growth factor
CYR61	Cysteine-rich angiogenic inducer 61
DCK	Deoxycytidine kinase
dFdC	2′,2′-difluoro deoxycytidine
DMEM	Dulbecco’s modified Eagle’s medium
DMSO	Dimethyl sulfoxide
DNA	Deoxyribonucleic acid
dTMP	2′-deoxythymidine-5′-monophosphate
ECM	Extracellular matrix

EDTA	Ethylene diamine tetraacetic acid
ELISA	Enzyme-linked immunosorbent assay
ENO1	Alpha-enolase
ENO2	Gamma-enolase
ETC	Electron transport chain
FAD	Flavin adenine dinuckleotide
$FADH_2$	Dihydroflavine-adenine dinucleotide
FAP-α	Fibroblast activation protein α
FBS	Fetal bovine serum
FH	Fumarate hydratase
FSP-1	Fibroblast specific protein-1
G-CSF	Granulocyte colony-stimulating factor
G6P	Glucose-6-phosphate
GAPDH	Glyceraldehyde-3-phosphate dehydrogenase
GAS6	Growth Arrest Specific 6
GDP	Guanosine diphosphate
GEM-NAB	Gemcitabine combined with nanoparticle albumin-bound paclitaxel
GFAP	Fibrillary acidic protein
GLUL	Glutamate ammonia ligase
GLUT1	Glucose transporter 1
GM-CSF	Granulocyte-macrophage colony-stimulating factor
GOT1	Glutamic-oxaloacetic transaminase 1
GOT2	Glutamic-oxaloacetic transaminase 2
GPI	Glucose-6-phosphate isomerase
GTP	Guanosine triphosphate
H2-Ab1	H-2 class II histocompatibility antigen A beta chain
HBP	Hexosamine biosynthesis pathway
hCNT	Human concentrative nucleoside transporter
hENT1	Human equilibrative nucleoside transporter 1
HGF	Hepatocyte growth factor
HIF-1α	Hypoxia-inducible factor-1α
HK	Hexokinase
HPaSteC	Human Pancreatic Stellate Cells

HRP	Horseradish peroxidase
iCAFs	Inflammatory cancer-associated fibroblasts
IDH1	Isocitrate dehydrogenase [NADP] cytoplasmic
IFP	Interstitial fluid pressure
IGF	Insulin-like growth factor
IGF1R	Insulin like growth factor 1 receptor
II-SDHB	Succinate dehydrogenase iron-sulfur subunit of complex II
IL	Interleukin
IV-COXII	Cytochrome c oxidase II of complex IV
KCl	Potassium chloride
KRAS	Kirsten rat sarcoma viral oncogene homolog
KRH	Krebs Ringer HEPES
LDHA	Lactate dehydrogenase A
LFQ	Label-free quantification
LGM	Low glucose medium
LIF	Leukemia inhibitory factor
MCT	Monocarboxylate transporter
MDH	Malate dehydrogenase
ME1	Malic enzyme 1
MgSO4	Magnesium sulfate
MHC	Major histocompatibility complex
MMP	Matrix metalloproteinases
MMR	Mismatch repair
MR	Magnetic resonance
MTT	Thiazolyl blue tetrazolium bromide
myCAFs	Myofibroblastic cancer-associated fibroblasts
N_2	Nitrogen
NaCl	Sodium chloride
NAD	Nicotinamide adenine dinucleotide
NADPH	Reduced nicotinamide adenine dinucleotide phosphate
NaOH	Sodium hydroxide
NCAM	Neural cell adhesion molecule
NEAA	Non-essential amino acid

NGF	Nerve growth factor
OXPHOS	Oxidative phosphorylation
P53	Tumor protein P53
PBS	Phosphate-buffered saline
PCC	Pancreatic cancer cells
PDAC	Pancreatic ductal adenocarcinoma
PDGF	Platelet-derived growth factor
PDHA	Pyruvate dehydrogenase E1 component subunit alpha
PFK1	Phosphofructokinase 1
PGAM1	Phosphoglycerate mutase 1
PGD	Phosphogluconate dehydrogenase
PGK1	Phosphoglycerate kinase 1
PGLS	6-phosphogluconolactonase
PGM	Phosphoglycerate mutase
PI3K	Phosphoinositide 3-kinase
PKM1/2	Pyruvate kinase M1 and M2 isoforms
PP	Pancreatic polypeptide
PPP	Pentose phosphate pathway
PRSS1	Serine protease 1
PSAT1	Phosphoserine aminotransferase 1
PSC	Pancreatic stellate cells
PSC-CM	Pancreatic stellate cell conditioned medium
PSPH	Phosphoserine phosphatase
RAC1	Ras-related C3 botulinum toxin substrate 1
RNA	Ribonucleic acid
ROS	Reactive oxygen species
RPM	Revolutions per minute
SDS-PAGE	Sodium dodecyl sulfate polyacrylamide gel electrophoresis
SEM	Standard error mean
SFM	Serum free medium
SGLTs	Sodium-glucose cotransporters
SMAD4	Mothers against decapentaplegic homolog 4
STK11	Serine/threonine kinase 11

TALDO1	Transaldolase 1
TBST	Tris-buffered saline containing 0.1% Tween 20
TCA	Tricarboxylic acid cycle
TGF-β	Transforming growth factor β
TIMP	Tissue inhibitors of metalloproteinases
TKT	Transketolase
TMB	3,3′,5,5′-tetramethylbenzidine
TME	Tumor microenvironment
TNF-α	Tumor necrosis factor-α
TP53	Tumor protein P53
TPI1	Triosephosphate isomerase 1
V-ATP5A	ATP synthase subunit alpha of complex V
α-SMA	Smooth muscle alpha-actin